Diagrammatic Monte Carlo study of the Holstein polaron

Supervisor:

Prof. Cesare Franchini

Co-supervisor:

MSc. Thomas Hahn

Submitted by:

Stefano Ragni

Abstract

The aim of the thesis is to apply the Diagrammatic Monte Carlo numerical method [N. V. Prokof'ev and B. V. Svistunov, Phys. Rev. Lett. 81, 2514, 1998] to the Holstein model of the lattice polaron. As part of this work, the method was implemented in a computer program, and its results were collected and analyzed. The study focuses on ground state properties of the Holstein polaron, such as energy, effective mass and average number of phonons. Observables are computed via an improved approach using estimators developed by Mishchenko [A. Mishchenko et al., Phys. Rev. B, vol. 62, 09, 2009]. The dependency of polaron properties on coupling and momentum is investigated for different dimensionalities (1D, 2D and 3D). Results are compared to analytical expressions obtained in the weak-coupling and strong-coupling limits and to other approaches found in literature.

Contents

Chapter 1

Introduction

This part is intended as a brief summary of the main concepts required to understand both the Diagrammatic Monte Carlo algorithm and the physical system to which the algorithm is applied in this work. In Section 1.1 the standard Hamiltonian of condensed matter physics is recalled and its electronic and phononic parts are developed. Section 1.2 follows up with a discussion on the electron-phonon interaction and introduces the polaron problem. Section 1.3 traces the path from ordinary quantum mechanics to the many-body Green function expansion, explaining the meaning of Feynman diagrams. Lastly, Section 1.4 takes a break from the physics to present the techniques upon which Diagrammatic Monte Carlo is based.

1.1 Review of condensed matter physics fundamentals

The electrons and atoms that constitute matter are assumed as non-relativistic quantum particles. They interact via electromagnetic interaction, the dynamic effects of which are usually ignored so that it can be represented as a static potential $V(\mathbf{r})$. Often this is the Coulomb potential $V(\mathbf{r}) = Q/r$, where Q is the charge of

the particle. The starting point is the Hamiltonian [1]:

$$\hat{H} = \hat{H}_e + \hat{H}_a + \hat{H}_{ea} \tag{1.1}$$

$$\hat{H}_e = \sum_i^{N_e} \left(\frac{\hat{p}_i^2}{2m} + \frac{1}{2} \sum_{j \neq i} V_{ee}(\hat{\mathbf{r}}_i - \hat{\mathbf{r}}_j) \right) \tag{1.2}$$

$$\hat{H}_a = \sum_i^{N_a} \left(\frac{\hat{P}_i^2}{2M} + \frac{1}{2} \sum_{j \neq i} V_{aa}(\hat{\mathbf{R}}_i - \hat{\mathbf{R}}_j) \right) \tag{1.3}$$

$$\hat{H}_{ea} = \sum_i^{N_e} \sum_j^{N_a} V_{ea}(\hat{\mathbf{r}}_i - \hat{\mathbf{R}}_j) \tag{1.4}$$

where $\hat{\mathbf{r}}_i$ and $\hat{\mathbf{R}}_i$ are respectively the electronic and atomic coordinates, N_e is the number of electrons, N_a is the number of atoms, $\hat{p}_i$ and $\hat{P}_i$ the momentum operators for electrons and atoms, and m and M their masses. The first is the electronic term, the second is the atomic/ionic[1] term and the third term takes into account electron-ion interaction. As we will always deal with quantum observables, the hat symbol from operators will be dropped to ease notation.

The electron-ion term 1.4 is a summation of the interactions between the individual atoms at $\mathbf{R}_j$ and the electrons at $\mathbf{r}_i$. The position of each ion can be decomposed into a sum of the equilibrium position $\mathbf{R}_j^{(0)}$ and the displacement $\mathbf{Q}_j$:

$$\mathbf{R}_j = \mathbf{R}_j^{(0)} + \mathbf{Q}_j \tag{1.5}$$

Assuming small displacements, one can do a Taylor expansion of the interaction potential:

$$V_{ea}(\mathbf{r}_i - \mathbf{R}_j^{(0)} - \mathbf{Q}_j) = V_{ea}(\mathbf{r}_i - \mathbf{R}_j^{(0)}) - \mathbf{Q}_j \cdot \boldsymbol{\nabla} V_{ea}(\mathbf{r}_i - \mathbf{R}_j^0) + \mathcal{O}(Q^2) \tag{1.6}$$

The constant term:

$$V_{ea}(\mathbf{r}_i - \mathbf{R}_j^{(0)}) \tag{1.7}$$

is the potential for the electrons when the atoms are in their equilibrium positions, which forms a periodic potential in the crystal. The solution of the Hamiltonian for the motion of the electron in this periodic potential of fixed atoms gives the

---

[1]Here the word "ion" does not imply any particular charge state and it is used interchangeably with "atom"

Bloch states $|\eta\rangle$ of the solid, with associated eigenvalues $E_\eta(\mathbf{R})$. In the *Born-Oppenheimer* approximation, these eigenvalues are then substituted back into Eq. 1.1, acting as a potential energy for the dynamics of the ions. We will be interested in just the ground state term $E_0(\mathbf{R})$ which provides a "binding" contribution:

$$\langle H \rangle_0 = H_a + E_0(\mathbf{R}) \tag{1.8}$$

1.1.1 Phonons

If the crystal is finite with a number of cells $N = N_1 N_2 N_3$, its lattice points define a sequence over which displacement and momentum of the ions are defined. After applying *Born-Von Karman boundary conditions*, the sequence becomes periodic and can be treated by Fourier analysis:

$$\mathbf{Q}(\mathbf{R}) = \frac{1}{\sqrt{N}} \sum_{\mathbf{q}} e^{i\mathbf{q}\cdot\mathbf{R}} \tilde{\mathbf{Q}}(\mathbf{q}) \qquad \tilde{\mathbf{Q}}(\mathbf{q}) = \frac{1}{\sqrt{N}} \sum_{\mathbf{R}} e^{-i\mathbf{q}\cdot\mathbf{R}} \mathbf{Q}(\mathbf{R}) \tag{1.9}$$

$$\mathbf{P}(\mathbf{R}) = \frac{1}{\sqrt{N}} \sum_{\mathbf{q}} e^{i\mathbf{q}\cdot\mathbf{R}} \tilde{\mathbf{P}}(\mathbf{q}) \qquad \tilde{\mathbf{P}}(\mathbf{q}) = \frac{1}{\sqrt{N}} \sum_{\mathbf{R}} e^{-i\mathbf{q}\cdot\mathbf{R}} \mathbf{P}(\mathbf{R}) \tag{1.10}$$

The sum in $\mathbf{q}$ is over N equally spaced wavevectors over the first Brillouin Zone.

Displacements and their conjugate momenta must be real, which leads to the condition:

$$\tilde{\mathbf{Q}}^\star(\mathbf{q}) = \tilde{\mathbf{Q}}(-\mathbf{q}) \qquad \tilde{\mathbf{P}}^\star(\mathbf{q}) = \tilde{\mathbf{P}}(-\mathbf{q}) \tag{1.11}$$

The Born-Oppenheimer approximation introduced in the previous section allowed to decouple the ionic part from the electronic one. The new Hamiltonian 1.8 contains a repulsive (inside H_a) and attractive $E_0(\mathbf{R})$ term, which compete to form a minimum of the potential energy. In the harmonic approximation around the minimum, the system becomes a collection of coupled harmonic oscillators. The above mentioned Fourier transform can then be used to decouple the system of oscillators [1]. The result is:

$$H_{ph} = \frac{1}{2} \sum_{\xi=l,tr} \sum_{\mathbf{q}} \left[\frac{|\mathbf{P}_\xi(\mathbf{q})|^2}{M} + M\omega_\xi^2(\mathbf{q})|\mathbf{Q}_\xi(\mathbf{q})|^2 \right] \tag{1.12}$$

The transformed Hamiltonian is a sum of *independent* harmonic oscillators, each wavevector mode has its own characteristic frequency given by the dispersion re-

lation $\omega_\xi(\mathbf{q})$. ξ indicates the polarization state (longitudinal or transversal, with respect to the direction of $\mathbf{q}$).

The goal is to quantize this Hamiltonian. We recall the procedure in the case of a single harmonic oscillator in position space:

$$H = \frac{p^2}{2m} + \frac{m\omega^2 x^2}{2} = \frac{1}{2m}\left[p^2 + (m\omega x)^2\right]$$

The expression in square brackets is a sum of squares, which is natural to write as a product. However, position and momentum operator do not commute, so there is an additional term:

$$(ip + m\omega x)(-ip + m\omega x) = p^2 + (m\omega x)^2 + im\omega[p, x]$$

$$H = \hbar\omega\left(\frac{ip + m\omega x}{\sqrt{2m\hbar\omega}} \cdot \frac{-ip + m\omega x}{\sqrt{2m\hbar\omega}} + \frac{1}{2}\right) = \hbar\omega\left(b^\dagger b + \frac{1}{2}\right)$$

Where we defined two new operators: b and its adjoint $b^\dagger$

In this form, the Hamiltonian is easier to diagonalize.

The commutator $\left[b, b^\dagger\right]$ follows from the canonical commutation relations:

$$\left[b, b^\dagger\right] = \frac{-2im\omega[x, p]}{2m\hbar\omega} = 1$$

Now apply these results to 1.12:

$$\mathbf{b}_\xi^\dagger(\mathbf{q}) = -\frac{i}{\sqrt{2M\hbar\omega_\xi(\mathbf{q})}}\mathbf{P}_\xi(\mathbf{q}) + \sqrt{\frac{\omega_\xi(\mathbf{q})M}{2\hbar}}\mathbf{Q}_\xi(\mathbf{q}) \qquad (1.13)$$

$$\mathbf{b}_\xi(\mathbf{q}) = \frac{i}{\sqrt{2M\hbar\omega_\xi(\mathbf{q})}}\mathbf{P}_\xi(-\mathbf{q}) + \sqrt{\frac{\omega_\xi(\mathbf{q})M}{2\hbar}}\mathbf{Q}_\xi(-\mathbf{q}) \qquad (1.14)$$

these create/destroy an elementary excitation of bosonic type called *phonon*, with energy $\hbar\omega_\xi(\mathbf{q})$, momentum $\hbar\mathbf{q}$ and polarization ξ. Here a single phonon branch is assumed. In this formalism, the Hamiltonian takes the simpler form:

$$H_{ph} = \sum_{\xi=l,tr}\sum_{\mathbf{q}} \hbar\omega_\xi(\mathbf{q})\left[\mathbf{b}_\xi^\dagger(\mathbf{q}) \cdot \mathbf{b}_\xi(\mathbf{q}) + 1/2\right] \qquad (1.15)$$

where $\mathbf{b}_\xi^\dagger(\mathbf{q}) \cdot \mathbf{b}_\xi(\mathbf{q})$ is the phonon number operator.

From 1.13 and 1.14 it follows immediately:

$$\mathbf{Q}_\xi(\mathbf{q}) = \sqrt{\frac{\hbar}{2M\omega_\xi(\mathbf{q})}} \left[\mathbf{b}_\xi^\dagger(\mathbf{q}) + \mathbf{b}_\xi(-\mathbf{q}) \right] \tag{1.16}$$

which, substituted into 1.9, allows to express the displacement in terms of creation/annihilation operators:

$$\mathbf{Q}(\mathbf{R}) = \frac{1}{\sqrt{N}} \sum_{\xi,\mathbf{q}} \sqrt{\frac{\hbar}{2M\omega_\xi(\mathbf{q})}} \left[\mathbf{b}_\xi^\dagger(\mathbf{q}) + \mathbf{b}_\xi(-\mathbf{q}) \right] e^{i\mathbf{q}\cdot\mathbf{R}} \tag{1.17}$$

1.1.2   Tight binding

The Holstein Hamiltonian describes the kinetic electronic term using a second-quantized tight binding approach. For this reason this section introduces tight binding and derives its form in second quantization.

The electrons in this model are considered tightly bound to the atom to which they belong and they should have limited interaction with states and potentials on surrounding atoms of the solid.

It is often used in a variational context, where the following form for the electronic wavefunction is chosen:

$$\psi_m(\mathbf{r}) = \sum_{\mathbf{R}} c_m(\mathbf{R}) \phi_m(\mathbf{r} - \mathbf{R})$$

where the expansion is in terms of the atomic orbitals ϕ_m, and the free parameters $c_m(\mathbf{R})$ are to be obtained via energy minimization.

Another possible approach is to pick instead a set of "desirable" localized states and define an approximate electronic Hamiltonian in terms of them. This is the approach used in the following, where the second-quantized form of the tight-binding Hamiltonian is derived.

Tight binding in second quantization

Consider the electronic Hamiltonian[2] for the single electron plus the fixed-nuclei term, which is the sum of the potentials $U(\mathbf{r} - n\mathbf{a})$ generated by the n-th ion:

$$\hat{H} = \frac{\hat{p}^2}{2m} + \sum_n U(\mathbf{r} - n\mathbf{a}) \tag{1.18}$$

As single particle states we pick localized orbitals $\langle \mathbf{r} | n \rangle = \phi(\mathbf{r} - n\mathbf{a})$ that are lowest energy eigenstates of the Hamiltonian of the single site:

$$\hat{H} = \frac{\hat{p}^2}{2m} + U(\mathbf{r} - n\mathbf{a}) \tag{1.19}$$

$$\hat{H} |n\rangle = \epsilon_0 |n\rangle \tag{1.20}$$

Note that the eigenvalues do not depend on n: the localized orbital states are all degenerate in energy. The tight-binding Hamiltonian in second quantization reads:

$$\hat{H}_{tb} = \sum_{i,j} \langle i | \hat{H} | j \rangle \, \hat{c}_i^\dagger \hat{c}_j \tag{1.21}$$

The matrix elements are:

$$
\begin{aligned}
\langle i | \hat{H} | j \rangle &= \int d\mathbf{r} \, \phi(\mathbf{r} - i\mathbf{a}) \left[\frac{\hat{p}^2}{2m} + \sum_n U(\mathbf{r} - n\mathbf{a}) \right] \phi(\mathbf{r} - j\mathbf{a}) \\
&= \int d\mathbf{r} \, \phi(\mathbf{r} - i\mathbf{a}) \left[\frac{\hat{p}^2}{2m} + U(\mathbf{r} - j\mathbf{a}) + \sum_{n \neq j} U(\mathbf{r} - n\mathbf{a}) \right] \phi(\mathbf{r} - j\mathbf{a}) \\
&= \epsilon_0 \int d\mathbf{r} \, \phi(\mathbf{r} - i\mathbf{a}) \phi(\mathbf{r} - j\mathbf{a}) + \sum_{n \neq j} \int d\mathbf{r} \, \phi(\mathbf{r} - i\mathbf{a}) U(\mathbf{r} - n\mathbf{a}) \phi(\mathbf{r} - j\mathbf{a}) \\
&= \epsilon_0 S(i,j) + \sum_{n \neq j} U(i,j,n)
\end{aligned}
\tag{1.22}
$$

Now the nearest neighbor approximation is used: we postulate nonzero S and U for nearest neighbors only. We also assume a 1D lattice, so that:

---

[2]correlation effects due to electron-electron interaction are neglected in this work

$$\hat{H}_{tb} = \sum_i \left(\langle i | \hat{H} | i-1 \rangle \hat{c}_i^\dagger \hat{c}_{i-1} + \langle i | \hat{H} | i \rangle \hat{c}_i^\dagger \hat{c}_i + \langle i | \hat{H} | i+1 \rangle \hat{c}_i^\dagger \hat{c}_{i+1} \right) \tag{1.23}$$

The following properties can be shown:

$$S(i, i-1) = S(i, i+1) \equiv \mathcal{S}(1) \tag{1.24}$$

$$U(i, i-1, n) = U(i, i+1, n-1) \tag{1.25}$$

$$\sum_n U(i, i-1, n) = \sum_n U(i, i+1, n) \equiv \mathcal{U}(1) \tag{1.26}$$

After introducing the definitions:

$$E \equiv \epsilon_0 + \mathcal{U}(0) \tag{1.27}$$

$$t \equiv \epsilon_0 \mathcal{S}(1) + \mathcal{U}(1) \tag{1.28}$$

one finally gets to:

$$\hat{H}_{tb} = E \sum_i \hat{c}_i^\dagger \hat{c}_i + t \sum_i \hat{c}_i^\dagger (\hat{c}_{i-1} + \hat{c}_{i+1}) \tag{1.29}$$

The first term only results in a shift in energy of the Hamiltonian and will be dropped.

It is also possible to express the same Hamiltonian in momentum space. To do so it's sufficient to apply a discrete Fourier transform to the sequence of operators c_i and $c_i^\dagger$:

$$c_j = \frac{1}{\sqrt{N}} \sum_k e^{ikja} c_k \qquad c_j^\dagger = \frac{1}{\sqrt{N}} \sum_k e^{-ikja} c_k^\dagger \tag{1.30}$$

In this way the tight-binding term becomes:

$$t \sum_j \hat{c}_j^\dagger (\hat{c}_{j-1} + \hat{c}_{j+1}) =$$

$$\frac{t}{N} \sum_j \left(\sum_{k,k'} e^{i(k'-k)ja} e^{-ik'a} c_k^\dagger c_{k'} + \sum_{k,k''} e^{i(k''-k)ja} e^{ik''a} c_k^\dagger c_{k''} \right) =$$

$$\frac{t}{N} \left(\sum_{k,k'} N\delta_{k',k} e^{-ik'a} c_k^\dagger c_{k'} + \sum_{k,k''} N\delta_{k'',k} e^{ik''a} c_k^\dagger c_{k''} \right) =$$

$$t \sum_k \left(e^{ika} + e^{-ika} \right) c_k^\dagger c_k \quad (1.31)$$

which can be written in the usual form (single band, 1D):

$$\sum_k \epsilon(k) c_k^\dagger c_k \qquad \epsilon(k) = 2t\cos(k) \tag{1.32}$$

Compare this to the dispersion of free electrons ($\hbar = 1$):

$$\epsilon^{\text{free}}(k) = \frac{k^2}{2m}$$

k is discrete for a crystal of finite size and becomes continuous in the thermodynamic limit. The curves are similar in the proximity of $k = 0$.

The tight binding Hamiltonian 1.29 is often [2] written in the equivalent form:

$$\hat{H}_{tb} = -t \sum_{<i,j>} (\hat{c}_i^\dagger \hat{c}_j + \hat{c}_i \hat{c}_j^\dagger) \tag{1.33}$$

Here the angular brackets denote nearest neighbor pairs and the hopping integral t corresponds to the transfer integral J, also called interatomic matrix element, bond energy or two center integral. It is the fundamental ingredient of the tight-binding model:

$$J_{ml}(\mathbf{R}_n) = -\int d\mathbf{r}\, \phi_m^*(\mathbf{r}) U(\mathbf{r}) \phi_l^*(\mathbf{r} - \mathbf{R}_n) \tag{1.34}$$

For $t \to 0$ it is impossible for an electron to hop into neighboring sites (isolated atomic system). If the hopping term is turned on, electrons can stay in both sites lowering their kinetic energy.
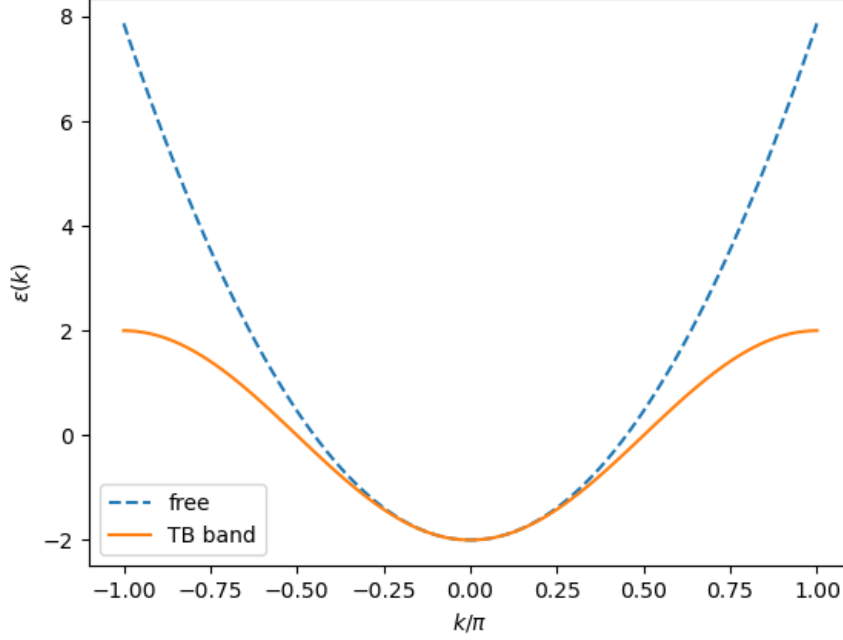
Figure 1.1: Tight binding band for a monoatomic chain of atoms in 1D compared to the free electron.

1.2 Polaron physics

1.2.1 The electron-phonon interaction

The linear term of Eq. 1.6 is the electron-phonon interaction, which is the focus of this section:

$$V_{ep} = \sum_{j} \mathbf{Q}_j \cdot \boldsymbol{\nabla} V_{ea}(\mathbf{r}_i - \mathbf{R}_j^0) \tag{1.35}$$

Now the goal is to write this interactions in terms of operators, that is to express it in second quantization formalism. For this we need the second quantized form of the displacement operator that was derived in Section 1.1.1.

Being periodic, the electron-atom potential can be written in a Fourier series:

$$V_{ea}(\mathbf{r}) = \frac{1}{N} \sum_{\mathbf{q}} V_{ea}(\mathbf{q}) e^{i\mathbf{q}\cdot\mathbf{r}} \tag{1.36}$$

and its gradient is:

$$\boldsymbol{\nabla} V_{ea}(\mathbf{r}) = \frac{i}{N} \sum_{\mathbf{q}} \mathbf{q} V_{ea}(\mathbf{q}) e^{i\mathbf{q}\cdot\mathbf{r}} \tag{1.37}$$

which inserted into 1.35 gives:

$$V_{ep}(\mathbf{r}) = \frac{i}{N} \sum_{\mathbf{q}} \mathbf{q} V_{ea}(\mathbf{q}) e^{i\mathbf{q}\cdot\mathbf{r}} \sum_{j} \mathbf{Q}_j e^{i\mathbf{q}\cdot\mathbf{R}_j^{(0)}} \tag{1.38}$$

Inserting now the expression 1.17 for $\mathbf{Q}_j$ and using the properties of Fourier transforms, the second quantized form of V_{ep} can be obtained:

$$V_{ep}(\mathbf{r}) = -\sum_{\mathbf{q}\mathbf{G}} e^{i\mathbf{r}(\mathbf{q}+\mathbf{G})} V_{ea}(\mathbf{q}+\mathbf{G})(\mathbf{q}+\mathbf{G}) \cdot \xi_{\mathbf{q}} \sqrt{\frac{\hbar}{2MN\omega_q}} (b_{\mathbf{q}} + b_{-\mathbf{q}}^{\dagger}) \tag{1.39}$$

now the summation has been divided into a $\mathbf{q}$ variable ranging over the first Brillouin Zone of the crystal and $\mathbf{G}$ which is the set of reciprocal lattice vectors. The product MN can also be expressed as $\rho\nu$ (density and volume) in view of the continuum limit. The different modes λ were dropped for simplicity.

The electron-phonon interaction is finally obtained by integrating this potential over the charge density of the solid $\rho(\mathbf{r})$:

$$H_{ep} = \int \mathrm{d}^3 r \, \rho(\mathbf{r}) V_{ep}(\mathbf{r}) =$$

$$-\sum_{\mathbf{q}\mathbf{G}} \rho(\mathbf{q}+\mathbf{G}) V_{ea}(\mathbf{q}+\mathbf{G})(\mathbf{q}+\mathbf{G}) \cdot \xi_{\mathbf{q}} \sqrt{\frac{\hbar}{2MN\omega_q}} (b_{\mathbf{q}} + b_{-\mathbf{q}}^{\dagger}) \tag{1.40}$$

This matrix element is often written as:

$$M_{\mathbf{q}+\mathbf{G}} = -V_{ea}(\mathbf{q}+\mathbf{G})(\mathbf{q}+\mathbf{G}) \cdot \xi_{\mathbf{q}} \sqrt{\frac{\hbar}{2MN\omega_q}} \tag{1.41}$$

$$H_{ep} = \sum_{\mathbf{q}\mathbf{G}} M_{\mathbf{q}+\mathbf{G}} \, \rho(\mathbf{q}+\mathbf{G})(b_{\mathbf{q}} + b_{-\mathbf{q}}^{\dagger}) \tag{1.42}$$

The most common forms of electron-phonon interactions in semiconductors are three [3]:

- Deformation potential coupling to acoustical phonons

- Piezoelectric coupling to acoustical phonons

- Polar coupling to optical phonons

Deformation potential

The deformation potential coupling to acoustical phonons is the long-wavelength limit of 1.42. The terms with $G \neq 0$ are discarded and the electron-ion potential is taken to be a constant D at $\mathbf{q} \to 0$, called the *deformation constant*. At long wavelength ξ approaches the direction of $\mathbf{q}$ and only longitudinal phonons are important when there is no degeneration. The interaction becomes: [3]

$$H_{ep}^{def} = D \sum_{\mathbf{q}} \sqrt{\frac{\hbar}{2\rho\nu\omega_{\mathbf{q}}}} |\mathbf{q}| \rho(\mathbf{q})(b_{\mathbf{q}} + b_{-\mathbf{q}}^{\dagger}) \qquad (1.43)$$

where the summation is over longitudinal acoustic phonons. However, it often happens in semiconductors that valence bands are degenerate at the band maximum, so the holes have a deformation coupling to transverse phonon that must be taken into account when dealing with a multi-band model.

A detailed derivation of this type of coupling can be found for example in [1].

Piezoelectric interaction

Many semiconductors are piezoelectric, that is an electric field is produced when a crystal is deformed and vice-versa. Acoustical phonons are periodic deformations, so they create electric fields if the crystal is piezoelectric. Examples of strongly piezoelectric materials are CdS and ZnO. Without going into the details of this type of interaction, the final result is shown: [3]

$$H_{ep}^{piezo} = i \sum_{\mathbf{q}} \sqrt{\frac{\hbar}{2\rho\nu\omega_{\mathbf{q}}}} M_{\lambda}(\hat{q}) \rho(\mathbf{q})(b_{\mathbf{q}} + b_{-\mathbf{q}}^{\dagger}) \qquad (1.44)$$

It is characterized by a matrix element $M_{\lambda}(\hat{q})$ that depends only on the direction of $\mathbf{q}$. Moreover, $M_{\lambda}(-\hat{q}) = -M_{\lambda}(\hat{q})$ so that 1.44 is hermitian.

Polar coupling

In ionic crystals, the polar coupling between electrons and optical phonons can be very large. Some of the atoms are positively charged, while others are negatively

charged. An optical phonon has the different ions in the crystal vibrating out of phase, so that when the plus and minus ions oscillate, they set up a dipole polarization field. Such polarization causes a long-range electric field which scatters the electrons. The form of the Hamiltonian has been derived by Fröhlich [4]:

$$H_{ep} = \sum_{\mathbf{q}} \frac{M}{q\sqrt{\nu}} \rho(\mathbf{q})(b_{\mathbf{q}} + b^{\dagger}_{-\mathbf{q}}) \tag{1.45}$$

$$M^2 = 2\pi e^2 \hbar \omega_{LO} \left(\frac{1}{\epsilon_{\infty}} - \frac{1}{\epsilon_0} \right) \tag{1.46}$$

the high-frequency (electronic, ion-clamped) dielectric constant ϵ_{∞} is the square of the refractive index, and the static (electronic and ionic) dielectric constant ϵ_0 can be measured by putting the solid between the parallel plates of a capacitor.

1.2.2 Pekar's polaron

The first and simplest model of a polaron was proposed by Pekar in the 1940s. [5] Its goal was to try to describe localization without performing very difficult calculations, by introducing only the minimal ingredients required to have some localized solution. [6]

Consider an electron wavefunction and add the kinetic energy to the total energy. It is the standard kinetic energy with some kind of effective mass. Instead of describing ions as discrete objects one can describe the system as a dielectric continuum and therefore the energy associated with it comes from the electrostatic energy (the integral of the energy density).

$$E = \frac{\hbar^2}{2m^*} \int d\mathbf{r} \, |\boldsymbol{\nabla}\psi|^2 + \frac{1}{2} \int d\mathbf{r} \, \mathbf{E} \cdot \mathbf{D} \tag{1.47}$$

Ideally one wants to find this wavefunction, which requires connecting it to the electric field and displacement. The first relation to be used is the Gauss Law:

$$\boldsymbol{\nabla} \cdot \mathbf{D} = -e|\psi(\mathbf{r})|^2 \tag{1.48}$$

Then one can relate the displacement to the electric field by the dielectric constant (assuming linear, homogeneous, etc.).

$$\mathbf{D} = \varepsilon_0 \epsilon_0 \mathbf{E} \tag{1.49}$$

Inverting these two relations, one gets a Coulomb integral in the charge density:

$$\frac{1}{2} \int d\mathbf{r}\, \mathbf{E} \cdot \mathbf{D} = \frac{1}{2} \frac{e^2}{4\pi\varepsilon_0} \left(\frac{1}{\epsilon_0} - \frac{1}{\epsilon_\infty} \right) \int d\mathbf{r}\, d\mathbf{r}'\, \frac{|\psi(\mathbf{r})|^2 |\psi(\mathbf{r}')|^2}{|\mathbf{r} - \mathbf{r}'|} \tag{1.50}$$

The screening comes from the total electric screening (ionic plus electronic contribution). A problem arises: by using the total screening we are double counting the electronic contribution. We are already considering an effective mass so the electronic screening was already taken into account. It has to be canceled with a subtraction of the electronic dielectric screening.

Plugging back into Eq. 1.47 one gets an expression involving only the wavefunction of the polaron. At this point one does a variational minimization with constraint (normalization of the wavefunction). One arrives at an equation that looks a lot like the Schrödinger equation, but a nonlinear equation of third order in the wavefunction. It is the Landau-Pekar equation:

$$\boxed{-\frac{\hbar^2}{2m^*}\nabla^2\psi(\mathbf{r}) - \frac{e^2}{4\pi\varepsilon_0}\left(\frac{1}{\epsilon_0} - \frac{1}{\epsilon_\infty}\right) \int d\mathbf{r}'\, \frac{|\psi(\mathbf{r}')|^2}{|\mathbf{r} - \mathbf{r}'|}\psi(\mathbf{r}) = \lambda\psi(\mathbf{r})} \tag{1.51}$$

To gain insight into this equation, one tries a simple trial solution, to see if something with localized features solves the problem. Consider an exponentially decaying function:

$$\psi(\mathbf{r}) = (\pi r_p^3)^{-1/2} \exp(-|\mathbf{r}|/r_p) \tag{1.52}$$

The energy becomes a sum of two terms (kinetic and Coulomb), one scaling as the inverse of the square of the polaron radius with a plus sign, and the other one scaling as the inverse of the polaron radius with a minus sign:

$$\frac{\hbar^2}{2m^*}\frac{1}{r_p^2} - \frac{5}{16}\frac{e^2}{4\pi\varepsilon_0}\left(\frac{1}{\epsilon_0} - \frac{1}{\epsilon_\infty}\right)\frac{1}{r_p} \tag{1.53}$$

Since there is different scaling at infinity and opposite sign, there will be a competition between the kinetic and Coulomb part, and this competition leads to the formation of a minimum, which corresponds to the self-trapped polaron (qualitatively described in Figure 1.2).

Some problems of this model are:

- In the case of a *non-polar semiconductor* or *insulator* the Coulomb term
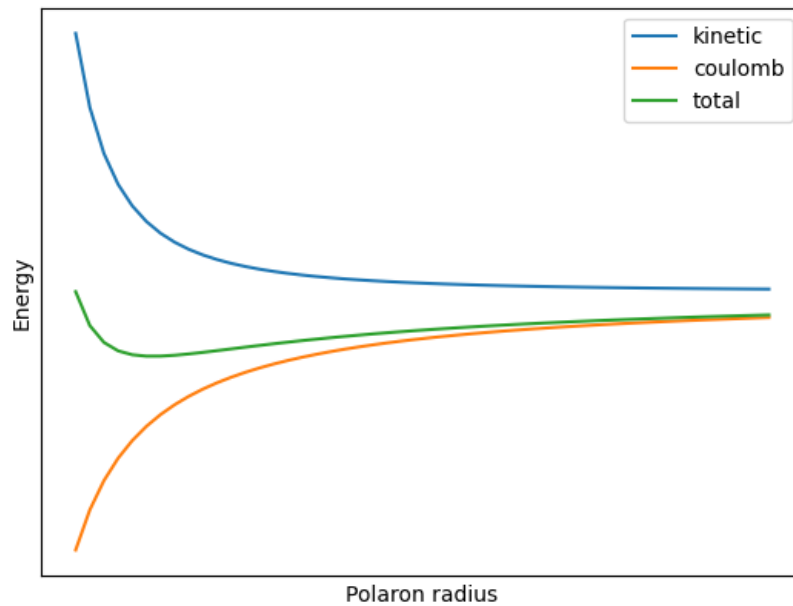
Figure 1.2: Kinetic and Coulomb terms compete to form a minimum in the total energy.

vanishes because the dielectric constant including the ionic contribution will be equal to the electronic dielectric constant

- The model doesn't consider any granularity in the crystal, no atoms, no multiple electronic bands, no multiple phonon branches, so it is not something that can be used for quantitative calculations.

1.3 Many body physics

Diagrammatic Monte Carlo requires the mathematical tools of many-body quantum physics, which are introduced here. The fundamental quantity of interest is the many-body Green function of the system and its expansion in a diagrammatic series. The main steps towards this expansion are outlined in this section, and its first terms will be derived for the case of electron-phonon interaction.

We start by recalling the main pictures (equivalent representations) of quantum mechanics ($\hbar = 1$ is assumed throughout this section). Consider a Hamiltonian H

that doesn't explicitly depend on time:

- Schrödinger picture: the quantum state evolves in time

$$\psi(t) = e^{-iHt}\psi(0) \tag{1.54}$$

- Heisenberg picture: the operators evolve in time

$$O(t) = e^{iHt}Oe^{-iHt} \tag{1.55}$$

These are equivalent point of views because they lead to the same expectation values. In Schrödinger picture:

$$\langle\psi(t)|\,O\,|\psi(t)\rangle = \psi^\star(t)O\psi(t) = \psi^\star e^{iHt}Oe^{-iHt}\psi \tag{1.56}$$

In Heisenberg picture:

$$\langle\psi|\,O(t)\,|\psi\rangle = \psi^\star O\psi = \psi^\star e^{iHt}Oe^{-iHt}\psi \tag{1.57}$$

which yields the same result as 1.56.

1.3.1 Interaction picture

Consider an Hamiltonian decomposed into an unperturbed, exactly solvable part H_0 and a perturbation V:

$$H = H_0 + V \tag{1.58}$$

In the interaction picture both states and operators evolve with time. Operators evolve under the influence of the unperturbed Hamiltonian, while state evolution is driven by the perturbation only (the latter is not immediately obvious, but will become apparent later in Eq. 1.64).

$$\begin{aligned}
\hat{O}(t) &= e^{iH_0t}Oe^{-iH_0t} \\
\hat{\psi}(t) &= e^{iH_0t}e^{-iHt}\psi
\end{aligned} \tag{1.59}$$

where operators and states are marked with a hat to distinguish them from other pictures.

The main purpose of introducing this picture is to remove the explicit appearance of the unperturbed Hamiltonian H_0 in the time-dependent Schrödinger equation:

$$\frac{\partial}{\partial t}\psi(t) = -iH\psi(t) \tag{1.60}$$

In order to transform 1.60 into the interaction picture, we calculate the derivative:

$$\frac{\partial}{\partial t}\hat{\psi}(t) = iH_0 e^{iH_0 t}\psi(t) + e^{iH_0 t}\frac{\partial}{\partial t}\psi(t) \tag{1.61}$$

Using the time dependent Schrödinger equation 1.60 and the fact that H_0 commutes with $e^{iH_0 t}$ one gets:

$$\frac{\partial}{\partial t}\hat{\psi}(t) = ie^{iH_0 t}(H_0 - H)\psi(t) = -ie^{iH_0 t}V\psi(t) \tag{1.62}$$

At this point it's easy to cast the right-hand side into the interaction picture:

$$\frac{\partial}{\partial t}\hat{\psi}(t) = -ie^{iH_0 t}Ve^{-iH_0 t}e^{iH_0 t}\psi(t) = -i\hat{V}\hat{\psi}(t) \tag{1.63}$$

This equation shows that the time dependence of $\hat{\psi}(t)$ is determined by $\hat{V}(t)$. Taking the state at time 0 as reference, one can define an equivalent equation in terms of the evolution operator $U(t)$:

$$\frac{\partial}{\partial t}U(t) = -i\hat{V}U(t) \quad \text{with} \quad \hat{\psi}(t) = U(t)\psi(0) \tag{1.64}$$

The above can be solved in an iterative manner. The first step is to integrate the equation from time 0 to t:

$$U(t) - U(0) = -i\int_0^t dt_1\, \hat{V}(t_1)U(t_1) \tag{1.65}$$

Now, iterating:

$$U(t) = 1 - i \int_0^t \mathrm{d}t_1 \, \hat{V}(t_1) \left[1 - i \int_0^{t_1} \mathrm{d}t_2 \, \hat{V}(t_2) U(t_2) \right] \tag{1.66}$$

$$= 1 - i \int_0^t \mathrm{d}t_1 \, \hat{V}(t_1) - \int_0^t \mathrm{d}t_1 \int_0^{t_1} dt_2 \, \hat{V}(t_1)\hat{V}(t_2) \tag{1.67}$$

$$= \sum_{n=0}^{\infty} (-i)^n \int_0^t \mathrm{d}t_1 \int_0^{t_1} dt_2 \ldots \int_0^{t_{n-1}} \mathrm{d}t_n \, \hat{V}(t_1)\hat{V}(t_2)\ldots\hat{V}(t_n) \tag{1.68}$$

The last expression is similar to the series expansion of an exponential, but not exactly: it's missing the $n!$ factor, and the integration limits depend on previous integration variables, so that it cannot be written as a product of identical terms.

However, it is possible to rearrange the above expression into a compact, exponential form. It is done by introducing the *time-ordering* operator, which acts on time dependent operators and arranges them so that earlier times appear on the right (so that they are the first to be applied). An example with three times:

$$t_2 < t_3 < t_1 : \quad T[\hat{V}(t_1)\hat{V}(t_2)\hat{V}(t_3)] = \hat{V}(t_1)\hat{V}(t_3)\hat{V}(t_2) \tag{1.69}$$

The time ordering operator can be given an explicit expression through the Heaviside $\theta(t)$ function. For two operators it reads:

$$T[\hat{V}(t_1)\hat{V}(t_2)] = \theta(t_1 - t_2)\hat{V}(t_1)\hat{V}(t_2) + \theta(t_2 - t_1)\hat{V}(t_2)\hat{V}(t_1) \tag{1.70}$$

Let us now use the above to rearrange the evolution operator restricting ourselves to just the $n = 2$ term for clarity:

$$\int_0^t \mathrm{d}t_1 \int_0^{t_1} dt_2 \, \hat{V}(t_1)\hat{V}(t_2) =$$
$$\frac{1}{2}\left(\int_0^t \mathrm{d}t_1 \int_0^{t_1} dt_2 \, \hat{V}(t_1)\hat{V}(t_2) + \int_0^t dt_2 \int_0^{t_2} dt_1 \, \hat{V}(t_2)\hat{V}(t_1) \right) =$$
$$\frac{1}{2} \int_0^t \mathrm{d}t_1 \int_0^t dt_2 \left(\theta(t_1 - t_2)\hat{V}(t_1)\hat{V}(t_2) + \theta(t_2 - t_1)\hat{V}(t_2)\hat{V}(t_1) \right) =$$
$$\frac{1}{2!} \int_0^t \mathrm{d}t_1 \int_0^t dt_2 \, T[\hat{V}(t_1)\hat{V}(t_2)] \tag{1.71}$$

where we performed the relabeling $t_1 \leftrightarrow t_2$ in the second term of the second row above. This argument can be readily generalized to the arbitrary n case, obtaining

the full expansion for $U(t)$:

$$U(t) = \sum_{n=0}^{\infty} \frac{(-i)^n}{n!} \int_0^t \mathrm{d}t_1 \int_0^t \mathrm{d}t_2 \ldots \int_0^t \mathrm{d}t_n \, T[\hat{V}(t_1)\hat{V}(t_2)\ldots\hat{V}(t_n)] \quad (1.72)$$

which can also be written in the more compact form:

$$U(t) = T \exp\left(-i \int_0^t \mathrm{d}t_1 \, \hat{V}(t_1)\right) \quad (1.73)$$

S matrix

Define the operator S as:
$$S(t,t') = U(t)U^\dagger(t') \quad (1.74)$$

S evolves the state from an arbitrary point in time to another. It may be broken down to:

1. backward evolution from t' to 0

2. forward evolution from 0 to t

where backwards evolution is achieved by $U^\dagger$.

S satisfies the following properties:

$$S(t,t) = 1 \quad (1.75)$$
$$S^\dagger(t,t') = S(t',t) \quad (1.76)$$
$$S(t,t')S(t',t'') = S(t,t'') \quad (1.77)$$

which are easily verifiable using the fact that U is unitary. S obeys a differential equation very similar to that of U, with solution analogous to 1.73:

$$S(t,t') = T \exp\left(-i \int_{t'}^t \mathrm{d}t_1 \, \hat{V}(t_1)\right) \quad (1.78)$$

1.3.2 Green function

A quantity of fundamental importance in the Diagrammatic Monte Carlo method is the *Green function* or *propagator*. At zero temperature, it is proportional to the probability amplitude of finding the system in its interacting ground state with an

added particle at time t if a particle in the same state was added at a previous time t'.

For example, in the case of an electron in state $\mathbf{k}$ one has:

$$G(\mathbf{k}, t - t') = -i \langle \Psi_0 | c_{\mathbf{k}}(t) c_{\mathbf{k}}^\dagger(t') | \Psi_0 \rangle \tag{1.79}$$

To make this definition clearer, let us break down the formula into a series of steps:

1. Start from the real ground state of the interacting system Ψ_0

2. An electronic excitation in state $\mathbf{k}$ at time t' is created

3. The same excitation at a later time t is destroyed

4. The resulting state is projected along the ground state

If $|\mathbf{k}\rangle$ were an eigenstate of H, this state would propagate with a simple time dependence reduced to multiplication by a phase factor. Instead, the particle initially created in step 2 undergoes a series of "scattering events" between t' and t, and the Green function tells how much amplitude is left in the state $\mathbf{k}$.

Now a procedure to actually calculate the Green function from quantities that are known is presented. The first step is to change the creation/annihilation operators from Heisenberg picture to interaction picture:

$$c_{\mathbf{k}}(t) = S(0, t)\hat{c}_{\mathbf{k}}(t)S(t, 0) \tag{1.80}$$

where the definitions of the time evolution and S-matrix operators were used.

The main problem of the formalism used up to this point is that it is based on the ground state of the interacting system Ψ_0 which is not known. A way to bridge this state to the ground state of the non-interacting system ϕ_0 was established by Gell-Mann and Low [7]:

$$\psi(0) = S(0, -\infty)\phi_0 \tag{1.81}$$

which means that $\hat{\Psi}_0(-\infty)$ is equal to ϕ_0. An additional assumption is also needed for $\hat{\Psi}_0(\infty)$:

$$\hat{\psi}(\infty) = e^{iL}\phi_0 \tag{1.82}$$

relating it to ϕ_0 via a phase factor. 1.81 and 1.82 allow the intermediate result:

$$\langle \Psi_0 | = \langle \phi_0 | \, S(-\infty, 0) = \frac{\langle \phi_0 | \, S(\infty, 0)}{\langle \phi_0 | \, S(\infty, -\infty) \, | \phi_0 \rangle} \tag{1.83}$$

Finally, applying 1.80 and 1.83 to the definition of the propagator 1.79:

$$\boxed{G(\mathbf{k}, t - t') = -i \frac{\langle \phi_0 | \, TS(\infty, -\infty) \hat{c}_{\mathbf{k}}(t) \hat{c}_{\mathbf{k}}^\dagger(t') \, | \phi_0 \rangle}{\langle \phi_0 | \, TS(\infty, -\infty) \, | \phi_0 \rangle}} \tag{1.84}$$

Together with 1.78, this formula represents the crucial result that the Green function of the interacting system can be represented as an expansion of matrix elements between the non-interacting ground state.

1.3.3   Diagrammatic expansion of the Green function

Consider for now just the numerator of 1.84 with the expansion 1.78 for S. The $n = 0$ term of the exponential expansion is always the free propagator G_0:

$$M^{(0)} = \langle \psi_0 | \, T\{\hat{c}_{\mathbf{k}_2}(t_2) \hat{c}_{\mathbf{k}_1}^\dagger(t_1)\} \, | \psi_0 \rangle \tag{1.85}$$

By 1.59, the creation/annihilation operators in interaction picture can be expressed as:

$$\hat{c}_{\mathbf{k}}(t) = e^{iH_0 t} c_{\mathbf{k}} e^{-iH_0 t} \tag{1.86}$$

The commutator is:

$$[H_0, c_{\mathbf{k}}] = \sum_{\mathbf{k}'} \epsilon(\mathbf{k}')[c_{\mathbf{k}'}^\dagger c_{\mathbf{k}'}, c_{\mathbf{k}}] = \sum_{\mathbf{k}'} \epsilon(\mathbf{k}')\Big([c_{\mathbf{k}'}^\dagger, c_{\mathbf{k}}]c_{\mathbf{k}'} + c_{\mathbf{k}'}^\dagger[c_{\mathbf{k}'}, c_{\mathbf{k}}]\Big) \tag{1.87}$$

where the first commutator is a delta and the second is zero because it is between two annihilation operators:

$$[H_0, c_{\mathbf{k}}] = \sum_{\mathbf{k}'} \epsilon(\mathbf{k}')\delta_{\mathbf{k}',\mathbf{k}} c_{\mathbf{k}'} = \epsilon(\mathbf{k}) c_{\mathbf{k}} \tag{1.88}$$

Substituting this for the commutators:

$$\hat{c}_{\mathbf{k}}(t) = c_{\mathbf{k}} - i\epsilon(\mathbf{k})t c_{\mathbf{k}} + \frac{i^2}{2!}\epsilon^2(\mathbf{k})t^2 c_{\mathbf{k}} + \cdots = c_{\mathbf{k}} e^{-i\epsilon(\mathbf{k})t} \tag{1.89}$$

Now, going back to 1.85 with the time ordering $t_2 > t_1$:

$$M^{(0)} = \langle\psi_0| c_{\mathbf{k}_1} c_{\mathbf{k}_2}^\dagger |\psi_0\rangle \, e^{-i(\epsilon(\mathbf{k}_2)t_2 - \epsilon(\mathbf{k}_1)t_1)} = \delta_{\mathbf{k}_1,\mathbf{k}_2} e^{-i\epsilon(\mathbf{k}_1)(t_2 - t_1)} \tag{1.90}$$

which is just the free propagator $iG_0^+(\mathbf{k}_2, \mathbf{k}_1, t_2 - t_1)$

Now take V as the electron-phonon interaction:

$$V = \sum_{\mathbf{qk}} M_{\mathbf{q}} \, A_{\mathbf{q}} \, c_{\mathbf{k+q}}^\dagger \, c_{\mathbf{k}} \tag{1.91}$$

which is 1.42 with a new annihilation operator $A_{\mathbf{k}}$ defined as:

$$A_{\mathbf{k}} = b_{\mathbf{k}} + b_{-\mathbf{k}}^\dagger \qquad A_{\mathbf{k}}^\dagger = b_{\mathbf{k}}^\dagger + b_{-\mathbf{k}} = A_{-\mathbf{k}} \tag{1.92}$$

The propagator for phonons may be defined in two different ways [8]. The one with a more direct physical interpretation is:

$$G_{ph}(\mathbf{k}, t) = -i \langle\psi_0| T\{b_{\mathbf{k}}(t) b_{\mathbf{k}}^\dagger(0)\} |\psi_0\rangle \tag{1.93}$$

where the ket vector $|\psi_0\rangle$ is the exact ground state for the system of phonons, also called the "interacting vacuum". Analogously to the electronic case, this propagator has the physical significance of being the probability amplitude to observe a phonon in state $\mathbf{k}$ at time t if a phonon in state $\mathbf{k}$ was introduced into the system at time 0. In the case of zero interaction, $G(\mathbf{k}, t)$ becomes the free propagator:

$$G_{ph}^{(0)}(\mathbf{k}, t) = -i(\theta_t \langle 0| b_{\mathbf{k}}(t) b_{\mathbf{k}}^\dagger(0) |0\rangle + \theta_{-t} \langle 0| b_{\mathbf{k}}(t) b_{\mathbf{k}}^\dagger(0) |0\rangle) = -i\theta_t e^{-i\omega(\mathbf{k})t} \tag{1.94}$$

where θ_t is the Heaviside function and $|0\rangle$ is the ket for the non-interacting vacuum.

An alternative definition, harder to interpret physically but more convenient mathematically is:

$$D(\mathbf{k}, t) = -i \langle\psi_0| T\{A_{\mathbf{k}}(t) A_{\mathbf{k}}^\dagger(0)\} |\psi_0\rangle \tag{1.95}$$

$D(\mathbf{k}, t)$ may be viewed as propagating a "displacement wave" in the interacting

vacuum. The free propagator is:

$$D^{(0)}(\mathbf{k}, t) = -i(\theta_t e^{-i\omega(\mathbf{k})t} + \theta_{-t} e^{i\omega(\mathbf{k})t}) \tag{1.96}$$

When there is a mixture of phonon and electron operators, the bracket can be immediately factored into separate parts for electron and phonons, because the two different kinds of operators commute.

The $n = 1$ term vanishes because it contains the factor $\langle\phi_0|\, T\hat{A}_{\mathbf{q}}\,|\phi_0\rangle$ which is zero since $\langle 0|\, a_{\mathbf{q}}\,|0\rangle$ and $\langle 0|\, a_{\mathbf{q}}^\dagger\,|0\rangle$. This can be generalized to the statement: [3]

> Only the terms even in n contribute to the propagator expansion for the electron-phonon interaction.

Computing now the $n = 2$ term:

$$G(\mathbf{k}, t - t') = G^{(0)}(\mathbf{k}, t - t') + \frac{(-1)^3}{2!} \int dt_1 \int dt_2$$
$$\sum_{\mathbf{q}_1, \mathbf{q}_2} M_{\mathbf{q}_1} M_{\mathbf{q}_2} \langle\phi_0|\, T\hat{A}_{\mathbf{q}_1}(t_1)\hat{A}_{\mathbf{q}_2}(t_2)\,|\phi_0\rangle$$
$$\times \sum_{\mathbf{k}_1, \mathbf{k}_2} \langle\phi_0|\, T\hat{c}_{\mathbf{k}}(t)\hat{c}_{\mathbf{k}_1+\mathbf{q}_1}^\dagger(t_1)\hat{c}_{\mathbf{k}_1}(t_1)\hat{c}_{\mathbf{k}_2+q_2}^\dagger(t_2)\hat{c}_{\mathbf{k}_2}(t_2)\hat{c}_{\mathbf{k}}^\dagger(t')\,|\phi_0\rangle \tag{1.97}$$

The phonon bracket gives a single-phonon Green's function:

$$\langle\phi_0|\, T\hat{A}_{\mathbf{q}_1}(t_1)\hat{A}_{\mathbf{q}_2}(t_2)\,|\phi_0\rangle = i\delta_{\mathbf{q}_1+\mathbf{q}_2}D^{(0)}(\mathbf{q}_1, t_1 - t_2) \tag{1.98}$$

Note the Dirac delta, which imposes the condition $\mathbf{q}_1 = \mathbf{q}_2$ to the calculations that will follow.

The electron bracket instead has a lot of possible pairings. To decompose it, one makes use of *Wick's theorem*, which states that the only non-zero terms are the fully contracted ones:

$$\overline{\hat{c}_{\mathbf{k}}(t)\hat{c}_{\mathbf{k}_1+\mathbf{q}_1}^\dagger}(t_1)\overline{\hat{c}_{\mathbf{k}_1}(t_1)\hat{c}_{\mathbf{k}_2+\mathbf{q}_2}^\dagger}(t_2)\overline{\hat{c}_{\mathbf{k}_2}(t_2)\hat{c}_{\mathbf{k}}^\dagger}(t') =$$
$$i^3\delta_{\mathbf{k},\mathbf{k}_1+\mathbf{q}_1}\delta_{\mathbf{k},\mathbf{k}_2}G^{(0)}(\mathbf{k}, t - t_1)G^{(0)}(\mathbf{k} - \mathbf{q}_1, t_1 - t_2)G^{(0)}(\mathbf{k}, t_2 - t') \tag{1.99}$$

$$\hat{c}_{\mathbf{k}}(t)\hat{c}^{\dagger}_{\mathbf{k}_1+\mathbf{q}_1}(t_1)\hat{c}_{\mathbf{k}_1}(t_1)\hat{c}^{\dagger}_{\mathbf{k}_2+\mathbf{q}_2}(t_2)\hat{c}_{\mathbf{k}_2}(t_2)\hat{c}^{\dagger}_{\mathbf{k}}(t') =$$
$$i^2\delta_{\mathbf{q_1},0}\delta_{\mathbf{k},\mathbf{k}_1}G^{(0)}(\mathbf{k},t-t_1)G^{(0)}(\mathbf{k},t_1-t')n_F(\xi_{\mathbf{k_2}}) \quad (1.100)$$

$$\hat{c}_{\mathbf{k}}(t)\hat{c}^{\dagger}_{\mathbf{k}_1+\mathbf{q}_1}(t_1)\hat{c}_{\mathbf{k}_1}(t_1)\hat{c}^{\dagger}_{\mathbf{k}_2+\mathbf{q}_2}(t_2)\hat{c}_{\mathbf{k}_2}(t_2)\hat{c}^{\dagger}_{\mathbf{k}}(t') =$$
$$i^2\delta_{\mathbf{k},\mathbf{k}_1}\delta_{\mathbf{k},\mathbf{k}_2-\mathbf{q}_1}G^{(0)}(\mathbf{k},t-t_2)G^{(0)}(\mathbf{k}+\mathbf{q}_1,t_2-t_1)G^{(0)}(\mathbf{k},t_1-t') \quad (1.101)$$

$$\hat{c}_{\mathbf{k}}(t)\hat{c}^{\dagger}_{\mathbf{k}_1+\mathbf{q}_1}(t_1)\hat{c}_{\mathbf{k}_1}(t_1)\hat{c}^{\dagger}_{\mathbf{k}_2+\mathbf{q}_2}(t_2)\hat{c}_{\mathbf{k}_2}(t_2)\hat{c}^{\dagger}_{\mathbf{k}}(t') =$$
$$i^2\delta_{\mathbf{q_1},0}\delta_{\mathbf{k},\mathbf{k}_2}G^{(0)}(\mathbf{k},t-t_2)n_F(\xi_{\mathbf{k_1}})G^{(0)}(\mathbf{k},t_2-t') \quad (1.102)$$

$$\hat{c}_{\mathbf{k}}(t)\hat{c}^{\dagger}_{\mathbf{k}_1+\mathbf{q}_1}(t_1)\hat{c}_{\mathbf{k}_1}(t_1)\hat{c}^{\dagger}_{\mathbf{k}_2+\mathbf{q}_2}(t_2)\hat{c}_{\mathbf{k}_2}(t_2)\hat{c}^{\dagger}_{\mathbf{k}}(t') =$$
$$i\delta_{\mathbf{q_1},0}\delta_{\mathbf{k},\mathbf{k}_2}G^{(0)}(\mathbf{k},t-t')n_F(\xi_{\mathbf{k_1}})n_F(\xi_{\mathbf{k_1}}) \quad (1.103)$$

$$\hat{c}_{\mathbf{k}}(t)\hat{c}^{\dagger}_{\mathbf{k}_1+\mathbf{q}_1}(t_1)\hat{c}_{\mathbf{k}_1}(t_1)\hat{c}^{\dagger}_{\mathbf{k}_2+\mathbf{q}_2}(t_2)\hat{c}_{\mathbf{k}_2}(t_2)\hat{c}^{\dagger}_{\mathbf{k}}(t') =$$
$$- i^3\delta_{\mathbf{k}_1,\mathbf{k}_2-\mathbf{q}_1}G^{(0)}(\mathbf{k},t-t')G^{(0)}(\mathbf{k}_1,t_1-t_2)G^{(0)}(\mathbf{k}_1+\mathbf{q}_1,t_2-t_1) \quad (1.104)$$

where the definition $n_F(\xi_{\mathbf{k}}) = \langle\phi_0| c^{\dagger}_{\mathbf{k}}(t)c_{\mathbf{k}}(t) |\phi_0\rangle$ is used.

1.3.4 Feynman diagrams

Feynman introduced the idea of representing the terms in the propagator expansion by diagrams [9]. The diagrams in time domain are drawn by representing the electron unperturbed Green's function $G^{(0)}(\mathbf{k}, t - t')$ by a solid line with an arrow which goes from t' to t, while the phonon unperturbed propagator $D^{(0)}(\mathbf{q}, t - t')$ is represented by a wiggly line. The latter does not have a directional arrow because

$$D^{(0)}(\mathbf{q}, t - t') = D^{(0)}(-\mathbf{q}, t' - t) \quad (1.105)$$

so the sign of $\mathbf{q}$ is irrelevant: phonons can be viewed as going in either direction in time. The factor $n_F(\xi_k)$ is drawn as a solid line which loops and represents an

expression	symbol	factor
$G^{(0)}(\mathbf{k}, t - t')$	$\xrightarrow{\quad \mathbf{k} \quad}$	$-ie^{-i\epsilon(\mathbf{k})(t-t')}$
$D^{(0)}(\mathbf{q}, t - t')$	$\overset{\mathbf{q}}{\sim\!\sim\!\sim\!\sim\!\sim\!\sim}$	$-ie^{-i\omega(\mathbf{q})(t-t')}$
$n_F(\xi_k)$	$\bigcirc$	-1
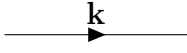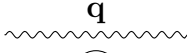
Table 1.1: Rules for translating mathematical expressions from diagrams and vice-versa. In addition, vertices carry a factor of $M_{\mathbf{q}}$.

electron line which starts and ends at the same point in time. By using these rules (also summarized in Table 1.1) the diagrams representing each of the six terms 1.99 to 1.104 are constructed in Figure 1.3. However, not all of them are actually contributing to the perturbed Green function.

The terms (b), (d) and (e) in Figure 1.3 vanish because they exist only if the phonon wave vector can assume the value of zero, but a phonon with $\mathbf{q} = 0$ is either a translation of the crystal as a whole or a permanent strain, and neither of these are included in the Hamiltonian. Sums over $\mathbf{q}$ are implicitly excluding the $\mathbf{q} = 0$ term.

The terms (a) and (c) are not zero, and are the kind of terms to be dealt with in the Diagrammatic Monte Carlo algorithm:

$$
\frac{1}{2!} \int dt_1 \int dt_2 \sum_{\mathbf{q}} |M_{\mathbf{q}}|^2 D^{(0)}(\mathbf{q}, t_1 - t_2)
$$
$$
\times \left[G^{(0)}(\mathbf{k}, t - t_1) G^{(0)}(\mathbf{k} - \mathbf{q}, t_1 - t_2) \times G^{(0)}(\mathbf{k}, t_2 - t') \right.
$$
$$
\left. + G^{(0)}(\mathbf{k}, t - t_2) G^{(0)}(\mathbf{k} + \mathbf{q}, t_2 - t_1) \times G^{(0)}(\mathbf{k}, t_1 - t') \right] \quad (1.106)
$$

These term really differ only in the labeling of the variables $t_1, t_2, \mathbf{q}_i$, which can be relabeled so that only one term needs to be written and the factor $1/2$ gets canceled.

The term (f) as the property that part of it is not topologically connected to the electron propagator $G^{(0)}(\mathbf{k}, t - t')$. This kind of diagram is called *disconnected* diagram. The disconnected parts provide just a constant which multiplies the contribution from the connected parts.
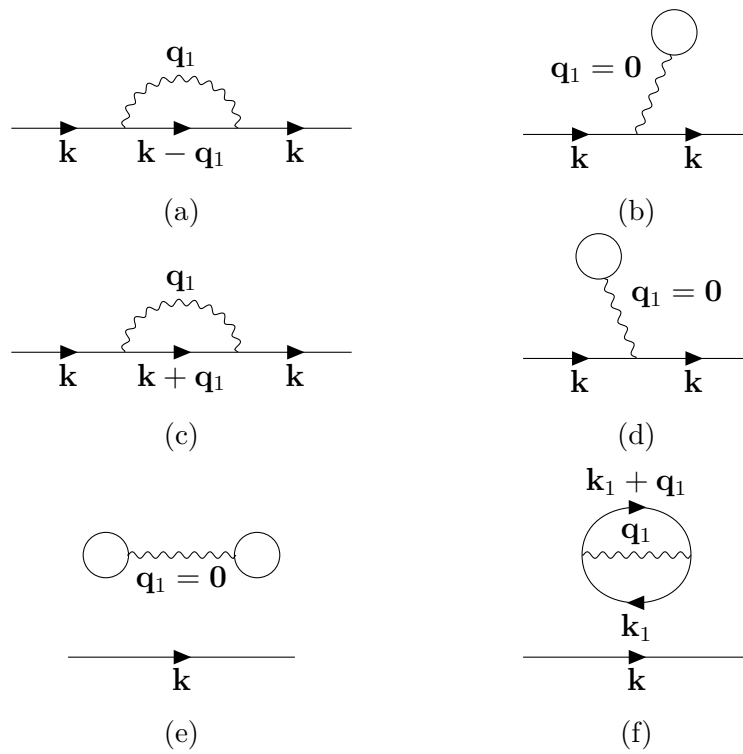
Figure 1.3: Diagrammatic representation of the first terms (1.99 to 1.104) entering the expansion of the single electron Green function.

Vacuum polarization terms

Now the denominator of 1.84 which was ignored up to this point should be considered. $\langle\psi_0|\,S(-\infty,\infty)\,|\psi_0\rangle$ can be expanded exactly in the same way as it was done for the numerator. At the end of the calculations one obtains the following result up to term $n=2$:

$$\langle\psi_0|\,S(-\infty,\infty)\,|\psi_0\rangle = 1 + F_1 + \dots \tag{1.107}$$

where F_1 is exactly the same constant obtained before from the term (f), which corresponds in the diagram representation to the closed bubble of Figure 1.3 (f).

The evaluation of the vacuum polarization terms is unnecessary because of a cancellation theorem known as *linked cluster theorem*, which states that:

The vacuum polarization diagrams exactly cancel the disconnected diagrams in the expansion of $G(\mathbf{k}, t - t')$.

Thanks to this theorem one only needs to take into account connected diagrams when calculating $G(\mathbf{k}, t-t')$. This is not only very convenient, but often necessary since disconnected diagrams can give infinities when evaluated.

1.4 Monte Carlo methods

1.4.1 Monte Carlo integration

Monte Carlo integration [10] is a technique for numerical integration using random numbers. Consider the integral of a function f of a real variable:

$$\int f(x)\,\mathrm{d}x = \int \frac{f(x)}{p(x)} p(x)\,\mathrm{d}x = \left\langle \frac{f(x)}{p(x)} \right\rangle_p \tag{1.108}$$

The law of large numbers states that the mean of a large number of samples drawn from a distribution tends to its expected value:

$$\frac{1}{N} \sum_i^N \frac{f(x_i)}{p(x_i)} \xrightarrow[N\to\infty]{} \left\langle \frac{f(x)}{p(x)} \right\rangle_p \tag{1.109}$$

this gives a way to approximate an integral by drawing samples from an arbitrary distribution.

1.4.2 Metropolis-Hastings algorithm

Metropolis-Hastings is a Markov Chain Monte Carlo (MCMC) method based on two postulates:

1. Existence of stationary distribution: ensured by detailed balance

2. Uniqueness of stationary distribution: ensured by ergodicity

Detailed balance: the probability (π) of being in state x and transitioning (P) to state x' is equal to the probability of being in state x' and transitioning to state x. In symbols, this proposition reads:

$$P(x'|x)\pi(x) = P(x|x')\pi(x') \tag{1.110}$$

The aim is to design a Markov process[3] which fulfills detailed balance such that after a given amount of transitions (also called updates) we reach the target equilibrium distribution $\pi(x)$. The detailed balance condition can be rewritten as:

$$\frac{\pi(x')}{\pi(x)} = \frac{P(x'|x)}{P(x|x')} \tag{1.111}$$

Now separate the transition into two independent sub-steps:

1. *Proposal*: a new state is proposed according to the probability distribution $p(x'|x)$

2. *Accept-reject*: the proposal is only accepted with a probability $A(x', x)$

The transition probability can thus be written as their product:

$$\begin{aligned} P(x'|x) &= p(x'|x)A(x', x) \\ P(x|x') &= p(x|x')A(x, x') \end{aligned} \tag{1.112}$$

---

[3]A Markov process is a stochastic process for which predictions regarding future outcomes can be made based solely on its present state.

Inserting this relation into 1.111 we find:

$$\frac{A(x', x)}{A(x, x')} = \frac{\pi(x')p(x|x')}{\pi(x)p(x'|x)} \tag{1.113}$$

So far we simply reshaped the detailed balance condition into another form. Designing the Markov process now amounts to choose an appropriate A such that 1.113 is satisfied. Let us consider the *Metropolis choice*:

$$\boxed{A(x', x) = \min\left(1, \frac{\pi(x')p(x|x')}{\pi(x)p(x'|x)}\right)} \tag{1.114}$$

It's easy to see that this choice satisfies 1.113: exchanging x and x' the ratio on the right side of 1.114 becomes the reciprocal so that either $A(x', x)$ or $A(x, x')$ is 1.

Prescription 1.114 has the remarkable feature that the complete knowledge of the form of $\pi(x)$ is not actually needed, but only its form *up to a multiplicative constant* (independent of x). This is important because it allows to draw samples from a distribution whose normalization factor is unknown: the factor cancels in the ratio on the right side of 1.114 so that the non-normalized form of $\pi(x)$ can be used instead.

Another observation is that we didn't impose any requirement on the proposal distribution $p(x'|x)$. In practice it will be some distribution from which we can draw samples easily by direct sampling. The simplest possible form is to use a uniform distribution independent of the current state x, but this means that proposal values systematically try to escape the high density region, and the accepted ratio will be low. So a better idea is to use a distribution that *approximates* our target distribution: if we could directly sample from it, we would have $\pi(x) = p(x)$, which substituted into 1.114 means that every proposed update is always accepted, and the whole procedure becomes pointless, since we already have the target distribution.

The downside of the Metropolis-Hastings algorithm versus direct sampling is that it introduces correlation in the sequence it generates. This means that the error estimation for observables extracted from the distribution of states has to be adapted. The naive way of computing the standard deviation of samples underestimates the error. So we must resort to a slightly more involved procedure known as *blocking analysis*.

1.4.3 Blocking analysis

In this context blocking means arranging of sampling units in groups (blocks) that are similar to one another.

The variance satisfies the following properties:

$$\text{Var}(aX) = a^2 \, \text{Var}(X) \tag{1.115}$$

$$\text{Var}(X + Y) = \text{Var}(X) + \text{Var}(Y) \quad \text{if X,Y independent} \tag{1.116}$$

Split the M measurements into N blocks of length L so that $M = NL$:

$$\text{Var}(\bar{X}) = \text{Var}\left(\frac{1}{NL}\sum_{n=0}^{N-1}\sum_{m=nL}^{(n+1)L-1} X_m\right) = \text{Var}\left[\frac{1}{N}\sum_{n=0}^{N-1}\left(\frac{1}{L}\sum_{m=nL}^{(n+1)L-1} X_m\right)\right] \tag{1.117}$$

The expression in the inner brackets is the *block average* of X inside block n:

$$\bar{X}_n \equiv \frac{1}{L}\sum_{m=nL}^{(n+1)L-1} X_m \tag{1.118}$$

Applying properties 1.115 and 1.116 to 1.117:

$$\text{Var}\left(\frac{1}{N}\sum_{n=0}^{N-1}\bar{X}_n\right) = \frac{1}{N^2}\text{Var}\left(\sum_{n=0}^{N-1}\bar{X}_n\right) = \frac{1}{N^2}\sum_{n=0}^{N-1}\text{Var}(\bar{X}_n) \tag{1.119}$$

Now assume common variance for block averages [11]:

$$\forall n \; \text{Var}(X_n) =: \text{Var}(\bar{X}_{block}) \tag{1.120}$$

This is true for sufficiently big block size L. To ensure such requirement, one can study the behavior of correlation for increasing block sizes (see [11] for more information on this).

With this assumption, the sum $\sum_n \text{Var}(\bar{X}_n)$ reduces to $N \, \text{Var}(\bar{X}_{block})$:

$$\boxed{\text{Var}(\bar{X}) = \frac{1}{N}\text{Var}(\bar{X}_{block})} \tag{1.121}$$

This relation allows to calculate the variance of the correlated outcomes of X from the variance of the uncorrelated (or better, less correlated) block averages,

for which the usual formula applies:

$$\mathrm{Var}(\bar{X}_{block}) = \sigma^2(\bar{X}_{block}) = \frac{1}{N-1} \sum_{n=0}^{N-1} (\bar{X}_n - \bar{X})^2 \qquad (1.122)$$

The adaptation of the MCMC Metropolis-Hastings algorithm to deal with a stochastic process in which states are represented by Feynman diagrams will be discussed in Chapter 3.

Chapter 2

Holstein model

2.1 Holstein Hamiltonian

The discussion of the Holstein Hamiltonian starts from the original model presented by Holstein in [12][13] and then develops into the second quantized form used in the Diagrammatic Monte Carlo algorithm. Analytical approaches to the weak-coupling and strong-coupling regimes are also described.

2.1.1 The molecular-crystal model
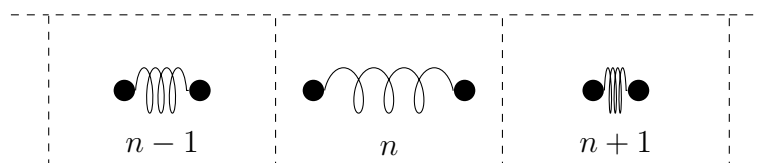
Figure 2.1: Holstein's molecular-crystal model.

The system is taken to be a linear chain of N identical diatomic molecules. [12] The only degree of freedom they possess is their internuclear separation x_n. The potential energy curve for the bond of each individual molecule is assumed to be parabolic, and there is no coupling between different molecules. Thus the lattice Hamiltonian reads:

$$H_L = \sum_n^N \left(\frac{P_n^2}{2M} + \frac{1}{2} M \omega_0^2 x_n^2 \right) \tag{2.1}$$

Where M is the reduced mass of the molecule and ω_0 the vibrational frequency. The system can be thought as an ensemble of N uncoupled harmonic oscillators with the same frequency. Figure 2.1 shows site n and their nearest neighbors $n-1$ and $n+1$. As an example, the system is depicted in a state where the molecule on site $n-1$ is in equilibrium $(x_{n-1} = 0)$, the molecule on site n is stretched $(x_n > 0)$ and the molecule on site $n+1$ is compressed $(x_{n+1} < 0)$.

In addition, a single electron moves in this environment. The electron interacts with each molecule through the potential $U(r-na, x_n)$. The electronic Hamiltonian reads:

$$H_e = \frac{p^2}{2m} + \sum_n^N U(r - na, x_n) \tag{2.2}$$

The key feature of the model is that U depends on the internuclear separation x_n, coupling the electronic degree of freedom with the lattice vibrations. This kind of electron-phonon interaction is called *Holstein coupling.*

The Hamiltonian of the whole system is the sum of the lattice and electron Hamiltonians:

$$H = H_e + H_L \tag{2.3}$$

As stressed above, the electronic term also contains a coupling to the lattice. In what follows, the coupling will be extracted from the electronic term, resulting in a purely electronic term and an interaction term in the Hamiltonian. Now we switch to a quantum mechanical description of the system, where all observables are replaced by operators acting on a Hilbert space.

The full Hamiltonian of the system (Equation 2.3 quantized) is:

$$\hat{H} = -\frac{\hbar^2}{2m}\nabla^2 + \sum_n U(r - na, x_n) + \sum_n \left(-\frac{\hbar^2}{2M}\frac{\partial^2}{\partial x_n^2} + \frac{1}{2}M\omega_0^2 x_n^2 \right)$$

A tight-binding approach is used to express the electronic wavefunction as a linear combination of localized[1] orbitals ϕ:

---

[1] In this context, localized doesn't mean exactly localized at position **r** but rather a state in which the electron is most of the time around a certain position (the lattice site). The probability to find the electron far from the site vanishes exponentially.

$$\psi(r, x_1, ..., x_N) = \sum_n a_n(x_1, ..., x_N)\phi(r - na, x_n)$$

The electron states ϕ used in the expansion are the energy eigenstates of a system comprised of the electron and a single molecule at n:

$$\left[-\frac{\hbar^2}{2m}\nabla^2 + U(r - na, x_n)\right]\phi(r - na, x_n) = E(x_n)\phi(r - na, x_n)$$

The equations obeyed by the expansion coefficients are obtained by a standard "projection" procedure. The calculation can be found in the Appendix of Holstein's paper [12]. The result is:

$$\hat{H}a_n(x_1, ..., x_n) = -\sum_{\pm} J(x_n, x_{x\pm1})a_{n\pm1}(x_1, ..., x_n)$$
$$+ \sum_n \left(-\frac{\hbar^2}{2M}\frac{\partial^2}{\partial x_n^2} + \frac{1}{2}M\omega_0^2 x_n^2\right)a_n(x_1, ..., x_n) \qquad (2.4)$$
$$- E(x_n)a_n(x_1, ..., x_n)$$

where:

$$J(x_n, x_m) \equiv \int \mathrm{d}r\, \phi^*(r - na, x_n)\Delta U(r - na)\phi^*(r - ma, x_m) \qquad (2.5)$$

is the two center transfer integral mentioned in the tight-binding section (Eq. 1.34).

A number of simplifications are introduced into 2.4:

1. The neglect of the x-dependence of the $J(x_n, x_{n\pm1})$; this simplification means that the $J(x_n, x_{n\pm1})$ are all to be taken equal to a single constant $-J$

2. The x-dependence of $E(x_n)$ is taken to be linear:

$$E(x_n) = -Ax_n \qquad (2.6)$$

Introducing the approximations into 2.4 we get:

$$\hat{H}a_n = -J(a_{n+1} + a_{n-1}) + \sum_n \left(-\frac{\hbar^2}{2M}\frac{\partial^2}{\partial x_n^2} + \frac{1}{2}M\omega_0^2 x_n^2 \right)a_n - Ax_n a_n \qquad (2.7)$$

which is an equation for the coefficients a_n.

However, we will not try to solve 2.7 in this form. In order for the Diagrammatic Monte Carlo algorithm to be applied, the Hamiltonian must be translated into the second quantization framework.

2.1.2 Second quantized form

The Hamiltonian 2.3 can be represented as a sum of three terms:

$$H^{hol} = H_{el}^{hol} + H_{ph}^{hol} + H_{el-ph}^{hol} \qquad (2.8)$$

To obtain the second quantized form, all the terms must be rewritten using creation/annihilation operators. In Section 1.1.2 the tight binding term 1.33 was derived, and the phonon term is just the standard treatment of a set of independent harmonic oscillators at each site discussed in 1.1.1, all vibrating at the same frequency ω_0. The interaction term, which was presented in general in Eq. 1.42, has a constant coefficient g independent of phonon momentum. For $\hbar = 1$ and lattice constant $a = 1$: [14]

$$H_{el}^{hol} = -J \sum_n \hat{c}_n^\dagger (\hat{c}_{n+1} + \hat{c}_{n-1}) \qquad (2.9)$$

$$H_{ph}^{hol} = \omega_0 \sum_n \hat{b}_n^\dagger \hat{b}_n \qquad (2.10)$$

$$H_{el-ph}^{hol} = g \sum_n \hat{c}_n^\dagger \hat{c}_n (\hat{b}_n^\dagger + \hat{b}_n) \qquad (2.11)$$

Sometimes the kinetic integral J is denoted by t, and the creation/annihilation operators written in the equivalent form 1.33 [15]:

$$H_{el}^{hol} = -t \sum_{\langle n,m \rangle} (\hat{c}_n^\dagger \hat{c}_m + \hat{c}_n \hat{c}_m^\dagger) \qquad (2.12)$$

where $\langle n, m \rangle$ means summing over nearest neighbor pairs. The hopping parameter t will be taken as unity of energy ($t = 1$).

The same Hamiltonian can be expressed in momentum space by Fourier transforming its terms (as was done in Sections 1.1.2 and 1.2.1):

$$H_{el}^{hol} = \sum_{\mathbf{k}} \epsilon(k) \hat{c}_{\mathbf{k}}^{\dagger} \hat{c}_{\mathbf{k}} \tag{2.13}$$

$$H_{ph}^{hol} = \omega_0 \sum_{\mathbf{q}} \hat{b}_{\mathbf{q}}^{\dagger} \hat{b}_{\mathbf{q}} \tag{2.14}$$

$$H_{el-ph}^{hol} = \frac{g}{\sqrt{N}} \sum_{\mathbf{k},\mathbf{q}} \hat{c}_{\mathbf{k}+\mathbf{q}}^{\dagger} \hat{c}_{\mathbf{k}} (\hat{b}_{-\mathbf{q}}^{\dagger} + \hat{b}_{\mathbf{q}}) \tag{2.15}$$

This Hamiltonian describes the *lattice* or *Holstein* polaron, in which the electron is spread over a small region of space, accompanied by a strong local distortion of the lattice.

Assuming a simple z-dimensional hypercubic lattice with unitary lattice constant, the electron dispersion is:

$$\epsilon(k) = -2t \sum_{i=1}^{z} \cos(k_i)$$

Phonons are instead assumed dispersionless:

$$\omega(q) = \omega_0$$

The behavior of the Hamiltonian depends on two parameters. It is customary to define the following combinations, respectively called *dimensionless coupling* α (which measures the strength of the electron-phonon coupling) and *adiabaticity ratio* γ:

$$\alpha = \frac{g^2}{z\omega_0 t} \qquad \gamma = \frac{\omega_0}{t} \tag{2.16}$$

Summarizing, the Holstein model is a simple model for the lattice polaron which:

- only considers optical phonons

- features a momentum-independent coupling

2.2 Weak-coupling limit

At small coupling, the limiting behavior is obviously that of the unperturbed system. The unperturbed states consist of the bare electron plus a number of phonons.

Let's redefine $\mathbf{k}$ here to refer to the total momentum of the polaron, and call $\mathbf{k}_e$ the momentum of the bare electron instead. Looking at the total energy, the bare electron brings a contribution $\epsilon(\mathbf{k}_e)$ dependent on its momentum, while phonons are present with a fixed energy cost of ω_0 each.

Let's now consider a system with just a single phonon. The ensemble of states with one phonon of momentum $q_i \in [-\pi, \pi]$ forms a continuum in the energy spectrum. Figure 2.2 depicts these energy states, where each different $\mathbf{q}$ introduces a horizontal shift of the original electron dispersion (due to conservation of total momentum). For a finite-sized crystal, $\mathbf{q}$ assumes discrete values, but in the continuum limit the orange curves densely fill the graph and the black points marking the intersection with a given total momentum become a line.
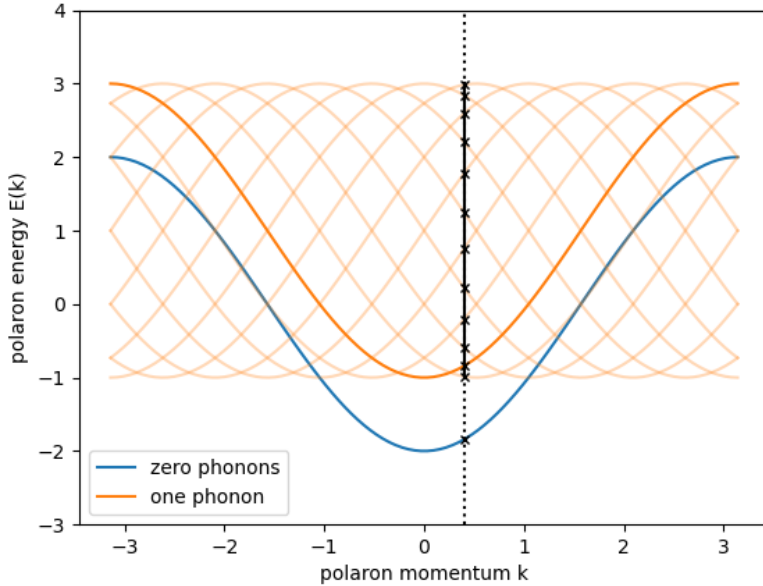
Figure 2.2: Energy of the lowest unperturbed states of Holstein Hamiltonian. The blue curve is a state with zero phonons, and coincides with the bare electron dispersion. The orange curves are an ensemble of states with one phonon of momentum $\mathbf{q}$, vertically shifted from the blue curve by the phonon energy ω_0. The vertical black line indicates a given value of the total polaron momentum.

2.2.1 Weak-coupling perturbation theory

When turning on the coupling, the electron becomes lightly dressed by phonons spread over a large region of space, and the effective mass increases slightly. This regime is the large-radius Holstein polaron for which a quasi-classical approximation (the continuum polaron) is also valid. Rayleigh-Schrödinger (RS) perturbation theory provides accurate results, but only at small momentum where there is no degeneracy with the upper states of the continuum.

Call $\{|n^0\rangle\}$ the set of unperturbed eigenstates, assumed non-degenerate. The index n here represents the momentum index of the polaron. The perturbed eigenstate is given by the expansion:

$$|n\rangle = |n^0\rangle + |n^1\rangle + |n^2\rangle + \cdots \tag{2.17}$$

and the energy is:

$$E_n = E_n^0 + E_n^1 + E_n^2 + \cdots \tag{2.18}$$

where the exponent is the order of the correction. Standard time-independent perturbation theory provides expressions to calculate the correction terms.

Let's evaluate corrections to the ground state energy. It's easy to see that the first order energy term vanishes:

$$\langle n^0 | H_{el-ph} |n^0\rangle = 0 \tag{2.19}$$

because the interaction creates a state with one more phonon, which is orthogonal to the original one.

The first non-vanishing correction to the energy is:

$$E_n^2 = \sum_{m \neq n} \frac{|\langle m^0 | H_{el-ph} |n^0\rangle|^2}{E_n^0 - E_m^0} \tag{2.20}$$

while the first non-vanishing correction to the state is:

$$|n^1\rangle = \sum_{m \neq n} |m^0\rangle \frac{\langle m^0 | H_{el-ph} |n^0\rangle}{E_n^0 - E_m^0} \tag{2.21}$$

We are interested in the ground state, therefore $|n^0\rangle$ contains zero phonons. H_{el-ph} then acts by adding one phonon and finally the projection on $\langle m^0|$ makes

all states with a number of phonon different from one vanish.

Thus the summation only runs on states containing a single phonon, and the denominator of 2.20 becomes the difference between the bare electron dispersion (state n) and the energy of one of the orange states of Figure 2.2 (state m):

$$E_n^0 \to \epsilon(k) \qquad E_m^0 \to \epsilon(k - q) + \omega_0 \tag{2.22}$$

Let's recall the form of H_{el-ph} (Eq. 2.15). As for its matrix element, the electron part gives 1 and in the phonon part the b term vanishes when applied to a zero phonon state. So we are left with a delta from the $b^\dagger$ operator, and a factor of $1/2\pi$ arises as a consequence of the continuum limit taken for both the perturbation theory sum and the sum inside H_{el-ph}.

Substituting the matrix elements and the expression for the unperturbed energy in 2.20, one gets the following expression:

$$E_k = -2t \cos(k) - \int \frac{\mathrm{d}q}{2\pi} \frac{t\omega_0\alpha}{2t \cos(k) + \omega_0 - 2t \cos(k - q)} \tag{2.23}$$

If the phonon energy ω_0 is below $4t$ there will be a momentum value at which the denominator becomes zero, and perturbative corrections will diverge. This corresponds to the point where the one-phonon continuum starts to intersect the bare electron (blue) curve in Figure 2.2.

Also the effective mass m^* can be obtained analytically [15] with RS perturbation theory:

$$\frac{m^*}{m_0} = \left(1 - \frac{\alpha}{4}\sqrt{\frac{t}{\omega_0}}\frac{1 + \omega_0/2t}{(1 + \omega_0/4t)^{3/2}}\right)^{-1} \tag{2.24}$$

where m_0 is the mass of the bare electron. In the limit of $\alpha \to 0$, Assuming all other parameters constant, the effective mass enhancement is proportional to g^2:

$$m^* = m_0(1 - k\alpha)^{-1} \approx m_0(1 + k\alpha) \implies \Delta m \propto g^2 \tag{2.25}$$

2.3 Strong-coupling limit

If the electron-phonon interaction is strong, the hopping term H_{el}^{hol} can be treated as a perturbation. The two terms 2.14 and 2.15 can be diagonalized using the

Lang-Firsov canonical transformation.

A slightly simpler case with a single energy level will be discussed first to introduce the Lang-Firsov transformation, and the results will be generalized to the Holstein case.

2.3.1 Lang-Firsov transformation

Consider a system where a particle possessing a single energy level ϵ interacts with a set of phonons of energy $\omega_{\mathbf{q}}$: [3]

$$H = \epsilon\, c^\dagger c + \sum_{\mathbf{q}} M_{\mathbf{q}}(b_{\mathbf{q}}^\dagger + b_{\mathbf{q}})\, c^\dagger c + \sum_{\mathbf{q}} \omega_{\mathbf{q}} b_{\mathbf{q}}^\dagger b_{\mathbf{q}} \qquad (2.26)$$

where the interaction term has the form 1.42. By making a canonical transformation (the Lang-Firsov transformation [16]), the Hamiltonian may be transformed into the following form:

$$H' = (\epsilon - \Delta)\, c'^\dagger c' + \sum_{\mathbf{q}} \omega_{\mathbf{q}} b_{\mathbf{q}}'^\dagger b_{\mathbf{q}}' \qquad (2.27)$$

where the effect of the interaction has been reduced to just a shift of energy by a term Δ, which has to be found.

The right transformation is:

$$O' = e^S O e^{-S} \qquad (2.28)$$

$$S = \sum_{\mathbf{q}} \frac{M_{\mathbf{q}}}{\omega_{\mathbf{q}}} (b_{\mathbf{q}}^\dagger - b_{\mathbf{q}})\, c^\dagger c \qquad (2.29)$$

The operator S and the transformed operators O' enjoy the following properties:

$$S^\dagger = -S \qquad (2.30)$$

$$\left(\prod_n O_n \right)' = \prod_n O_n' \qquad (2.31)$$

Property 2.30 is trivial while property 2.31 is easily shown by inserting the

identity operator $1 = e^S e^{-S}$ between each pair of factors:

$$(AB)' = e^S AB e^{-S} = e^S A e^S e^{-S} B e^{-S} = A'B' \qquad (2.32)$$

The transformed operators can be evaluated from their commutators with S thanks to the expansion of the exponential:

$$
\begin{aligned}
e^S O e^{-S} &= \left(1 + S + \frac{S^2}{2!} + \mathcal{O}(S^3)\right) O \left(1 - S + \frac{S^2}{2!} + \mathcal{O}(S^3)\right) = \\
&\left(O + SO + \frac{S^2 O}{2!} + \mathcal{O}(S^3)\right)\left(1 - S + \frac{S^2}{2!} + \mathcal{O}(S^3)\right) = \\
&O + SO - OS + \frac{S^2 O}{2!} - SOS + \frac{OS^2}{2!} + \mathcal{O}(S^3) = \\
&O + [S, O] + \frac{S[S, O]}{2!} - \frac{[S, O]S}{2!} + \mathcal{O}(S^3) = \\
&O + [S, O] + \frac{[S[S, O]]}{2!} + \mathcal{O}(S^3) \quad (2.33)
\end{aligned}
$$

Now the transformed creation/annihilation operators can be computed:

$$[S, c] = \sum_{\mathbf{q}} \frac{M_{\mathbf{q}}}{\omega_{\mathbf{q}}} (b_{\mathbf{q}}^\dagger - b_{\mathbf{q}}) [c^\dagger c, c] = -\sum_{\mathbf{q}} \frac{M_{\mathbf{q}}}{\omega_{\mathbf{q}}} (b_{\mathbf{q}}^\dagger - b_{\mathbf{q}})\, c \qquad (2.34)$$

$$[S, [S, c]] = -\left(\sum_{\mathbf{q}} \frac{M_{\mathbf{q}}}{\omega_{\mathbf{q}}} (b_{\mathbf{q}}^\dagger - b_{\mathbf{q}})\right)^2 [c^\dagger c, c] = \left(\sum_{\mathbf{q}} \frac{M_{\mathbf{q}}}{\omega_{\mathbf{q}}} (b_{\mathbf{q}}^\dagger - b_{\mathbf{q}})\right)^2 c \qquad (2.35)$$

and similar formulas for higher order commutators. For phonons:

$$[S, b_{\mathbf{q}}] = \sum_{\mathbf{q}'} \frac{M_{\mathbf{q}'}}{\omega_{\mathbf{q}'}} c^\dagger c [b_{\mathbf{q}'}^\dagger - b_{\mathbf{q}'}, b_{\mathbf{q}}] = -\sum_{\mathbf{q}'} \frac{M_{\mathbf{q}'}}{\omega_{\mathbf{q}'}} \delta_{\mathbf{q}', \mathbf{q}}\, c^\dagger c = -\frac{M_{\mathbf{q}}}{\omega_{\mathbf{q}}}\, c^\dagger c \qquad (2.36)$$

$$[S, [S, b_{\mathbf{q}}]] = 0 \qquad (2.37)$$

so that only the first order is actually relevant in this case.

$$c' = X\,c \qquad X = \exp\left\{-\sum_{\mathbf{q}} \frac{M_{\mathbf{q}}}{\omega_{\mathbf{q}}}(b_{\mathbf{q}}^{\dagger} - b_{\mathbf{q}})\right\} \tag{2.38}$$

$$b_{\mathbf{q}}' = b_{\mathbf{q}} - \frac{M_{\mathbf{q}}}{\omega_{\mathbf{q}}}\,c^{\dagger}c \tag{2.39}$$

and the corresponding creation operators follow by taking the adjoint. Substituting the above back into 2.26 we get 2.27 with:

$$\Delta = \sum_{\mathbf{q}} \frac{M_{\mathbf{q}}^{2}}{\omega_{\mathbf{q}}} \tag{2.40}$$

Turning now to the Holstein Hamiltonian (without the hopping term, to be treated perturbatively), the same argument can be repeated but adding an index i for the site to the $c, c^{\dagger}$ operators and assuming $M_{\mathbf{q}} = -g/\sqrt{N}$ and $\omega_{\mathbf{q}} = \omega_0$. The result (in position space) is [17]:

$$S = -\frac{g}{\omega_0}\sum_i c_i^{\dagger}c_i(b_i^{\dagger} + b_i) \tag{2.41}$$

$$c_i' = X_i\,c_i \qquad X_i = \exp\left(\frac{g}{\omega_0}(b_i^{\dagger} - b_i)\right) \tag{2.42}$$

$$H' = \omega_0 \sum_i b_i'^{\dagger} b_i' - \frac{g^2}{\omega_0}\sum_i c_i'^{\dagger} c_i' \tag{2.43}$$

From 2.40, the lattice deformation energy gained due to the electron presence is:

$$E_p = \frac{g^2}{\omega_0} \tag{2.44}$$

so that the α coupling constant defined earlier in 2.16 can be thought as the ratio between this energy and the bare electron kinetic energy proportional to the hopping t. E_p is typically referred to as *polaron energy* or *polaron binding energy.*

2.3.2 Strong-coupling perturbation theory

The transformed Hamiltonian 2.43 is now diagonal, and there are N degenerate unperturbed single-electron ground states $|GS, i\rangle_0' = c_i'^{\dagger}|0\rangle$ that can be projected into the original basis by considering the inverse transform. This leads to the

following condition for the ground state in the original basis:

$$c_i'^\dagger \left| 0 \right\rangle = e^S \left| GS, i \right\rangle_0 \tag{2.45}$$

the solution of which can be obtained by using fermion algebra and the Baker-Campbell-Hausdorff formula for the exponential operator:

$$
\begin{aligned}
\left| GS, i \right\rangle_0 = e^{-S} c_i'^\dagger \left| 0 \right\rangle &= \exp\left(\frac{g}{\omega_0}(b_i^\dagger - b_i) \right) c_i'^\dagger \left| 0 \right\rangle = \\
&\exp\left(\frac{g}{\omega_0} b_i^\dagger \right) \exp\left(-\frac{g}{\omega_0} b_i \right) \exp\left(-\frac{g^2}{2\omega_0^2} \right) c_i'^\dagger \left| 0 \right\rangle = \\
&\exp\left(-\frac{g^2}{2\omega_0^2} \right) \exp\left(\frac{g}{\omega_0} b_i^\dagger \right) c_i'^\dagger \left| 0 \right\rangle \quad (2.46)
\end{aligned}
$$

The phononic part of the state turns out to be the so-called *coherent state* of the harmonic oscillator. Some properties of these states are briefly recalled before proceeding.

Coherent states of the harmonic oscillator

The eigenstates of the annihilation operator are known as coherent states of the harmonic oscillator:

$$b \left| \xi \right\rangle = \xi \left| \xi \right\rangle \tag{2.47}$$

where the eigenvalue ξ is an arbitrary complex number. Coherent states can be shown to possess the property of minimizing the uncertainty product: [18]

$$\sigma_x \sigma_p = \frac{\hbar}{2} \tag{2.48}$$

Like any other quantum state, coherent states can be expressed in terms of energy eigenstates:

$$\left| \xi \right\rangle = \sum_{n=0}^{\infty} \left| n \right\rangle \left\langle n | \xi \right\rangle \tag{2.49}$$

The expansion coefficients $c_n \equiv \left\langle n | \xi \right\rangle$ can be easily computed thanks to prop-

erty 2.47. Recall the expression for the energy eigenstates $|n\rangle$:

$$|n\rangle = \frac{\left(b^\dagger\right)^n}{\sqrt{n!}} |0\rangle \qquad \langle n| = \langle 0| \frac{b^n}{\sqrt{n!}} \tag{2.50}$$

substituting the bra state into 2.49 gives:

$$c_n = \langle n|\xi\rangle = \langle 0| \frac{b^n}{\sqrt{n!}} |\xi\rangle = \frac{\xi^n}{\sqrt{n!}} \langle 0|\xi\rangle = \frac{\xi^n}{\sqrt{n!}} c_0 \tag{2.51}$$

So that 2.49 becomes:

$$|\xi\rangle = c_0 \sum_{n=0}^{\infty} \frac{\xi^n}{\sqrt{n!}} |n\rangle \tag{2.52}$$

Note that c_0 can be considered to be real with no loss of generality, since a global phase has no physical effect on the state. With this in mind, c_0 can be found from the normalization condition $|\langle\xi|\xi\rangle|^2 = 1$, which translates into a condition for the coefficients:

$$c_0^2 \sum_{n=0}^{\infty} \left| \frac{\xi^n}{\sqrt{n!}} \right|^2 = 1 \implies \frac{1}{c_0^2} = \sum_{n=0}^{\infty} \frac{\left(|\xi|^2\right)^n}{n!} \implies c_0 = e^{-|\xi|^2/2} \tag{2.53}$$

so that:

$$|\xi\rangle = e^{-|\xi|^2/2} \sum_{n=0}^{\infty} \frac{\xi^n}{\sqrt{n!}} |n\rangle \tag{2.54}$$

and using 2.50 again, this time the ket expression:

$$|\xi\rangle = e^{-|\xi|^2/2} \sum_{n=0}^{\infty} \frac{\left(\xi b^\dagger\right)^n}{n!} |0\rangle = e^{-|\xi|^2/2} e^{\xi b^\dagger} |0\rangle \tag{2.55}$$

so that 2.46 indeed contains coherent states ($\xi = g/\omega_0$).

Going back to our original calculation, the property of coherent states to minimize the uncertainty product between the momentum and position operators implies that the ground state has $\xi = g/\omega_0$ unperturbed ground states in the real space and can be interpreted as an electron dressed by a phonon cloud with zero average momentum [17]. The phonon statistic is found to be a Poisson distribution (at zero order in the perturbation) [17]:

$$P_0(n) = |\langle n| c_i |GS, i\rangle_0|^2 = e^{-N_{p0}} \frac{(N_{ph,0})^n}{n!} \tag{2.56}$$

$$N_{ph,0} = {}_0\langle GS, i| b_i^\dagger b_i |GS, i\rangle_0 = \frac{g^2}{\omega_0^2} = \frac{\alpha z t}{\omega_0} \tag{2.57}$$

where $|n\rangle$ is a state with a well-defined number of phonons (n) and N_{ph} is the average number of phonons in the state.

As for the energy, as we have seen at zeroth order the electron is trapped by the lattice deformation at a given site, with energy given by 2.44. The expression can be recast into $-\alpha z t$ using 2.16. The first order correction lifts the degeneracy with an exponentially reduced nearest-neighbor hopping. The second order has a much stronger effect, corresponding to a virtual transition of the electron without carrying its lattice deformation to a nearest neighbor location [15]. Explicit calculations of the first and second order correction can be found in [19]. The total polaron dispersion is given by the sum of the three terms:

$$-\alpha z t - \frac{t}{\alpha} - 2t_{eff} \sum_{i=1}^{z} \cos(k_i) \qquad t_{eff} = t \exp\left(-\frac{\alpha z t}{\omega_0}\right) \tag{2.58}$$

The exponentially suppressed t_{eff} induces an exponentially large effective mass enhancement:

$$\frac{m^*}{m_0} = \exp\left(\frac{\alpha z t}{\omega_0}\right) \tag{2.59}$$

The quantities here derived in the weak-coupling and strong-coupling limits will be calculated using Diagrammatic Monte Carlo, which is described in the next section.

Chapter 3

Diagrammatic Monte Carlo

3.1 DMC applied to the polaron system

The method of Diagrammatic (Quantum) Monte Carlo was developed by Prokof'ev and Svistunov [20]. It allows direct simulation of entities specified in terms of diagrammatic expansions of the type encountered in Section 1.3. This method is very general since it imposes no restrictions on the particular form of particle-particle interaction and dimensionality of the problem.

The technique was shown to work well when applied to the polaron problem, both by the original paper and by follow-up studies [21][15][22]. This work is not based on or extending previously written codes, thus providing a completely independent verification of the methods employed.

The purpose of the algorithm is to calculate a function Q which is given in terms of a series of integrals with an ever increasing number of integration variables:

$$Q(\{y\}) = \sum_{n=0}^{\infty} \sum_{\xi_n} \int dx_1 \ldots dx_n \, \mathcal{D}_n(\xi_n, \{y\}, x_1, \ldots, x_n) \qquad (3.1)$$

here ξ_n indexes different terms of the same order n: the diagrams they represent are said to possess different *topologies*[1]. $\{y\}$ collects all the *external variables* on which Q depends, while $x_1, \ldots, x_n$ are the integration or *internal* variables. Both external and internal variables are allowed to be either continuous or discrete: in the latter case integrals are replaced by sums.

---

[1] In this context topologies mean terms with the same number of integration variables but with a different time ordering of the vertices, as discussed in Section 1.3.4.

Diagrammatic Monte Carlo (DMC) is based essentially on the Metropolis-Hastings algorithm presented in 1.4.2. It samples diagrams represented by points in the parameter space $\{y\}, n, \xi_n, \{x\}_n$ and collects statistics for $Q(\{y\})$ so that for a number of samples large enough the procedure converges to the exact answer. This process has a lot in common with standard Monte Carlo simulation of a distribution given by a multidimensional integral, except that in the expansion 3.1 the number of integration variables is increasing with the order n.

The Markov chain to be produced is a sequence of Feynman diagrams. One starts from an arbitrary diagram, such as a $n = 0$ term with some set values for the external variables. At every iteration of the algorithm, the *current* diagram has a chance to be modified into a *proposed* diagram via a transition called *update*. The update is chosen among a series of possible types by drawing a random integer, and every update further depends on some real parameters to be extracted from a distribution. Being a Markov chain, the probabilities can only depend on the current state[2], but not on the previous states (the chain is *memoryless*).

The proposed diagram is either *accepted* or *rejected* according to the *acceptance* probability associated with the update. Note that even when the update is rejected, the "new" diagram (which will be the current diagram again) must still be considered in the statistics.

The set of elementary updates chosen and their implementation is arbitrary and specific to the problem to which DMC is applied. The only necessary requirements are the Metropolis-Hastings postulates of ergodicity and detailed balance discussed in 1.4.2. The approach followed in this thesis is to first illustrate a *minimal* set of updates that allows the DMC procedure to be carried out, satisfying ergodicity for the Holstein Hamiltonian. Then, more updates will be added to be able to measure more observables and to improve the efficiency.

The main class of routines that a program implementing the DMC has to be able to perform are:

- Tracking and managing the state of the system, that is, performing the updates by changing the data structure where the current diagram is stored

- Calculating the acceptance probabilities from the current and proposed diagrams

---

[2]or even be independent of the state altogether

- Extracting the relevant statistics from the distribution, which is done once at every iteration to avoid the need of storing the full history

Consider the one-electron Green function for the many body polaron Hamiltonian:[3]

$$G(\mathbf{k}, \tau) = \langle \Psi_0 | c_{\mathbf{k}}(\tau) c_{\mathbf{k}}^{\dagger}(0) | \Psi_0 \rangle \tag{3.2}$$

this quantity can be expanded in an infinite-order perturbation series by the procedure described in Section 1.3.3 and recast in a series of integrals assimilable to Eq. 3.1:

$$\sum_{n=0}^{\infty} \sum_{\xi_n} \int \frac{\mathrm{d}\mathbf{q}_1}{(2\pi)^D} \cdots \frac{\mathrm{d}\mathbf{q}_n}{(2\pi)^D} \int \mathrm{d}\tau_1 \ldots \mathrm{d}\tau_{2n} \, \mathcal{D}_n(\xi_n, \mathbf{k}, \tau, \tau_1, \ldots, \tau_{2n}, \mathbf{q}_1, \ldots, \mathbf{q}_n) \tag{3.3}$$

here $\tau_1, \ldots, \tau_{2n}, \mathbf{q}_1, \ldots, \mathbf{q}_n$ play the role of internal variables, while $\mathbf{k}, \tau$ are the external ones. $\mathcal{D}$ is the quantity to be summed over, and the target distribution of the MCMC procedure. It will be referred to as *diagram weight*, and its mathematical expression is obtained by multiplying all the propagators appearing in the diagram and the vertex factors. The continuum limit has been applied, so that sums on $\mathbf{q}_i$ were replaced by integrals containing the k-space density factor $a^D/(2\pi)^D$, where a (the dimension of the primitive cell) was set to unity.

The integrand $\mathcal{D}$ can be expressed by the formula:

$$\mathcal{D}(\ldots) = g^{2n} \prod_i \exp\left(-\epsilon(\mathbf{k}_i)\Delta\tau_i\right) \prod_j \exp\left(-\omega(\mathbf{q}_j)\Delta\tau_j\right) \tag{3.4}$$

where i runs over all the electron propagator and j over all the phonon propagators.

Mischenko et al. [21] improved the original method by introducing the one-electron-N-phonons Green function, where the external variables include momenta of the phonons that constitute the starting (0) and final (τ) state:

$$G_N(\mathbf{k}, \tau, \mathbf{q}_1, \ldots, \mathbf{q}_N) = \langle \Psi_0 | b_{\mathbf{q}_N}(\tau) \ldots b_{\mathbf{q}_1}(\tau) c_{\mathbf{k}}(\tau) c_{\mathbf{k}}^{\dagger}(0) b_{\mathbf{q}_1}^{\dagger}(0) \ldots b_{\mathbf{q}_N}^{\dagger}(0) | \Psi_0 \rangle \tag{3.5}$$

---

[3]Here the formalism slightly differs from the one used in Section 1.3.2 in that we switch to *imaginary time* defined as $\tau = it$. This approach is known as Matsubara method. [3]

Another quantity of interest will be the sum of all one-electron-N-phonons Green functions, which is relevant when the DMC simulation explores states with a number of external phonons:

$$P(\mathbf{k}, \tau) = G(\mathbf{k}, \tau) + \sum_{N=1}^{\infty} \int \frac{d\mathbf{q}_1}{(2\pi)^D} \cdots \frac{d\mathbf{q}_N}{(2\pi)^D} \, G_N(\mathbf{k}, \tau, \mathbf{q}_1, \dots, \mathbf{q}_N) \qquad (3.6)$$

Ground state properties from the propagator

The usefulness of the Green function is rooted in the fact that its long-imaginary time behavior gives information about ground state properties of the system, such as its energy. To prove this statement, insert a complete set of eigenstates of the full Hamiltonian (with interaction) into the definition 3.2:

$$H \ket{n_{\mathbf{k}}} = E_{\mathbf{k}} \qquad (3.7)$$

$$1 = \sum_{n_{\mathbf{k}}} \ket{n_{\mathbf{k}}} \bra{n_{\mathbf{k}}} \qquad (3.8)$$

so that the Green function becomes:

$$G(\mathbf{k}, \tau) = -\bra{\Psi_0} c_{\mathbf{k}}(\tau) \, 1 \, c_{\mathbf{k}}^\dagger(0) \ket{\Psi_0} = \sum_{n_{\mathbf{k}}} -\bra{\Psi_0} c_{\mathbf{k}}(\tau) \ket{n_{\mathbf{k}}} \bra{n_{\mathbf{k}}} c_{\mathbf{k}}^\dagger(0) \ket{\Psi_0} \quad (3.9)$$

Using the equivalent of 1.57 for the evolution of operators in imaginary time

$$c_{\mathbf{k}}(\tau) = e^{\mathcal{H}\tau} c_{\mathbf{k}}(0) e^{-\mathcal{H}\tau} \qquad (3.10)$$

the above expression reduces to:

$$\sum_{n_{\mathbf{k}}} \bra{\Psi_0} e^{\mathcal{H}\tau} c_{\mathbf{k}}(0) e^{-\mathcal{H}\tau} \ket{n_{\mathbf{k}}} \bra{n_{\mathbf{k}}} c_{\mathbf{k}}^\dagger(0) \ket{\Psi_0}$$

$$= \sum_{n_{\mathbf{k}}} e^{E_{vac}\tau} e^{-E_{\mathbf{k}}\tau} \bra{\Psi_0} c_{\mathbf{k}}(0) \ket{n_{\mathbf{k}}} \bra{n_{\mathbf{k}}} c_{\mathbf{k}}^\dagger(0) \ket{\Psi_0}$$

$$= \sum_{n_{\mathbf{k}}} e^{-E_{\mathbf{k}}\tau} \left| \bra{n_{\mathbf{k}}} c_{\mathbf{k}}^\dagger(0) \ket{\Psi_0} \right|^2 \quad (3.11)$$

This means that the Green function is a sum of terms decaying exponentially with τ. The behavior at large times is thus dictated by the term with the smallest

coefficient $E_{\mathbf{k}}$, that it is the ground state. After introducing the definition of the quasiparticle weight $Z_{n_{\mathbf{k}}}$, which represents the overlap between the polaron (perturbed) state $\langle n_{\mathbf{k}} |$ and the free electron state $c_{\mathbf{k}}^{\dagger}(0) | \Psi_0 \rangle$

$$Z_{n_{\mathbf{k}}} = \left| \langle n_{\mathbf{k}} | c_{\mathbf{k}}^{\dagger}(0) | \Psi_0 \rangle \right|^2 \tag{3.12}$$

one gets to the final result:

$$G(\mathbf{k}, \tau) \xrightarrow{\tau \to \infty} Z_0(\mathbf{k}) e^{-E_0(\mathbf{k})\tau} \tag{3.13}$$

A similar result is found for the N-phonons Green function:

$$G^{(N)}(\mathbf{k}, \tau, \mathbf{q}_1, \dots, \mathbf{q}_N) \xrightarrow{\tau \to \infty} Z_0^{(N)}(\mathbf{k}, \mathbf{q}_1, \dots, \mathbf{q}_N) e^{-E_0(\mathbf{k})\tau} \tag{3.14}$$

and for $P(\mathbf{k}, \tau)$, using the completeness relation:

$$P(\mathbf{k}, \tau) \xrightarrow{\tau \to \infty} e^{-E_0(\mathbf{k})\tau} \tag{3.15}$$

Scaling of the internal τ_i

In this thesis I chose to work with scaled internal τ_i in the DMC procedure rather than absolute values, which means that τ_i is now a real number between 0 and 1 that, once multiplied by τ, gives the absolute imaginary time. The reason is that it prevents some confusion when dealing with estimators (Section 3.4), and makes the Green function estimator derivation clearer. Mischenko et. al [21] observe that the relation 3.41 which is fundamental to the estimators derivation imply that the internal parameters of $\mathcal{D}_\nu(x')$ and $\mathcal{D}_\nu(x)$ have one and the same domain of definition, otherwise their ratio is not correctly defined. By introducing scaled times, always the same domain of $[0, 1]$ is achieved.

To be more precise, the scaled variables $\bar{\tau}_i \in [0, 1]$ are defined as:

$$\bar{\tau}_i = \frac{\tau_i}{\tau} \qquad \mathrm{d}\tau_i = \tau \mathrm{d}\bar{\tau}_i \tag{3.16}$$

As a result of the rules for the differentials, the diagram weight $\mathcal{D}$ must be modified as follows (consider the case of two τ variables for notational simplicity):

$$\int_0^\tau \mathrm{d}\tau_2 \int_0^{\tau_2} \mathrm{d}\tau_1 \mathcal{D}_{\tau_1 \tau_2}(\tau) = \int_0^1 \mathrm{d}\bar{\tau}_2 \int_0^{\bar{\tau}_2} \mathrm{d}\bar{\tau}_1 \tau^2 \mathcal{D}_{\tau\bar{\tau}_1, \tau\bar{\tau}_2}(\tau) \tag{3.17}$$

$$\int_0^1 \mathrm{d}\bar{\tau}_2 \int_0^{\bar{\tau}_2} \mathrm{d}\bar{\tau}_1 \bar{\mathcal{D}}_{\bar{\tau}_1 \bar{\tau}_2}(\tau) \qquad \bar{\mathcal{D}}_{\bar{\tau}_1 \bar{\tau}_2}(\tau) = \tau^2 \mathcal{D}_{\tau\bar{\tau}_1, \tau\bar{\tau}_2}(\tau) \tag{3.18}$$

In the rest of the thesis the scaled times will be referred to simply as τ_i without the line above for notational convenience.

As a result of this, 3.4 now becomes:

$$\mathcal{D}(\dots) = (g\tau)^{2n} \prod_i \exp\left(-\epsilon(\mathbf{k}_i)\tau\Delta\tau_i\right) \prod_j \exp\left(-\omega(\mathbf{q}_j)\tau\Delta\tau_j\right) \tag{3.19}$$

3.2 Updates

In this section the updates implemented in the code for the Holstein Hamiltonian are listed. The acceptance probability is calculated for each update and the distributions from which the parameters are drawn are shown. The usual [21] way to present the updates is to categorize them into two types:

  I: those which do not change the type of the diagram (change the values of parameters but not the function $\mathcal{D}_n$ itself)

 II: those which change the diagram order

Instead, here they will be listed in an order based on the information one would like to collect. For example, the minimal updates one must implement in order to get the perturbed one-electron Green function at a fixed imaginary time τ are the *add-internal* and *remove-internal* updates, therefore these two are the most "important" ones and should be discussed first. Further updates allow to obtain more observables, and finally there are some extra updates that don't expand the space of possible diagrams, but are there just to increase the frequency of accepted updates.

The naive way to calculate the weight ratio is to evaluate the formula 3.19 for the current diagram, copy the state into a temporary diagram, perform the proposed update on the temporary diagram and evaluate again the formula. The ratio between the two numbers will be the weight ratio, and this method holds true in general for all updates. However, it is more efficient to calculate the ratio explicitly for each update since the part of the diagram that doesn't change gets canceled and doesn't need to be considered; also this way the diagram doesn't need to be traversed twice, but just once. This matters when the diagram order

becomes big. Nevertheless, the first method is still good to check that the faster but more error-prone update specific calculations are correct.

The acceptance probability, defined in general by 1.114, here assumes the form:

$$\frac{\mathcal{D}_{new}}{\mathcal{D}_{cur}} \cdot \frac{p_{rev}}{p_{upd}} \tag{3.20}$$

to be calculated for each update. p_{upd} corresponds to $p(x'|x)$ and is the probability to transition to the new state x', while p_{rev} is the probability for the reverse process. The following discussion assumes that the choice of the type of update is uniformly distributed: if this is not the case one must ensure that the probability of choosing one type of update is the same as choosing its inverse[4].

3.2.1 add-internal

The *add-internal* update adds an internal phonon propagator with momentum $\mathbf{q}$ creating two new interaction vertices at times τ' and τ'', with $\tau'' > \tau'$. An example of this kind of update is provided in Figure 3.1, which highlights the portion of the diagram which has changed.

It will now be described how to calculate the weight ratio explicitly for this class of updates.

$$\frac{\mathcal{D}_{new}}{\mathcal{D}_{cur}} = \frac{(g\tau)^2}{(2\pi)^d} \exp\left\{ -\tau \sum_{i=i'}^{i''} \Delta\tau_i [\epsilon(\mathbf{k}_i - \mathbf{q}) - \epsilon(\mathbf{k}_i) + \omega(\mathbf{q})] \right\} \tag{3.21}$$

The portions of the diagram before τ' and after τ'' are left unchanged by the update, and since the weight of a diagram consists of the product of its propagators (and vertices), they simply cancel. In this way, we are left with a sum that goes from i' to i'', where these two indices refer respectively to the imaginary time segment that starts with τ' and to the one that ends with τ''. Inside this region, electron propagators change by being decreased by $\mathbf{q}$, and a new phonon propagator is added. These terms are respectively the first and third term in the square brackets of 3.21, and they appear with the plus sign since they are part of the proposed diagram, which is the numerator of the weight ratio. The second term instead comes from the current diagram, and its sign is opposite because it is in the denominator.

---

[4]if a class of updates contains its own inverse, this condition is trivially satisfied.

After taking care of the propagators, one must consider the vertex factors: since two vertices are added, there will be a factor of g^2 multiplying the exponential. The τ^2 factor comes instead from the fact that we chose to work with scaled imaginary times, and $1/(2\pi)^d$ comes from the continuum limit.

After the weight ratio, the second ingredient to be evaluated in order to obtain the full acceptance probability is p_{rev}/p_{upd}, which depends on which distributions we draw the parameters of the update from. The simplest choice for both $\mathbf{q}$ and τ', τ'' would be uniform distributions:

$$\mathbf{q} \leftarrow U^d(-\pi, \pi) \qquad \tau' \leftarrow U(0,1) \qquad \tau'' \leftarrow U(\tau', 1) \tag{3.22}$$

p_{upd} is just the product[5] of the update distributions, while p_{rev} is the probability that the reverse process happens, that is, the same phonon propagator is removed from the diagram. At this point one realizes that the DMC code can't run with just the *add-internal* update, but also *remove-internal* is at least required[6]. For this reason, the expression for p_{rev} will be justified later in Section 3.2.2.

$$\frac{p_{rev}}{p_{upd}} = \frac{1/(n+1)}{1/(2\pi)^d \cdot 1 \cdot 1/(1-\tau')} \tag{3.23}$$

where n is the diagram order (number of phonon propagators). A better choice that yields a higher acceptance ratio is to use an exponential distribution for τ''. As discussed in Section 1.4.2, the most effective way to draw the parameters is to use a distribution similar to the target equilibrium distribution, which contains the exponential dependence due to the phonon propagator.

$$E(t; \alpha, t_{max}, t_{min}) = C e^{-\alpha(t-t_{min})} \qquad C = \frac{\alpha}{1 - e^{-\alpha(t_{max}-t_{min})}} \tag{3.24}$$

so that:

$$\tau'' \leftarrow E(t; \omega(\mathbf{q})\tau, 1, \tau') \tag{3.25}$$

and the new p_{rev}/p_{upd} becomes:

$$\frac{p_{rev}}{p_{upd}} = \frac{1/(n+1)}{1/(2\pi)^d \cdot 1 \cdot E(\tau''; \omega(\mathbf{q})\tau, 1, \tau')} \tag{3.26}$$

At this point the total acceptance probability can be computed by 3.20.

---

[5] the variables are sampled independently

[6] the fundamental reason is that detailed balance must be satisfied in a Metropolis-Hastings algorithm
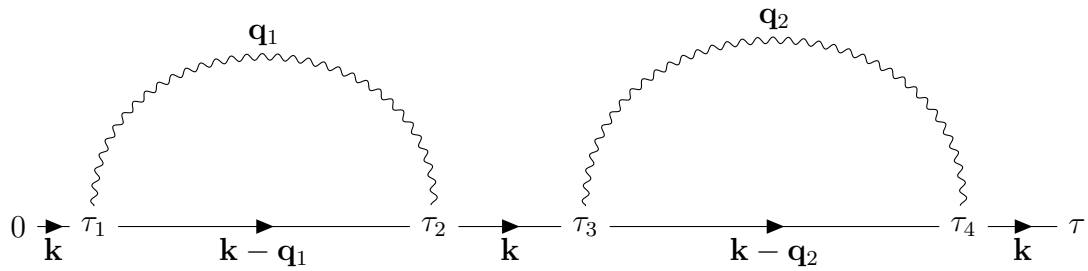
(a) A possible configuration for the current diagram.
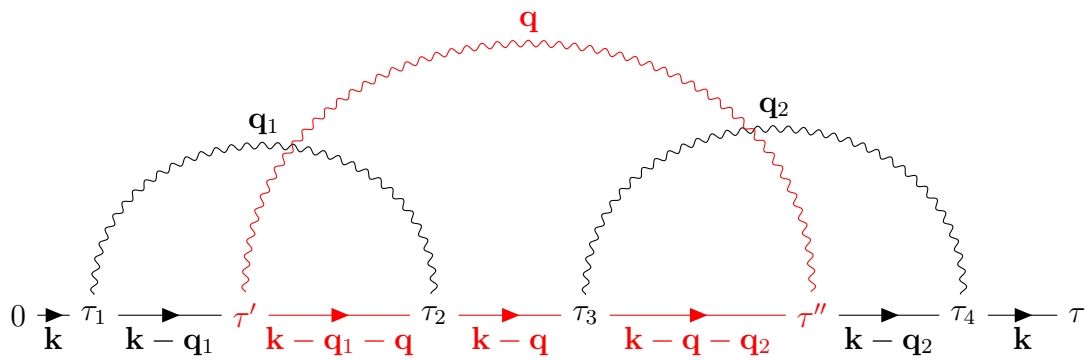
(b) A possible configuration for the proposed diagram.

Figure 3.1: An example of an add-internal update.

3.2.2 remove-internal

For this update we can refer again to Figure 3.1, but this time the reverse happens. The parameter of this update is an integer $m \in [0, n]$ which selects the phonon propagator to remove. The propagators are considered to be ordered by the time of their left (first) vertex, and the choice happens uniformly. Now the formula 3.23 is justified, since $1/(n+1)$ represents the probability that any particular propagator is chosen, reverting the *add-internal* update.

The weight ratio is the analog of 3.21:

$$\frac{\mathcal{D}_{new}}{\mathcal{D}_{cur}} = \frac{(2\pi)^d}{(g\tau)^2} \exp\left\{ -\tau \sum_{i=i'}^{i''} \Delta\tau_i [\epsilon(\mathbf{k}_i + \mathbf{q}) - \epsilon(\mathbf{k}_i) - \omega(\mathbf{q})] \right\} \tag{3.27}$$

here the factor multiplying the exponential is inverted, and signs inside the square brackets must be changed to reflect the phonon removal. Similarly, p_{rev}/p_{upd} becomes:

$$\frac{p_{rev}}{p_{upd}} = \frac{1/(2\pi)^d \cdot 1 \cdot E(t; \omega(\mathbf{q})\tau, 1, \tau')}{1/n} \tag{3.28}$$

where τ' is the left (first) vertex of the propagator about to be removed.

3.2.3 change-τ

After implementing the *add-internal* and *remove-internal* updates, the bare electron propagator can get dressed with virtual phonons and the perturbation comes into play. But since those updates don't change the total length (in imaginary time) of the diagram, one gets information about the one-electron Green function only at one fixed time, the one used to initialize the first diagram with zero virtual phonons. Hence further updates to change τ must be devised.

Given that we work with scaled times, we can change τ to a new value τ' leaving the scaled τ_i as they are. This corresponds to "stretching" the diagram to a new total length, maintaining the relative distances unaltered. The weight ratio for such an update is:

$$(\tau'/\tau)^{2n} \exp(-(\tau' - \tau)(\text{Arg} - \mu)) \tag{3.29}$$

where Arg is defined as:

(a) A possible configuration for the current diagram.

(b) A possible configuration for the proposed diagram.
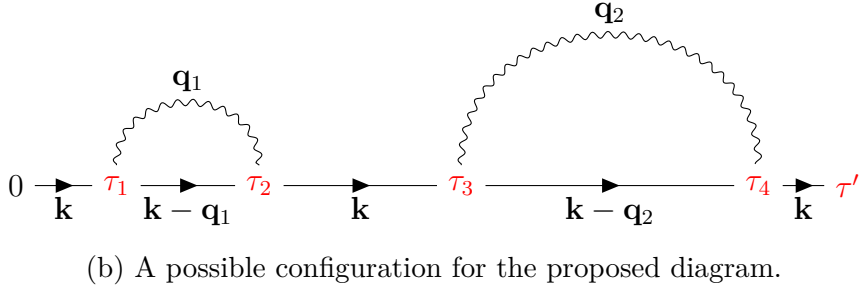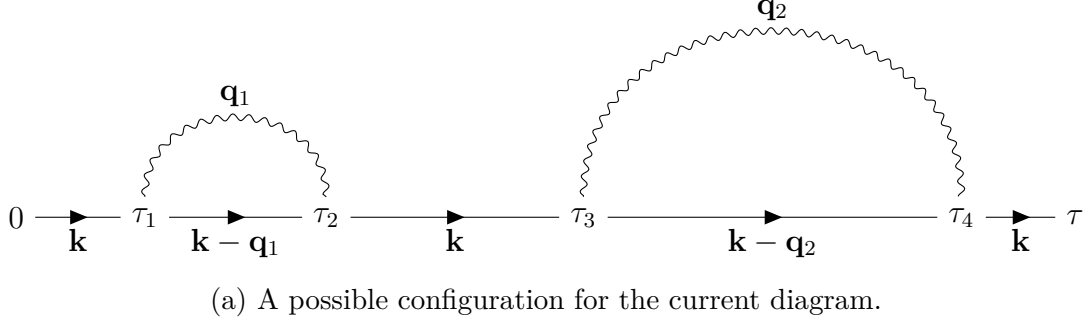
Figure 3.2: An example of a change-tau update.

$$\text{Arg} = \sum_i \epsilon(\mathbf{k}_i)\Delta\tau_i + \sum_j \omega(\mathbf{q}_j)\Delta\tau_j \tag{3.30}$$

and i, j indicate respectively electron and phonon lines.

Note that this update is self-balancing: the kind of update that reverts an instance of this class of updates belongs to this same class. But still, we must calculate the ratio p_{rev}/p_{upd}. If one chooses τ' uniformly distributed in $[0, \tau_{max}]$, the ratio becomes just 1 because each update and its reverse happen with the same probability.

3.2.4 add-external

Like *add-internal* and *remove-internal*, *add-external* and *remove-external* constitute a pair of updates that must exist at the same time in the code to fulfill the detailed balance requirement. This update adds an external phonon pair with the same $\mathbf{q}$ (momentum is conserved) to the beginning and end of the diagram, also adding two interaction vertices (Figure 3.3).

The calculation of this weight ratio requires distinguishing between the cases

$t' < t''$ and $t'' < t'$. For $t' < t''$ the update only affects the beginning an the end of the diagram:

$$\frac{\mathcal{D}_{new}}{\mathcal{D}_{cur}} = \frac{(g\tau)^2}{(2\pi)^d} \exp\left\{ -\tau \left[\sum_0^{i'} + \sum_{i''}^{n-1} \right] \right\} \tag{3.31}$$

where the summation symbols mean exactly the same kind of summation already seen in *add-internal*:

$$\sum_{i_1}^{i_2} = \sum_{i=i_1}^{i_2} \Delta\tau_i [\epsilon(\mathbf{k}_i - \mathbf{q}) - \epsilon(\mathbf{k}_i) + \omega(\mathbf{q})] \tag{3.32}$$

Instead, for $t'' < t'$ the whole diagram is changed and $\mathbf{k}_i$ is decreased by $2\mathbf{q}$ in the segment $[t'', t']$ because of the presence of both the added propagators (Figure 3.3).

$$\frac{p_{rev}}{p_{upd}} = \frac{1/(n_{ext}+1)}{1/(2\pi)^d \cdot E(\tau'; \omega(\mathbf{q})\tau, 1, 0) \cdot E(\tau''; -\omega(\mathbf{q})\tau, 1, 0)} \tag{3.33}$$

3.2.5   remove-external

remove-external complements *add-external* in the same way as in the internal phonon case. We can once again refer to Figure 3.3 with the process happening backwards. The weight ratio must be properly inverted, similarly to what was done for 3.27. For example, for $t' < t''$ one gets:

$$\frac{\mathcal{D}_{new}}{\mathcal{D}_{cur}} = \frac{(2\pi)^d}{(g\tau)^2} \exp\left\{ -\tau \left[\sum_0^{i'} + \sum_{i''}^{n-1} \right] \right\} \tag{3.34}$$

$$\sum_{i_1}^{i_2} = \sum_{i=i_1}^{i_2} \Delta\tau_i [\epsilon(\mathbf{k}_i + \mathbf{q}) - \epsilon(\mathbf{k}_i) - \omega(\mathbf{q})] \tag{3.35}$$

And p_{rev}/p_{upd} becomes:

$$\frac{p_{rev}}{p_{upd}} = \frac{1/(2\pi)^d \cdot E(\tau'; \omega(\mathbf{q})\tau, 1, 0) \cdot E(\tau''; -\omega(\mathbf{q})\tau, 1, 0)}{1/n_{ext}} \tag{3.36}$$
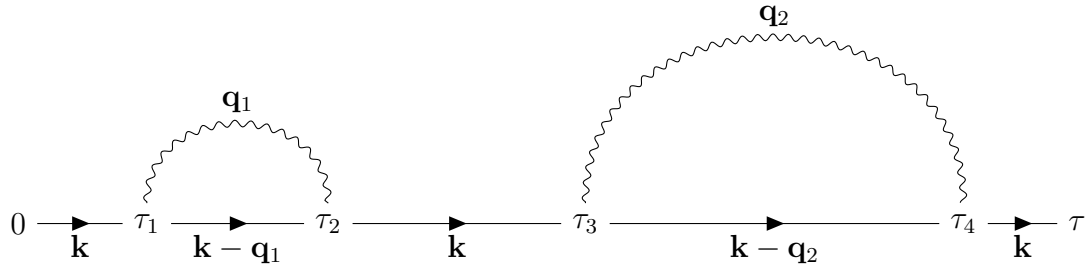
(a) A possible configuration for the current diagram.
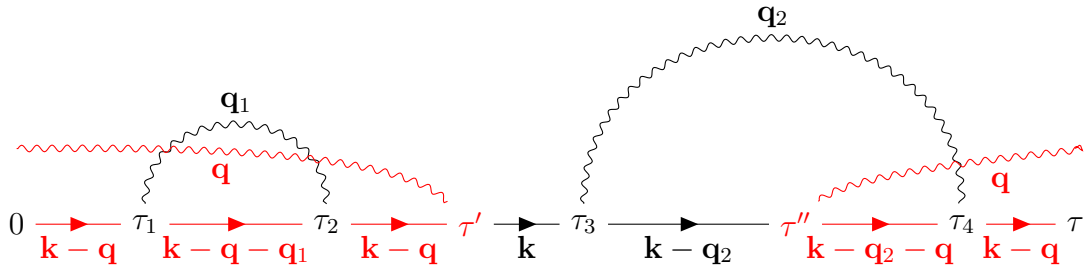
(b) A possible configuration for the proposed diagram for $\tau' < \tau''$.
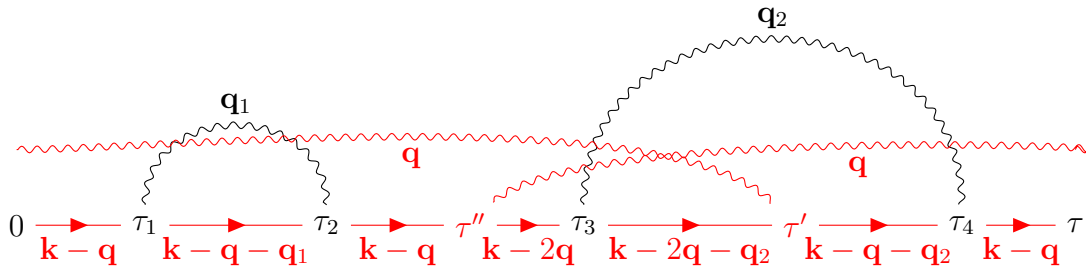
(c) A possible configuration for the proposed diagram for $\tau'' < \tau'$.

Figure 3.3: An example of an add-external update for both $\tau' < \tau''$ and $\tau'' < \tau'$.

(a) A possible configuration for the current diagram.

(b) A possible configuration for the proposed diagram.
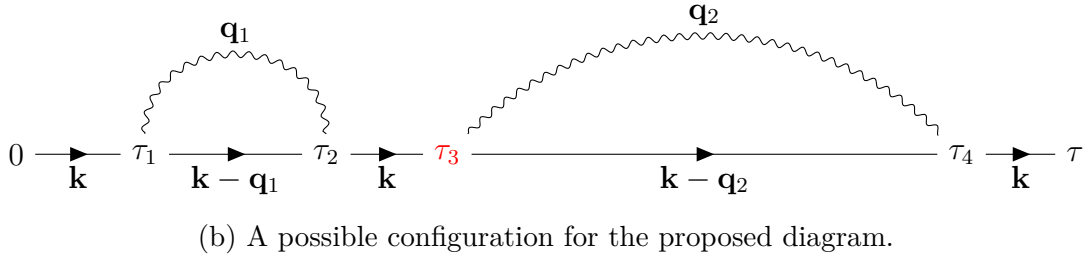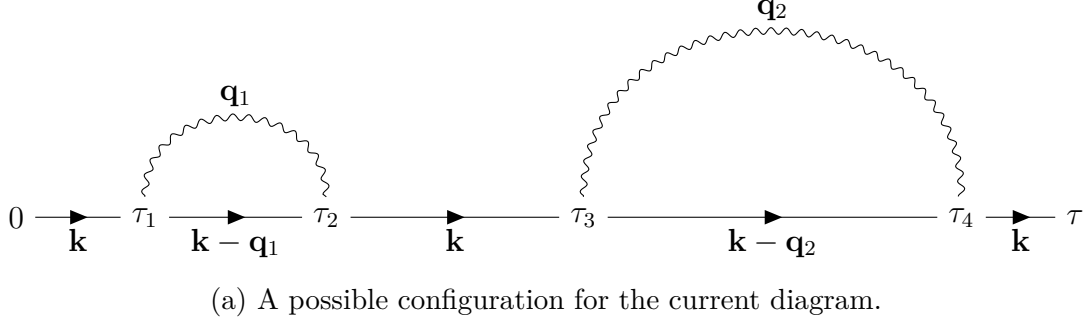
Figure 3.4: An example of a shift-vertex update.

3.2.6 shift-vertex

The *shift-vertex* update was added to improve the total ratio of accepted diagrams. A vertex of the diagram is chosen randomly, and its τ_i is shifted to a new value τ_i' between the previous τ_l and next τ_r times, so that the topology stays the same (Figure 3.4). It can be shown that the expression for the weight ratio is:

$$\frac{\mathcal{D}_{new}}{\mathcal{D}_{cur}} = \exp(-\tau\Delta E(\tau_i - \tau_i')) \qquad \Delta E = \epsilon(\mathbf{k}_{in}) - \epsilon(\mathbf{k}_{out}) \pm \omega(\mathbf{q}) \qquad (3.37)$$

where $\mathbf{k}_{in}$ is the incoming electron wave vector from the left, $\mathbf{k}_{out}$ is the outgoing wave vector and the sign on the phonon term depends on whether it is absorbed or emitted.

If τ_i' is drawn from the distribution:

$$\tau_i' \leftarrow E(t; \tau\Delta E, \tau_r, \tau_l) \qquad (3.38)$$

p_{rev}/p_{upd} becomes exactly equal to the weight ratio and the acceptance ratio for this kind of updates is unity, which is ideal.

3.3 The histogram method

The histogram method allows the calculation of the one-electron Green function from a single run of the simulation. It requires the implementation of the *change-τ* update (in addition to the always required *add-internal* and *remove-internal*) since one needs to probe diagrams with an arbitrary τ.

The idea behind this method is simple: one sets a maximum τ_{max} and divides the interval $[0, \tau_{max}]$ into an arbitrary number of bins, which controls the resolution with which the Green function is known. Then one keeps track of the number of occurrences of diagrams in each bin: after an update is accepted or rejected, one looks at the τ of the new diagram and increments the bin inside which this value falls.

However, note that this procedure doesn't directly yield the Green function: the first thing to do is to turn this histogram into a proper probability density histogram. This is a usual procedure that is accomplished by dividing each count by the total number of occurrences N and the bin length $\delta\tau$:

But this is not yet the Green function: being a probability distribution, it is the Green function divided by a normalization constant C which is unknown (it is the Green function integrated from 0 to τ). Nevertheless, this constant can be estimated by observing that:

$$\frac{N_0}{N} \approx \frac{C_0}{C} \rightarrow C \approx \frac{NC_0}{N_0} \tag{3.39}$$

where N_0 is the number of order 0 diagrams, C_0 is the normalization constant for the unperturbed electron Green function, and the approximation is valid for N big enough so that statistics approach the theoretical probability. C_0 can be obtained analytically.

Putting 3.39 together with the probability density normalization, one gets:

$$\frac{1}{N\delta\tau C} = \frac{C_0}{N_0\delta\tau} \tag{3.40}$$

which is the total factor to rescale the histogram.

3.3.1 The μ parameter

There is still an issue with the histogram method. Consider the bare electron propagator at the bottom of the band: its energy is negative, and the propagator has a minus sign in the argument of the exponential. This means that if one tries to simulate the Green function as it is, the behavior will resemble an increasing exponential, with very high values at large times and very small ones near zero. This is a problem since the statistics at small τ will be poor, leading to an inaccurate normalization [23].

For this reason the factor $e^{\mu\tau}$ is multiplied to the weight $\mathcal{D}$. The parameter is named μ because it has the same energy shifting effect as the chemical potential would have in the many-electron case.[7]

However, μ cannot be too large, otherwise the diagrams at large τ will be too few, which is bad for the exponential fit. So one has to tune μ to be a little lower than the perturbed ground state energy E_0 to obtain optimal results.

Of course, the effect of μ must be taken into account before extracting results from the Green function.

Examples of simulations of the Green function are presented in Figure 3.5 and 3.6. Table 3.1 and 3.2 report the parameters used and the results of the exponential fit to obtain E_0 and Z_0. Note that to obtain $P(0, \tau)$ the *add-external* and *remove-external* updates were enabled. The intercept in this case is close to 1, which is the expected result for the sum of the N-phonon quasiparticle weights.

N	α	γ	k	τ_{max}	μ	E_0	Z_0
10M	0.5	0.5	0	50.0	-2.2	-2.172	0.82

Table 3.1: Parameters and fit results for Figure 3.5.

N	α	γ	k	τ_{max}	μ	E_0	intercept
50M	0.5	0.5	0	50.0	-2.2	-2.172	0.99

Table 3.2: Parameters and fit results for Figure 3.6.

---

[7]here we work at zero temperature and with a single electron, so μ is just an unphysical addition that must be removed when collecting the results.
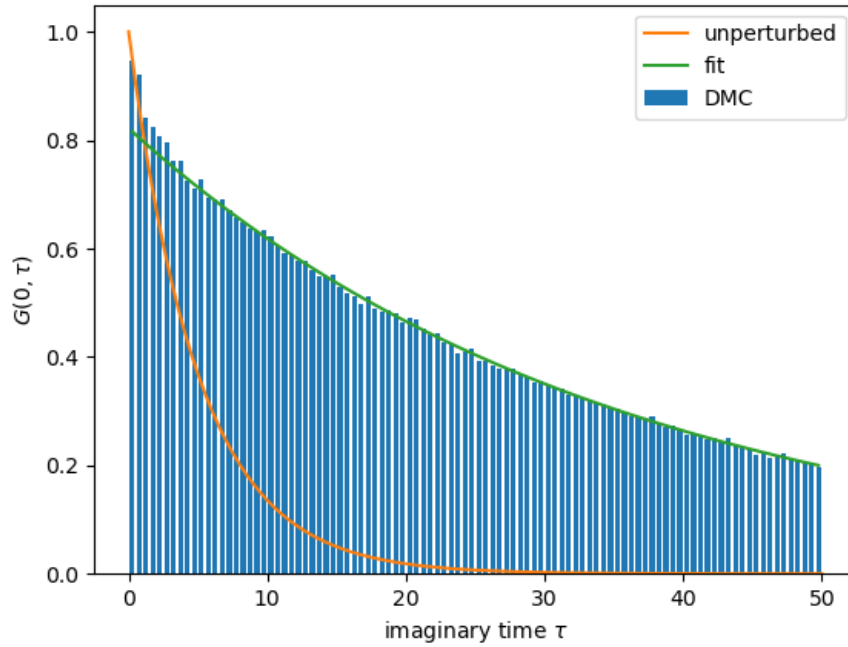
Figure 3.5: The one-electron Green function compared to the bare propagator.
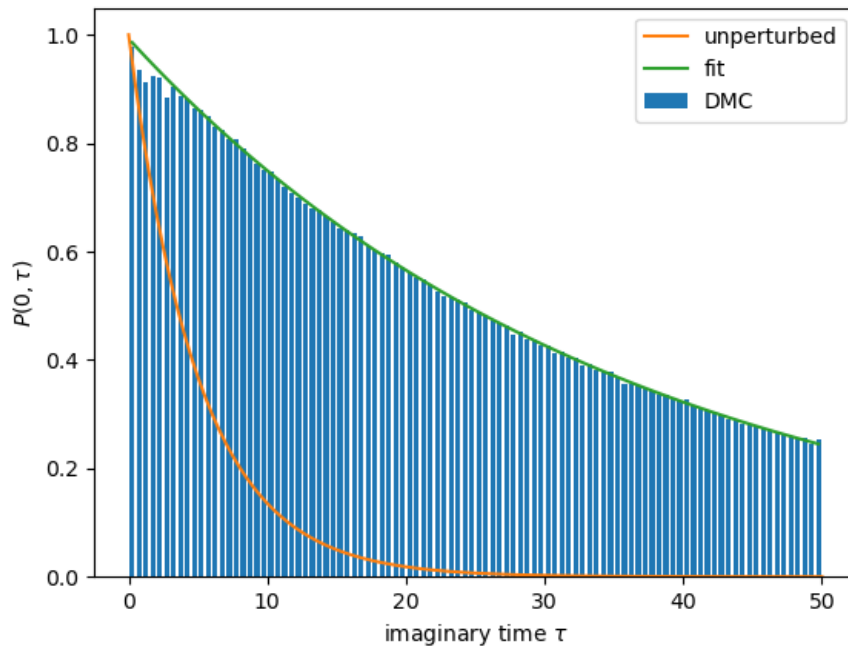
Figure 3.6: Sum of all the one-electron-N-phonons Green functions.

3.4 Direct estimators

Direct estimators, introduced by Mischenko *et al.* [21] for the Fröhlich Hamiltonian, are a convenient alternative to obtain directly many properties of the system without the need to compute the Green function histogram. The derivation of all estimators are fundamentally based on the following Monte Carlo integration result:

$$\frac{Q(x')}{Q(x)} = \frac{\sum_\nu \mathcal{D}_\nu(x')}{\sum_\mu \mathcal{D}_\mu(x)} = \sum_\nu \frac{\mathcal{D}_\nu(x)}{\sum_\mu \mathcal{D}_\mu(x)} \frac{\mathcal{D}_\nu(x')}{\mathcal{D}_\nu(x)} \approx \left\langle \frac{\mathcal{D}_\nu(x')}{\mathcal{D}_\nu(x)} \right\rangle_{MC} \tag{3.41}$$

where the last passage follows from:

$$p_{MC} = \frac{\mathcal{D}_\nu(x)}{\sum_\mu \mathcal{D}_\mu(x)} \tag{3.42}$$

Derivations of specific estimators used in this work are presented in the following subsections.

3.4.1 Energy estimator

Information about the ground state properties of the polaron is found in the long-time behavior of the polaron propagator.

Let us consider the following ratio between polaron propagators, for τ approaching infinity:

$$\frac{P(\mathbf{k}, (1+\lambda)\tau)}{P(\mathbf{k}, \tau)} \xrightarrow[\tau \to \infty]{} \frac{e^{-E_0(\mathbf{k})(1+\lambda)\tau}}{e^{-E_0(\mathbf{k})\tau}} = e^{-E_0(\mathbf{k})\lambda\tau} \tag{3.43}$$

where λ is a real number. Expanding the previous expression for small λ:

$$e^{-E_0(\mathbf{k})\lambda\tau} = 1 - \lambda E_0(\mathbf{k})\tau + \mathcal{O}(\lambda^2) \tag{3.44}$$

Developing the right side of equation 3.41:

$$\frac{\mathcal{D}(\mathbf{k}, (1+\lambda)\tau)}{\mathcal{D}(\mathbf{k}, \tau)} = (1+\lambda)^{2n} \prod_i \exp\left\{-\lambda\epsilon(\mathbf{k}_i)\tau\Delta\tau_i\right\} \prod_j \exp\left\{-\lambda\omega(\mathbf{q}_j)\tau\Delta\tau_j\right\}$$

$$= (1+\lambda)^{2n} \exp\left\{-\lambda\tau \sum_i \epsilon(\mathbf{k}_i)\Delta\tau_i - \lambda\tau \sum_j \omega(\mathbf{q}_j)\Delta\tau_j\right\}$$

$$= (1 + 2n\lambda + \mathcal{O}(\lambda^2))\left(1 - \lambda\tau\left[\sum_i \epsilon(\mathbf{k}_i)\Delta\tau_i + \sum_j \omega(\mathbf{q}_j)\Delta\tau_j\right] + \mathcal{O}(\lambda^2)\right)$$

$$= 1 + \lambda\left(2n - \tau \sum_i \epsilon(\mathbf{k}_i)\Delta\tau_i - \tau \sum_j \omega(\mathbf{q}_j)\Delta\tau_j\right) + \mathcal{O}(\lambda^2)$$

$$= 1 - \lambda\left(-2n + \tau \sum_i \epsilon(\mathbf{k}_i)\Delta\tau_i + \tau \sum_j \omega(\mathbf{q}_j)\Delta\tau_j\right) + \mathcal{O}(\lambda^2) \quad (3.45)$$

where n indicates the number of phonon propagators, and $2n$ is the number of interaction vertices. Comparing 3.45 to 3.44 one obtains the final result:

$$\boxed{E_0(\mathbf{k}) = \left\langle -\frac{2n}{\tau} + \sum_i \epsilon(\mathbf{k}_i)\Delta\tau_i + \sum_j \omega(\mathbf{q}_j)\Delta\tau_j \right\rangle_{MC}} \quad (3.46)$$

3.4.2   Effective mass and group velocity estimators

Similarly to the energy case, we look again at the long-time behavior of a ratio involving P, but this time $\mathbf{k}$ is varied instead of τ:

$$\frac{P(\mathbf{k} + \lambda\mathbf{e}, \tau)}{P(\mathbf{k}, \tau)} \xrightarrow[\tau\to\infty]{} \exp\left\{-\tau[E_0(\mathbf{k} + \lambda\mathbf{e}) - E_0(\mathbf{k}, \tau)]\right\} \quad (3.47)$$

Perform a Taylor expansion around $\mathbf{k}$ for small λ:

$$E_0(\mathbf{k} + \lambda\mathbf{e}) = E_0(\mathbf{k}) + \boldsymbol{\nabla}E_0(\mathbf{k}) \cdot \lambda\mathbf{e} + \lambda\mathbf{e}^{\mathrm{T}}\left[\frac{1}{2}\mathcal{H}_{E_0}(\mathbf{k})\right]\lambda\mathbf{e} + \mathcal{O}(\lambda^3) \quad (3.48)$$

Inserting 3.48 in 3.47 we get:

$$\exp\left\{-\tau\boldsymbol{\nabla}E_0(\mathbf{k})\cdot\lambda\mathbf{e} + \lambda\mathbf{e}^{\mathrm{T}}\left[-\frac{1}{2}\tau\mathcal{H}_{E_0}(\mathbf{k})\right]\lambda\mathbf{e} + \mathcal{O}(\lambda^3)\right\}$$

$$= 1 - \tau\boldsymbol{\nabla}E_0(\mathbf{k})\cdot\lambda\mathbf{e} + \lambda\mathbf{e}^{\mathrm{T}}\left[-\frac{1}{2}\tau\mathcal{H}_{E_0}(\mathbf{k})\right]\lambda\mathbf{e} + \frac{1}{2}[\tau\boldsymbol{\nabla}E_0(\mathbf{k})\cdot\lambda\mathbf{e}]^2 + \mathcal{O}(\lambda^3)$$

$$= 1 - \tau\boldsymbol{\nabla}E_0(\mathbf{k})\cdot\lambda\mathbf{e} + \frac{1}{2}\lambda\mathbf{e}^{\mathrm{T}}\left[-\tau\mathcal{H}_{E_0}(\mathbf{k}) + \tau^2\boldsymbol{\nabla}E_0(\mathbf{k})\otimes\boldsymbol{\nabla}E_0(\mathbf{k})\right]\lambda\mathbf{e} + \mathcal{O}(\lambda^3)$$

$$(3.49)$$

where $\otimes$ is the outer product between two vectors, yielding a matrix that consists of all the possible products between their components.

Perform the same expansion for the diagram weights:

$$\frac{\mathcal{D}(\mathbf{k}+\lambda\mathbf{e},\tau)}{\mathcal{D}(\mathbf{k},\tau)} = \prod_i \exp\left\{-[\epsilon(\mathbf{k}_i+\lambda\mathbf{e}) - \epsilon(\mathbf{k}_i)]\tau\Delta\tau_i\right\} \qquad (3.50)$$

$$\epsilon(\mathbf{k}_i+\lambda\mathbf{e}) - \epsilon(\mathbf{k}_i) = \lambda\boldsymbol{\nabla}\epsilon(\mathbf{k}_i)\cdot\mathbf{e} + \frac{1}{2}\lambda^2\mathbf{e}^{\mathrm{T}}\mathcal{H}_\epsilon(\mathbf{k}_i)\mathbf{e} + \mathcal{O}(\lambda^3) \qquad (3.51)$$

$$\exp\left\{-\sum_i\left[\lambda\boldsymbol{\nabla}\epsilon(\mathbf{k}_i)\cdot\mathbf{e} + \frac{1}{2}\lambda^2\mathbf{e}^{\mathrm{T}}\mathcal{H}_\epsilon(\mathbf{k}_i)\mathbf{e} + \mathcal{O}(\lambda^3)\right]\tau\Delta\tau_i\right\} =$$

$$\exp\left\{-\tau\left[\lambda\sum_i\boldsymbol{\nabla}\epsilon(\mathbf{k}_i)\Delta\tau_i\cdot\mathbf{e} + \frac{1}{2}\lambda^2\mathbf{e}^{\mathrm{T}}\sum_i\mathcal{H}_\epsilon(\mathbf{k}_i)\Delta\tau_i\mathbf{e} + \mathcal{O}(\lambda^3)\right]\right\} \quad (3.52)$$

It is convenient to define the following quantities:

$$k^\star \equiv \sum_i \boldsymbol{\nabla}\epsilon(\mathbf{k}_i)\Delta\tau_i \qquad (3.53)$$

$$\mathcal{H}^\star \equiv \sum_i \mathcal{H}_\epsilon(\mathbf{k}_i)\Delta\tau_i \qquad (3.54)$$

$$1 - \tau\mathbf{k}^\star\cdot\lambda\mathbf{e} - \frac{1}{2}\lambda^2\tau\mathbf{e}^{\mathrm{T}}\mathcal{H}^\star\mathbf{e} + \frac{1}{2}\lambda^2\tau^2(\mathbf{k}^\star\cdot\mathbf{e})^2 + \mathcal{O}(\lambda^3) =$$

$$1 - \tau\mathbf{k}^\star\cdot\lambda\mathbf{e} + \frac{1}{2}\lambda\mathbf{e}^{\mathrm{T}}\left[-\tau\mathcal{H}^\star + \tau^2\mathbf{k}^\star\otimes\mathbf{k}^\star\right]\lambda\mathbf{e} + \mathcal{O}(\lambda^3) \quad (3.55)$$

- $k \neq 0$: Group velocity

For $k \neq 0$ we get information about the group velocity. Comparing the first order terms in the expansions 3.55 and 3.49:

$$\boxed{\boldsymbol{\nabla} E_0(\mathbf{k}) = \langle \mathbf{k}^\star \rangle_{MC}} \tag{3.56}$$

- $k = 0$: Effective mass

The effective mass is related to the Hessian matrix of the energy dispersion relation, so the second order term must be considered. Note that the effective mass is calculated at the bottom of the band where the energy has a minimum, which means that all the terms in 3.49 containing the gradient vanish.

$$\boxed{\mathcal{H}_{E_0}(\mathbf{0}) = \langle \mathcal{H}^\star - \tau \mathbf{k}^\star \otimes \mathbf{k}^\star \rangle_{MC}} \tag{3.57}$$

Let us evaluate the gradient and Hessian of the energy dispersion in a couple of particular cases:

- Free electron dispersion (Fröhlich Hamiltonian [22] case)

$$\epsilon(\mathbf{k}) = \frac{\mathbf{k}^2}{2} \tag{3.58}$$

$$\boldsymbol{\nabla}\epsilon(\mathbf{k}) = \mathbf{k} \tag{3.59}$$

$$\mathcal{H}_\epsilon(\mathbf{k}) = \mathbb{1} \tag{3.60}$$

from which follows:

$$k^\star = \sum_i \mathbf{k}_i \Delta\tau_i \tag{3.61}$$

$$\mathcal{H}^\star = \mathbb{1} \sum_i \Delta\tau_i = \mathbb{1} \tag{3.62}$$

- Tight binding dispersion (Holstein Hamiltonian case)

Assuming a simple cubic lattice:

$$\epsilon(\mathbf{k}) = -2t \sum_i \cos(k_i) \tag{3.63}$$

$$\boldsymbol{\nabla}\epsilon(\mathbf{k}) = \partial_n \epsilon(\mathbf{k}) = 2t \sum_i \sin(k_i)\delta_{in} = 2t\sin(k_n) \tag{3.64}$$

$$\mathcal{H}_\epsilon(\mathbf{k}) = \partial_m \partial_n \epsilon(\mathbf{k}) = 2t \cos(k_n)\delta_{nm} \tag{3.65}$$

from which follows:

$$k_n^\star = 2t \sum_i \sin(k_{n,i})\Delta\tau_i \tag{3.66}$$

$$\mathcal{H}_{nm}^\star = 2t\delta_{nm} \sum_i \cos(k_{n,i})\Delta\tau_i \tag{3.67}$$

where index i is over electron propagators.

3.4.3   Z factors and average number of phonons

Let's start by observing that $Z_0^{(N)}(\mathbf{k})$ may be obtained as the limit of the following ratio for long times:

$$\frac{G^{(N)}(\mathbf{k},\tau)}{P(\mathbf{k},\tau)} \xrightarrow[\tau\to\infty]{} \frac{Z_0^{(N)}(\mathbf{k})e^{-E_0(\mathbf{k})\tau}}{e^{-E_0(\mathbf{k})\tau}} = Z_0^{(N)}(\mathbf{k}) \tag{3.68}$$

Using the definitions 3.5 and 3.6 the ratio becomes:

$$
\begin{aligned}
\frac{G^{(N)}(\mathbf{k},\tau)}{P(\mathbf{k},\tau)} &= \frac{\int d\mathbf{q}_1 \cdots \int d\mathbf{q}_N G^{(N)}(\mathbf{k},\tau,\mathbf{q}_1\ldots\mathbf{q}_N)}{\sum_{N'} \int d\mathbf{q}_1 \cdots \int d\mathbf{q}_{N'} G^{(N')}(\mathbf{k},\tau,\mathbf{q}_1\ldots\mathbf{q}_{N'})} \\
&= \sum_{N''} \int d\mathbf{q}_1 \cdots \int d\mathbf{q}_{N''} \frac{G^{(N'')}(\mathbf{k},\tau,\mathbf{q}_1\ldots\mathbf{q}_{N''})\delta_{N'',N}}{\sum_{N'} \int d\mathbf{q}_1 \cdots \int d\mathbf{q}_{N'} G^{(N')}(\mathbf{k},\tau,\mathbf{q}_1\ldots\mathbf{q}_{N'})} \\
&= \sum_{\nu''} \frac{\mathcal{D}_{\nu''}(\mathbf{k},\tau)}{\sum_{\nu'} \mathcal{D}_{\nu'}(\mathbf{k},\tau)}\delta_{N'',N} \approx \langle\delta_{N_m,N}\rangle_{MC}
\end{aligned}
\tag{3.69}
$$

where the Green functions were expressed in terms of diagram weights and the collective index ν was used to summarize all summation/integration variables.

Putting together the two results we get that at large τ the N-phonon Z factors for the ground state is simply the frequency of generating a diagram with N external phonons:

$$\boxed{Z_0^{(N)}(\mathbf{k}) \approx \langle\delta_{N_m,N}\rangle_{MC} \equiv \frac{1}{M}\sum_m^M \delta_{N_m,N}} \tag{3.70}$$

This result also allows to obtain the average number of phonons in the polaronic

cloud:

$$\boxed{\mathcal{N}_{ph} = \sum_{N=1}^{\infty} Z_0^{(N)}(\mathbf{k}) \cdot N} \tag{3.71}$$

3.4.4 Green function

The Green function itself may also be calculated via an estimator, providing a better alternative to the histogram method. This estimator is derived for the case of diagrams of order 2 for notational simplicity, the generalization to order n is trivial. Let's start by constructing the following estimator:

$$g_{\tau_0}(\tau_1, \tau_2, \tau) = \begin{cases} \frac{1}{\text{size}(\Gamma_{\tau_0})} \frac{\mathcal{D}_{\tau_1\tau_2}(\tau_0)}{\mathcal{D}_{\tau_1\tau_2}(\tau)} & \tau \in \Gamma_{\tau_0} \\ 0 & \text{otherwise} \end{cases}$$

where Γ_{τ_0} is an arbitrary interval containing τ_0 and τ_1, τ_2 are scaled times. In this way:

$$\langle g_{\tau_0} \rangle_{\text{MC}} = \int_0^{\tau_{max}} \mathrm{d}\tau \int_0^1 \mathrm{d}\tau_2 \int_0^{\tau_2} \mathrm{d}\tau_1 g_{\tau_0}(\tau_1, \tau_2, \tau) \frac{\mathcal{D}_{\tau_1\tau_2}(\tau)}{C} =$$

$$\frac{1}{C} \int_{\Gamma_{\tau_0}} \mathrm{d}\tau \int_0^1 \mathrm{d}\tau_2 \int_0^{\tau_2} \mathrm{d}\tau_1 \frac{\mathcal{D}_{\tau_1\tau_2}(\tau_0)}{\text{size}(\Gamma_{\tau_0})} = \frac{G(\tau_0)}{C} \tag{3.72}$$

So this estimator really reproduces the Green function, up to the multiplicative constant C which can be obtained by 3.40. Note that a factor of $(\tau_0/\tau)^2$ arises in the estimator as a consequence of the time scaling 3.18.

3.5 Implementation

In this section the implementation of the DMC algorithm that was written for this thesis is presented. The code is mainly divided into two parts:

1. The main loop

2. The implementation of the update procedures

After all the parameters characterizing a particular run have been supplied, the state is initialized with a zero-order diagram, and a burn-in loop of D thermalization steps is started. These steps are simply discarded (no measurements are taken)

because the initial steps of a MCMC procedure are clearly far away from the target equilibrium distribution, and would give an unwanted bias if included.

At this point the main loop starts. At every iteration, one (or more) updates are performed and statistics are collected on the resulting state. The variable `N_updates` defines how many updates are performed before each measurement. The structure in C code is:

```
1    init(diagram)
2
3    for (i=1; i<=D; i++)
4        // thermalization steps
5
6    for (i=1; i<=N; i++) {
7        for (j=1; j<=N_updates; j++) {
8            choice = rng_choice(n_sel_updates)
9            update[choice](diagram)
10       }
11       // collect statistics:
12       // histograms, estimators
13   }
```

`update[]` is an array of `n_sel_updates` procedures built dynamically depending on which type of updates were enabled at program launch. `rng_choice` draws one of them (for example, *try-add-internal*), and the chosen function is called. These functions share a common structure:

1. Draw parameters of the update $(\tau_1, \tau_2, \mathbf{q})$ from the distributions mentioned in 3.2.

2. Evaluate the weight ratio.

3. Draw a random number $\in [0, 1]$, and actually perform the update (changing the state) if the number is less than the acceptance calculated in step 2.

For example, the *try-add-internal* must call two other subroutines in order to do its job: *eval-add-internal*, which evaluates the weight ratio without changing the state, and finally *add-internal* to actually perform the update if step 3 was successful. Obviously, different types of updates require different parameters drawn from arbitrary distributions.

Up to this point no specific assumption was made about how the diagrams are represented in memory and how the updates are carried out. This is the second

(and lower-level) layer of the code. Each type of update x must implement the methods x and *eval-x*, like *add-internal* and *eval-add-internal* from the previous example. The clear separation into two layers makes it possible to replace initial implementations of the updates with eventual better performing ones without having to touch the higher-level layer. Moreover, the updates implementation is entirely deterministic, which means that it is easier to test for correctness.

Only the current state is kept in memory. The memory representation of a diagram is a collection of numeric variables such as order, τ, **k**, number of external phonons, etc. plus an array of vertices. A vertex contains information about its τ_i, the τ_j which is connected to by the internal phonon propagator, the phonon momentum **q**, whether the phonon is internal or external and whether it is absorbed or emitted.

The representation just described is simple but not optimal. More details about devising a more performant strategy for diagram representation in memory and related update algorithms can be found in [24].

3.5.1 Testing

A preliminary form of testing was carried out by restricting the simulations over low order diagrams to be compared with "exact" (non-random) standard numerical integration. Diagram order must be low enough so that numerical integration can provide the answer in a comfortable time. As the number of integration variables increases, standard integration simply can't compete with the Monte Carlo approach because it suffers an exponential increase in the integrand evaluations (this problem is commonly referred to as *curse of dimensionality* [25]). This test ensures that at least for low orders the implementation is correct (Figure 3.7).

The update procedures constitute the most important and critical section of the code. A small error could give totally wrong results and is difficult to spot in general. For this reason the following testing mechanism was conceived: the assumption is that a *reference implementation* that gives the correct results exists. Here the reference implementation is another code written by the author, in a higher level and safer language, with a focus on clarity rather than performance. The code to be tested is referred to as *fast implementation* instead. As mentioned in the previous section, updates are deterministic and they return a floating point number (the acceptance probability). The test then consists in producing a random
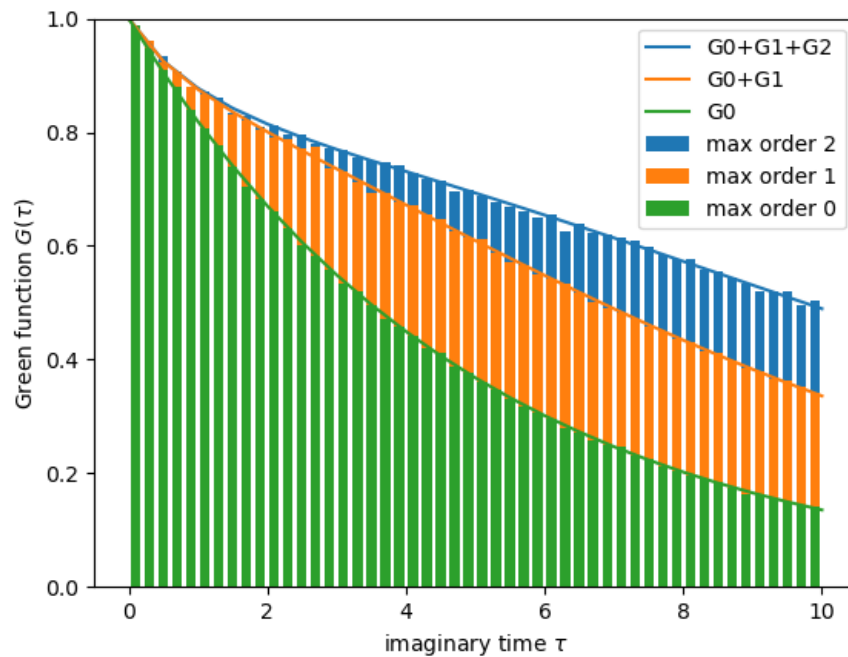
Figure 3.7: DMC agrees with standard N-dimensional integration by the quadrature method for low orders. DMC data is in histogram form while integration is represented by lines. The second order term needs to be calculated as a sum of the integrals for the three possible topologies.

"path" in diagram space for a large enough number of steps, running both the reference and fast implementations on it, and comparing the output of the update procedures, which should be the same in the limit of floating point errors.

Chapter 4

Results

In this part, results obtained with the author's implementation of DMC applied to the Holstein Hamiltonian are presented and discussed. The data is visualized in a series of graphs focusing on the dependence of each observable on one or more selected parameters.

Data from the author's implementation is always displayed as discrete points with associated error, which is then compared in the same graph to different kinds of reference data, when available:

- Analytic results from perturbation theory, which give expected behavior for limiting cases of the parameter space. These are labeled as "PT-hi" for the strong coupling limit (high α) and "PT-lo" for the weak coupling limit ($\alpha \approx 0$).

- Results from a different, independent implementation of the same DMC method, taken from Macridin's study [15] and labeled as "MACR".

- Results from another analytical approximation, which unlike perturbation theory allows to obtain good results at all couplings. It is based on the calculation of the Green function by summing over the class of the self-energy diagrams, but with each self-energy diagram averaged over the momenta of its free propagators [26]. These are labeled as "GDV".

- Results from the continuous-time path-integral quantum Monte Carlo algorithm employed by Kornilovitch in [27][28], labeled as "KOR". It is based on Feynman's integration of phonons and subsequent simulation of the resulting single-particle self-interacting system.

N	τ_{max}	O_{max}	D
5 M	12.0	300	1 M

Table 4.1: Standard initial settings employed in simulations ($M = 10^6$).

Settings

There are a few settings[1] that must be carefully tuned in order to run the program properly:

1. N, number of iterations. This is trivial because in a Monte Carlo simulation results will converge only when the number of iterations is high enough. The error introduced by this can be quantified by the size of the error bars calculated via the blocking method.

2. τ_{max}, diagram length. This parameter is important because in order to probe the ground state, the diagram length must be sufficiently high. How much exactly is not known a priori, so it must be discovered in a trial-and-error approach.

3. O_{max}, maximum order (the maximum number of internal vertices that can be placed in a diagram). If this number is reached by a diagram in a run, the distribution is artificially limited by that and will not reflect the true stationary distribution. The run must be restarted with a higher maximum order.

4. D, burn-in iterations

Raising the values of each one of these settings improves the simulation in some way, but it also increases the time required to complete it. Therefore I will refer to a set of *standard initial settings* which was found to be a reasonable default for most of the results presented in the following discussion. These settings are quick for debug purposes. Every time these settings are not sufficient anymore for the point of the physical parameter space that is being investigated, there will be a mention on how to adjust them.

---

[1]"settings" refers to parameters of the program, in contrast to the physical *parameters* of the Hamiltonian. τ_{max} is physical but will be treated as a setting nonetheless.

4.1 Ground state properties

4.1.1 1D

Energy

The values of the energy estimator as a function of the dimensionless coupling parameter α are presented in Figure 4.1. The most important feature of this graph is the possibility to recognize two regions with different behavior:

- A low-coupling region for $\alpha < 2$. Near 0, this part is well described by low-coupling perturbation theory and the dependence is approximately linear.

- A transition region near $\alpha = 2$ where the behavior changes quite rapidly.

- A high-coupling region for $\alpha > 2$. The dependence is again linear, but with a different slope.

Recall that α was defined as 2.16, which means that the transition takes place when the lattice deformation energy approaches the bare electron bandwidth (2.44). This is why most authors redefine α to include the factor of 2 so that the transition happens at the "normalized" value of 1.

The figure also shows how the other parameter of the Holstein Hamiltonian, $\gamma = \omega_0/t$, affects the curve. A smaller adiabaticity ratio results in a sharper transition (but there is no discontinuity, the curve is always smooth).

For the energy estimator, the agreement between data obtained in this work and previous DMC results (Figure 4.1), as well as path-integral QMC results (Figure 4.2) is very good.

Quasiparticle weights

In the one-dimensional lattice Z_0 drops at a steady rate which is determined by the adiabaticity constant: the smaller ω_0, the steeper the slope. This means that the electron gets dressed rapidly as the coupling increases. At high coupling the quasiparticle weight is zero, meaning that the perturbed state has no overlap with the bare electron state without phonons: the character of the state becomes totally different as expected from strong-coupling perturbation theory.

N	τ_{max}	O_{max}	D
150 M	34.0	600	1 M

Table 4.2: Settings for 1D $\gamma = 0.1$.

Number of phonons

The polaron ground state is not an eigenstate of the phononic number operator, but the average value of the observable can be considered. It follows directly from the quasiparticle weight distribution over a given number of phonons.

Figure 4.4 shows the bare electron progressively "dressing up" as the coupling increases, in a fashion consistent with 4.3. The number of phonons in the cloud surrounding the electron increases with decreasing γ.

Here the agreement with Macridin's results is still good, but not perfect as the $\gamma = 0.1$ curve deviates a bit, probably due to different τ_{max} settings used. In this case the high-coupling perturbation limit is still not reached. The effective mass results (Figure 4.5) show a similar trend, but reaching the high-coupling limit becomes even more difficult.

Effective mass

The effective mass was generally the most problematic observable to compute reliably. The main reason for this is apparent by its own definition: to get the effective mass one has to invert the estimator 3.57, so a good accuracy in the estimator is required for reliable results.

In the graph 4.5, the effective mass enhancement (ratio between the perturbed effective mass and the bare effective mass) is plotted. This value spans several order of magnitudes, so the logarithm is taken.

The cases $\gamma = 1.0$, $\gamma = 0.5$ could be obtained with the standard settings, while for the case $\gamma = 0.1$ an increase in τ_{max} and O_{max} was needed. Consequently, the number of iterations must be also increased. Table 4.2 shows the new settings.

A linear dependence in Figure 4.5 corresponds to an exponential enhancement: The polaron mass becomes quickly so high that external forces have little effect on it. Its ground state has therefore the character of a localized, trapped state.
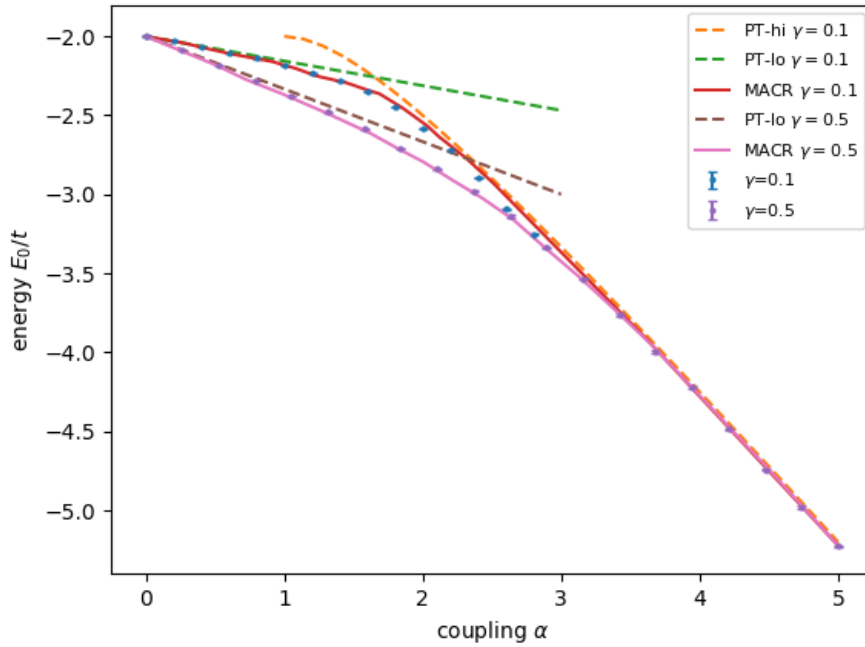
Figure 4.1: Energy vs. coupling, 1D lattice.
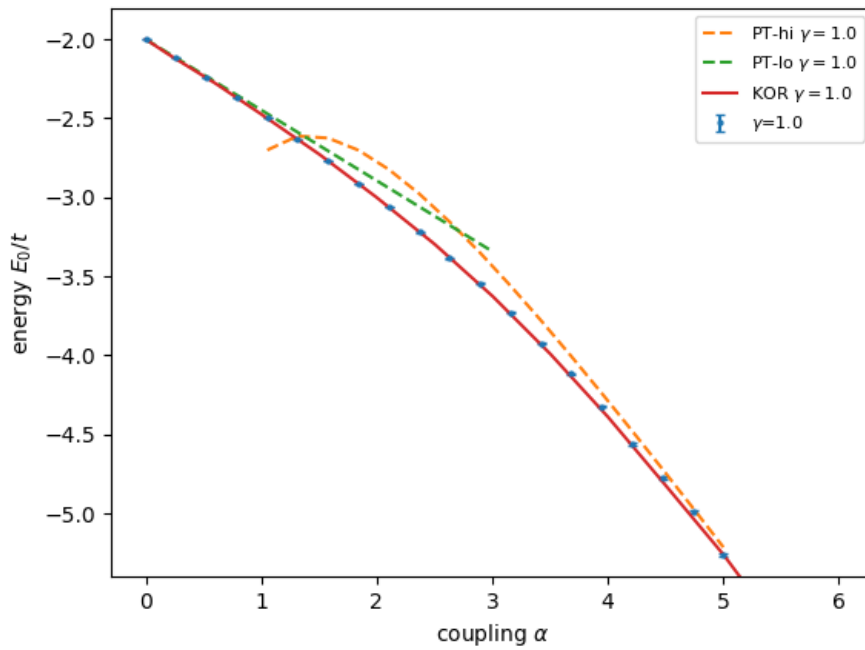
Figure 4.2: Energy vs. coupling, 1D lattice, $\gamma = 1$
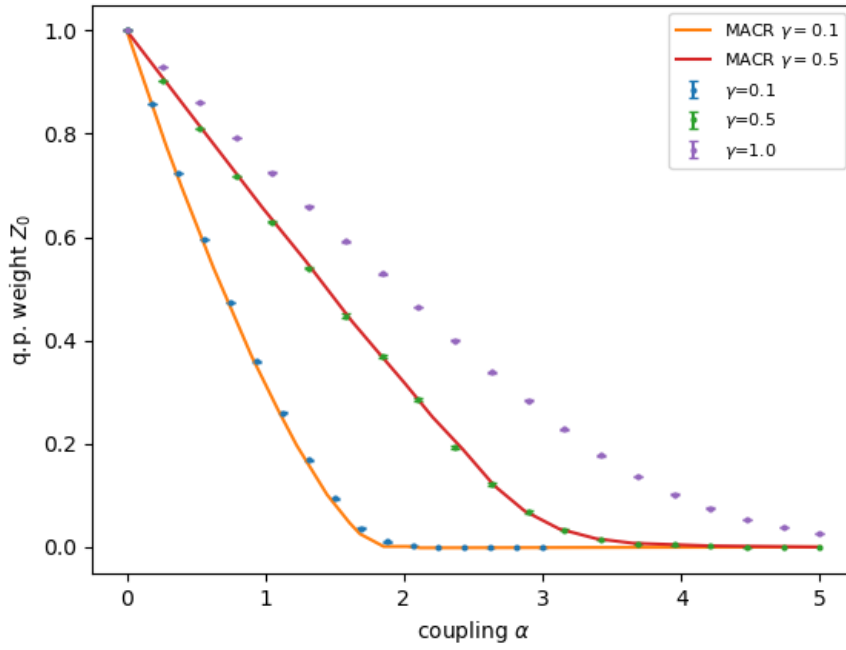
Figure 4.3: Z_0 q.p. weight vs. coupling, 1D lattice.
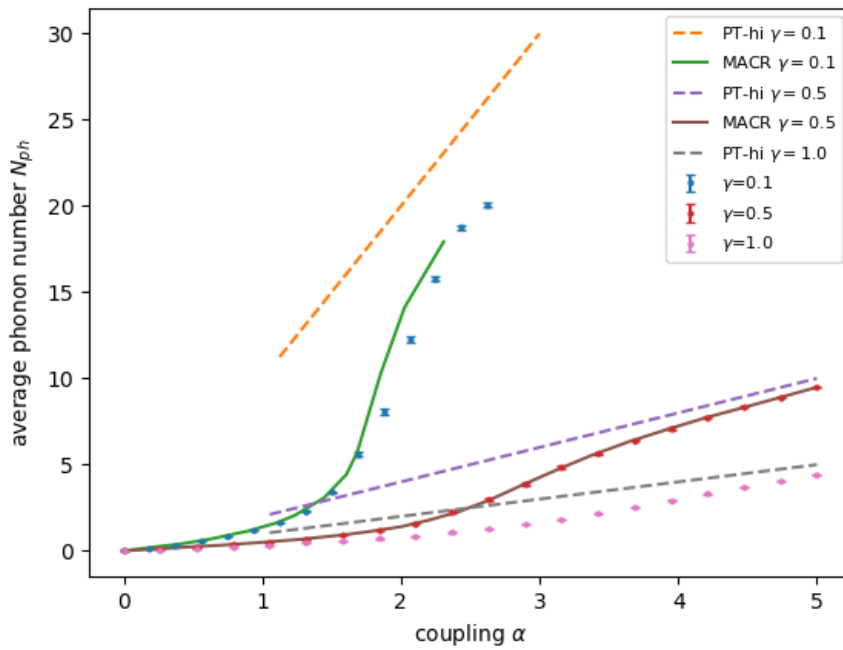
Figure 4.4: N_{ph} vs. coupling, 1D lattice.
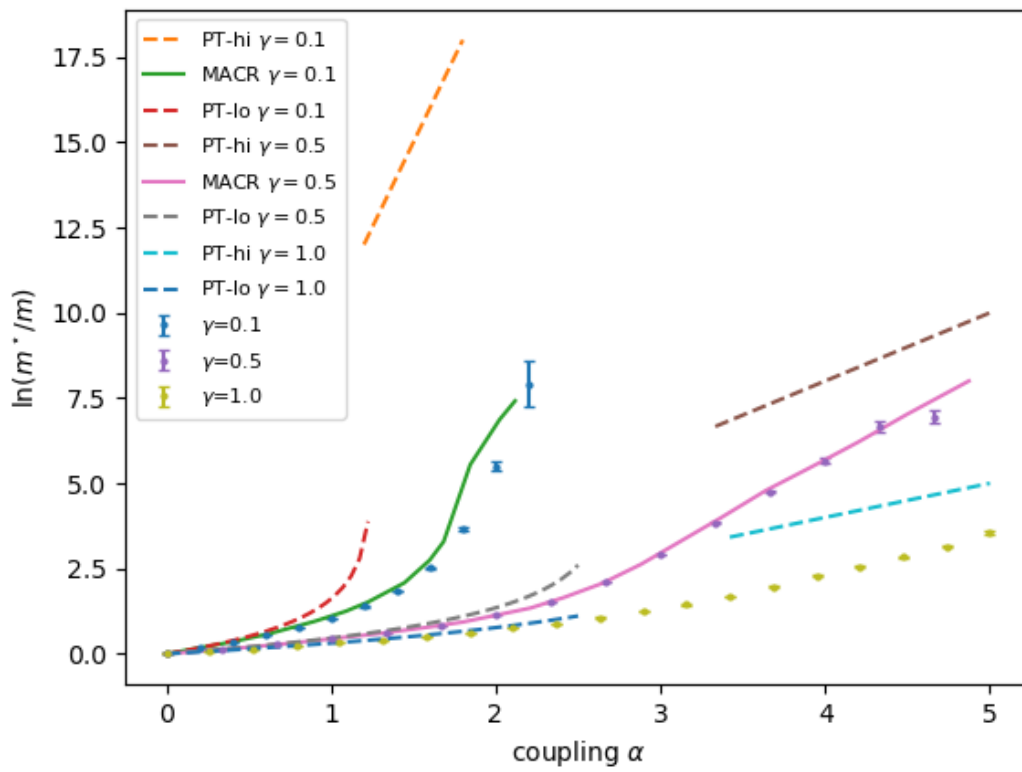
Figure 4.5: Logarithm of the effective mass enhancement vs. coupling, 1D lattice. The MCMC steps were increased to 400M, with measurements taken every 2 steps.

To summarize, the transition happens around $\alpha = 2$, the sharper the lower γ. Around this value, the quasiparticle weight drops abruptly while the effective mass starts to increase. In this region, the ground state is a mixture of both a large-radius polaron state, with its main contribution from the bare electron state, and a small polaron state, with a larger number of phonons.

4.1.2 2D and 3D

Adjusting the code for the N-dimensional case consisted basically in a couple of straightforward modifications:

- Summing over dimensions in the electronic "kinetic" term of the Hamiltonian

- Vectorizing all the operations involving momenta

- Remembering to include a factor of 2π for each component in the acceptance probability calculation when drawing a new **q**-vector

The bidimensional and tridimensional cases share the majority of features with the one-dimensional case, but different behavior was found in some aspects.

Comparing the 2D energy-coupling in 4.6 to the 1D case, one notes that the transition is sharper: the $\gamma = 0.5$ curve clearly shows the transition happening in a region very highly localized around 2, whereas the 1D plot required raising γ to higher values. Energies are overall scaled by a factor of 2 which is due to the added term in the electronic "kinetic" part.

The 3D results further confirm this observation: here the transition is so localized in coupling that the curve appears to possess almost a cusp-like singularity (Figure 4.10). Figure 4.14 compares the behavior of different dimensionalities for the same value of the γ parameter.

The Z_0 observable is affected by dimensionality in a very specific way: from 1D to 2D the curve changes its concavity from positive to negative. This means that the contribution of the bare electronic state decreases slower at the beginning

N	τ_{max}	O_{max}	D
60 M	34.0	1000	1 M

Table 4.3: Settings for 3D $\gamma = 0.5$.

and falls off abruptly at a certain point. Also in this case, the 3D behavior is even more pronounced, with the $\gamma = 0.5$ curve falling almost vertically.

Something similar happens to the N_{ph} estimator, which directly depends on phonon distribution. In the high coupling regime, the average number of phonon increases much more rapidly compared to 1D, in agreement with the perturbation theory results.

The effective mass was considerably more difficult to compute with respect to the one-dimensional case. As previously discussed, it was found that proper measurements could only be obtained by raising the total diagram length, which severely impacts the time required for running the simulation. This is made worse by the added time penalty due to vector operations in many dimensions.

Since we are working under the assumption of a simple cubic lattice, the isotropy can be exploited to take an average over the diagonal of the effective mass tensor, which has theoretically the same value along all directions. This helps a bit to reduce the error because three measurements are taken into account instead of a single one.

Similarly to the 1D case, the agreement with previous DMC data is overall very good for the values of γ considered. However, it is difficult to reach the high coupling perturbation limit for the effective mass as convergence gets more and more computationally expensive (Figures 4.9 and 4.13). There is also a slight deviation from Goodvin's analytical approximation for the quasiparticle weight Z_0 (Figure 4.7).
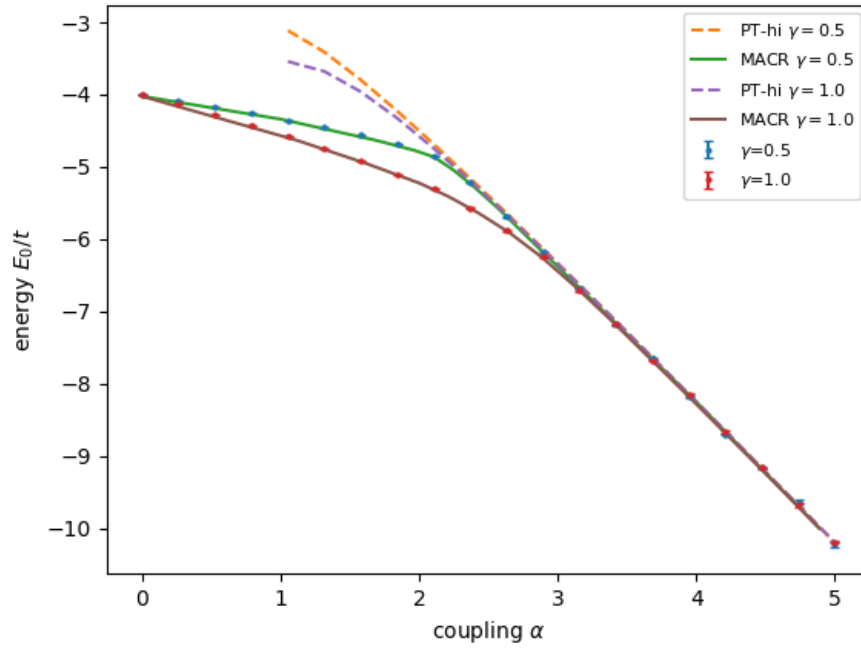
Figure 4.6: Energy vs. coupling, 2D lattice.
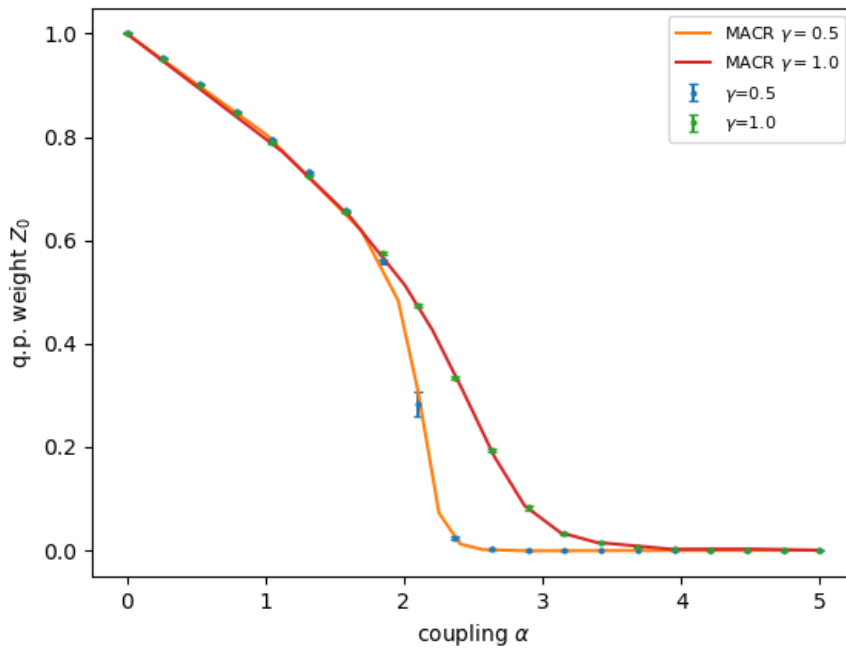
Figure 4.7: Z_0 q.p. weight vs. coupling, 2D lattice.
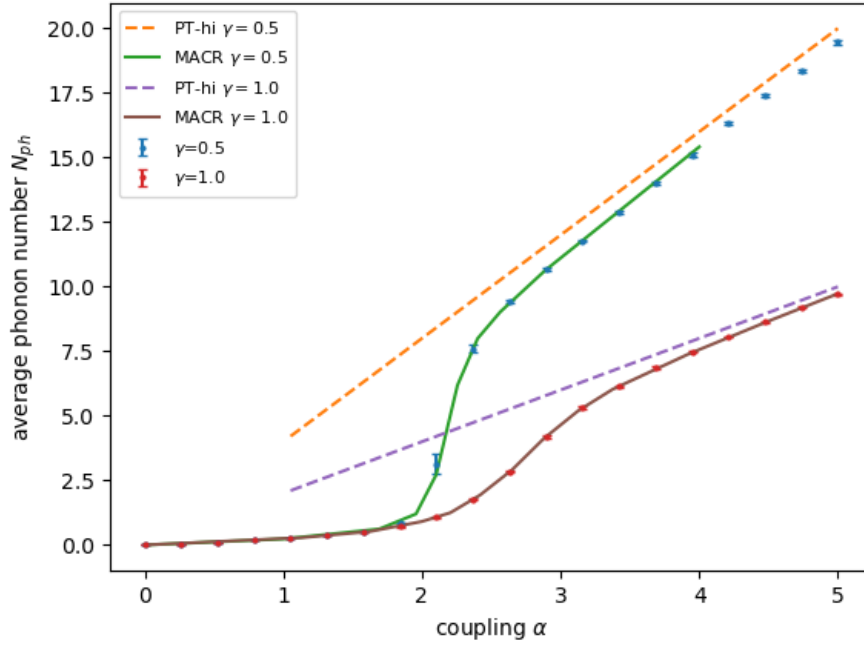
Figure 4.8: N_{ph} vs. coupling, 2D lattice.
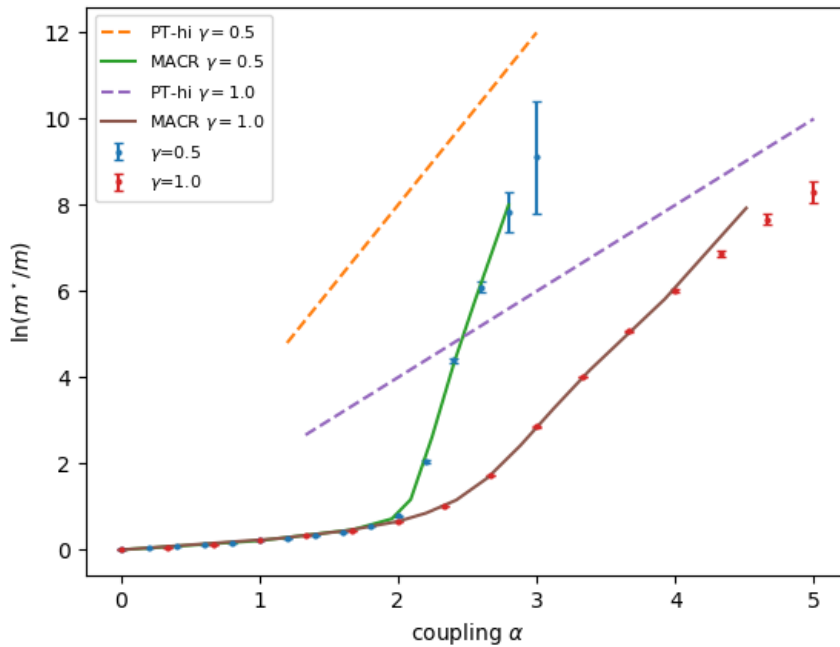
Figure 4.9: Logarithm of the effective mass enhancement vs. coupling, 2D lattice. The MCMC steps were increased to 200M, with measurements taken every 2 steps.
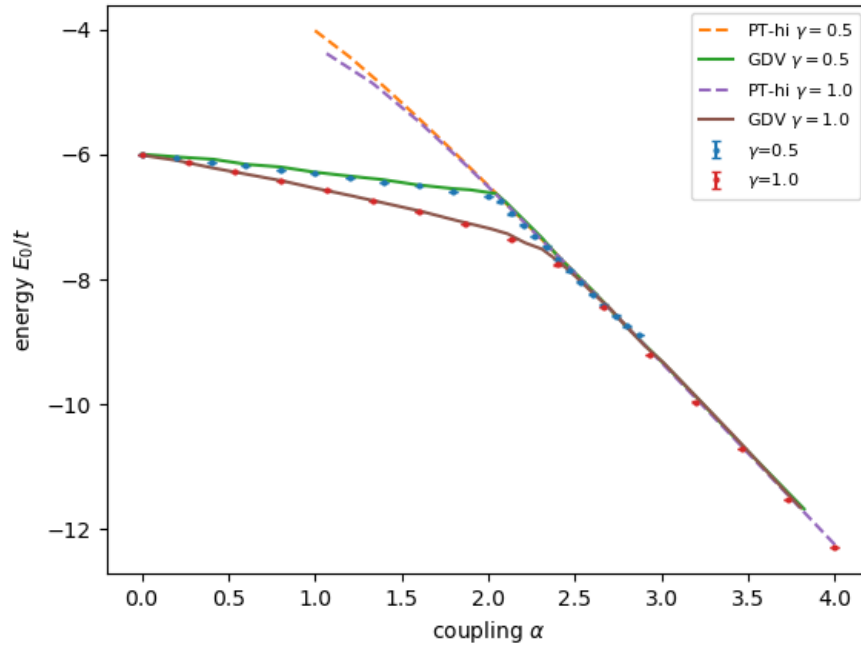
Figure 4.10: Energy vs. coupling, 3D lattice.
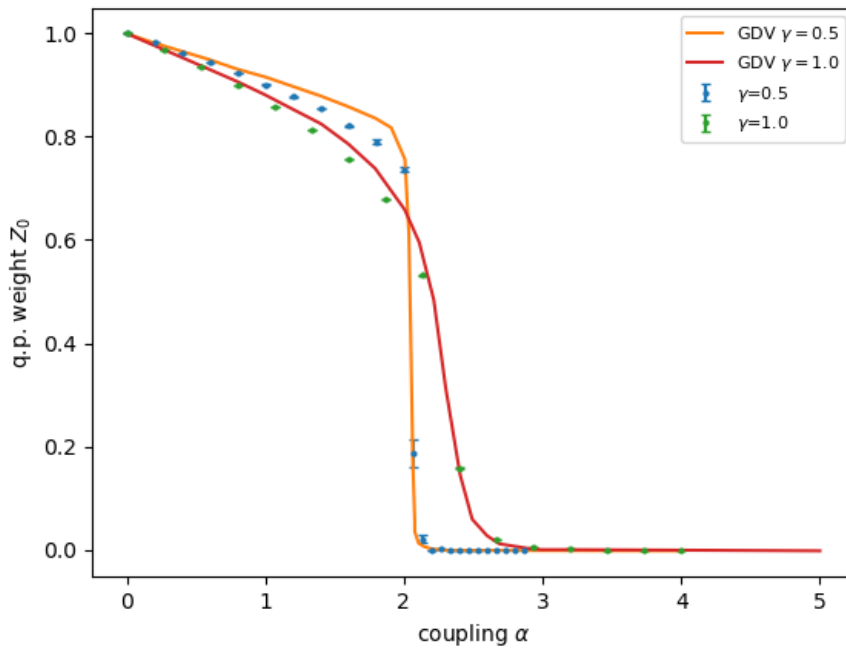
Figure 4.11: Z_0 q.p. weight vs. coupling, 3D lattice.
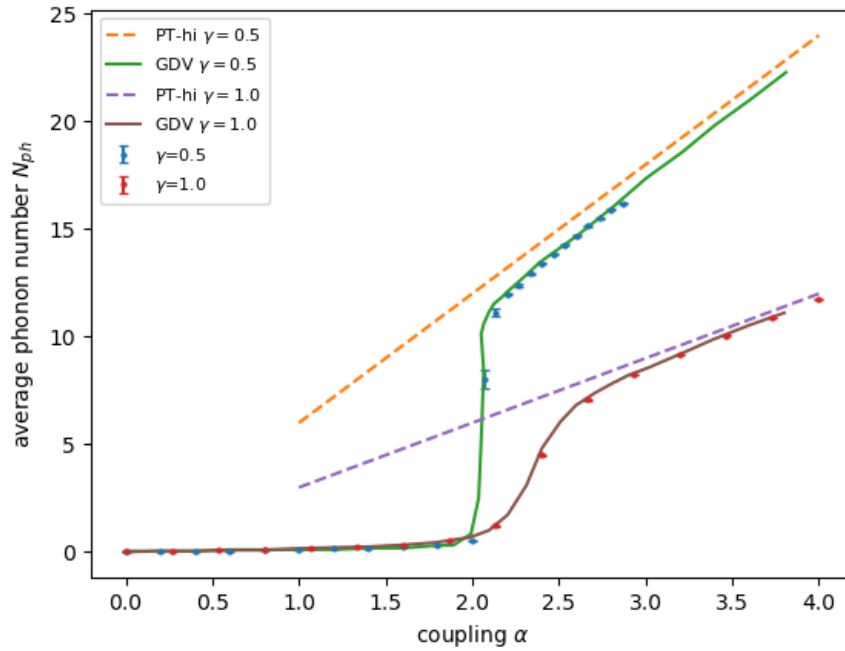
Figure 4.12: N_{ph} vs. coupling, 3D lattice.
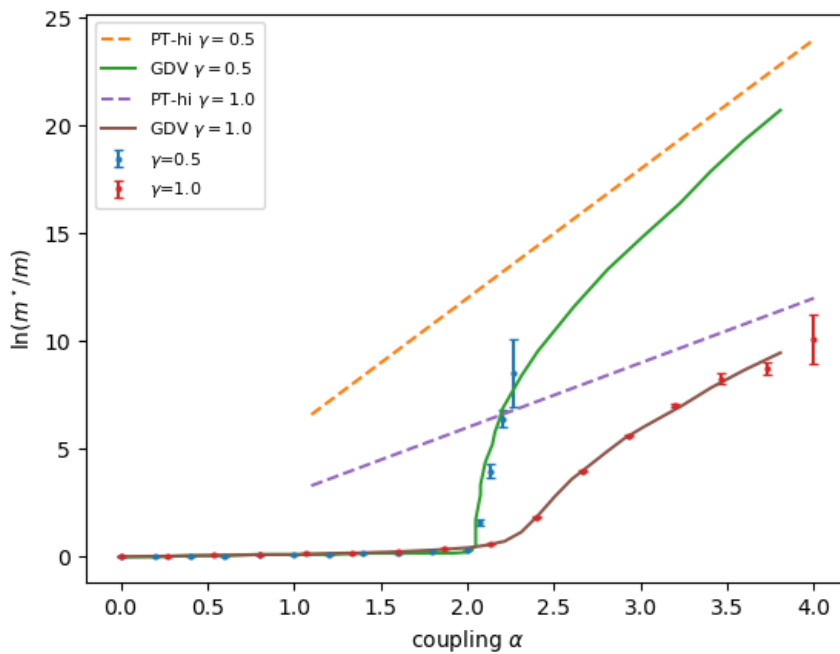
Figure 4.13: Logarithm of the effective mass enhancement vs. coupling, 3D lattice. The MCMC steps were increased to 200M, with measurements taken every 2 steps.
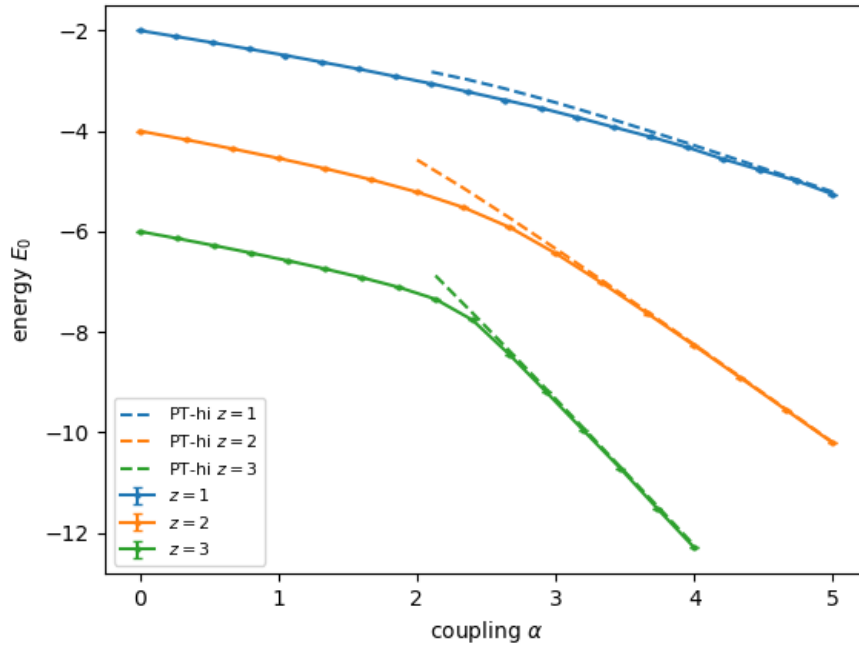
Figure 4.14: Energy vs. coupling for different dimensionalities z, $\gamma = 1.0$
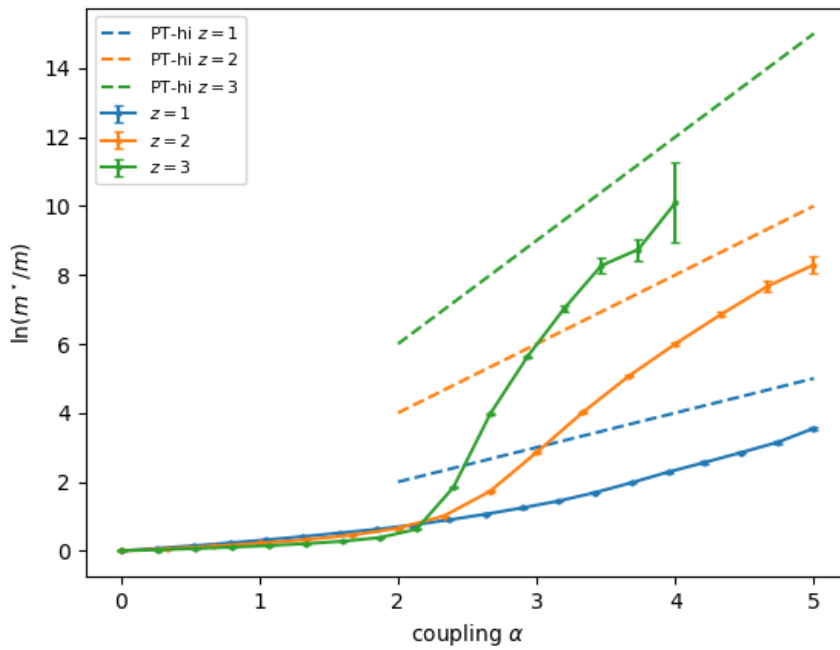
Figure 4.15: Logarithm of the effective mass enhancement vs. coupling, $\gamma = 1.0$

4.2 Momentum dependence

The large momentum polaron state was found to be very different from the small momentum state at both small and intermediate coupling:

- At small momentum, the electron is lightly dressed with a large quasiparticle weight and a dispersion very similar to that of a bare electron. At small coupling the number of phonons at large momentum is related to the number of phonons of the ground state by $N_{ph}(k \gg 0) \approx N_{ph}(k = 0) + 1$

- As momentum is increased, the polaron state starts to mix with the one-electron plus one-phonon continuum, The polaron dispersion flattens and looks more like the phonon dispersion. The Z_0 quasiparticle weight approaches 0 as the energy approaches the continuum edge.

4.2.1 1D

Energy

The results for the case of small coupling ($\alpha = 0.5$) and intermediate coupling ($\alpha = 2.0$) are reported in Figure 4.16. γ is kept at 0.5 throughout this section.

The weak coupling perturbation theory works well for small momentum, but it starts to fail at some point, producing an unphysical maximum in the polaron dispersion. This is due to the fact that below $\omega_0 = 4$ there is a momentum value at which the denominator of the energy correction becomes zero, which causes the perturbative expansion to diverge. [23]

In contrast, the DMC simulation shows that the polaron energy continues to increase, up to a point near the middle of the positive half of the Brillouin zone where the curve becomes almost flat, and tends towards the $E(0) + \omega_0$ value which is the energy of a state containing one more phonon[2]. This indicates that the polaron at large momentum is a weakly bound state.

In the intermediate coupling case perturbation theory fails as expected. The same flattening of the polaron dispersion at large k can be seen but now there is less difference from the $k = 0$ values due to the increased coupling with phonons. Its limit is not $E(0) + \omega_0$ anymore, which hints at a state containing a larger number of phonons, which is confirmed by the following results on phonon statistics.

---

[2]with respect to the $k = 0$ state of energy $E(0)$

	N	τ_{max}	O_{max}	D
$\alpha = 0.5$	20 M	60.0	600	1 M
$\alpha = 2.0$	10 M	12.0	600	1 M

Table 4.4: Settings for the upper half of the BZ in 1D momentum dependent simulations ($M = 10^6$).

	N	τ_{max}	O_{max}	D
$\alpha = 1.69$	500 M	12.0	600	1 M

Table 4.5: Settings for the zone boundary in 2D momentum dependent simulations.

Phonon statistics

At small coupling and small k the Z_0 quasiparticle weight is high, indicating that the polaron is still a lightly dressed electron (Figure 4.17). Figure 4.18 confirms that the high k state contains approximately one more phonon for $\alpha = 0.5$, while raising the coupling increases this number. The energy and average number of phonons curves are strongly correlated, showing similar behavior.

4.2.2 2D

For the 2D lattice case, the following path in k-space was chosen:

$$(0,0) \rightarrow (\pi, \pi) \rightarrow (\pi, 0) \rightarrow (0,0)$$

The results are reported in figures 4.19, 4.20 and 4.21. The behavior was found to be similar to the one-dimensional case:

- At the zone boundary the polaron is in the weakly bound state with a flat dispersion

- At the zone center the Z_0 quasiparticle weight is large, and is decreasing very rapidly with increasing k

Here the number of phonons is again larger by more than one than the corresponding $k = 0$ number, as in the one-dimensional case, but the effect seems to be enhanced by the higher dimensionality: the difference is larger even though the coupling is smaller ($\alpha = 1.69$ vs. $\alpha = 2.0$).
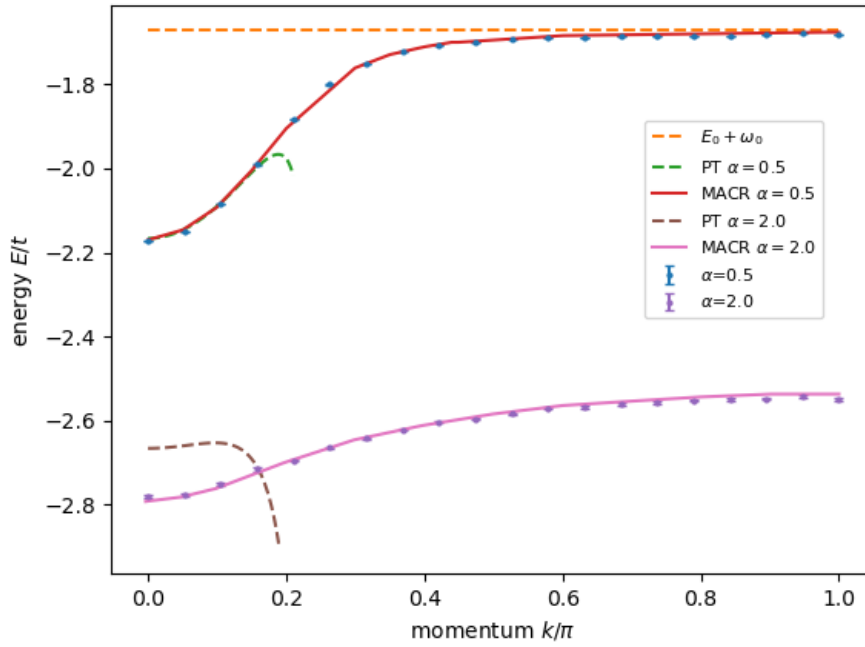
Figure 4.16: Energy vs. momentum, 1D lattice, $\gamma = 0.5$.
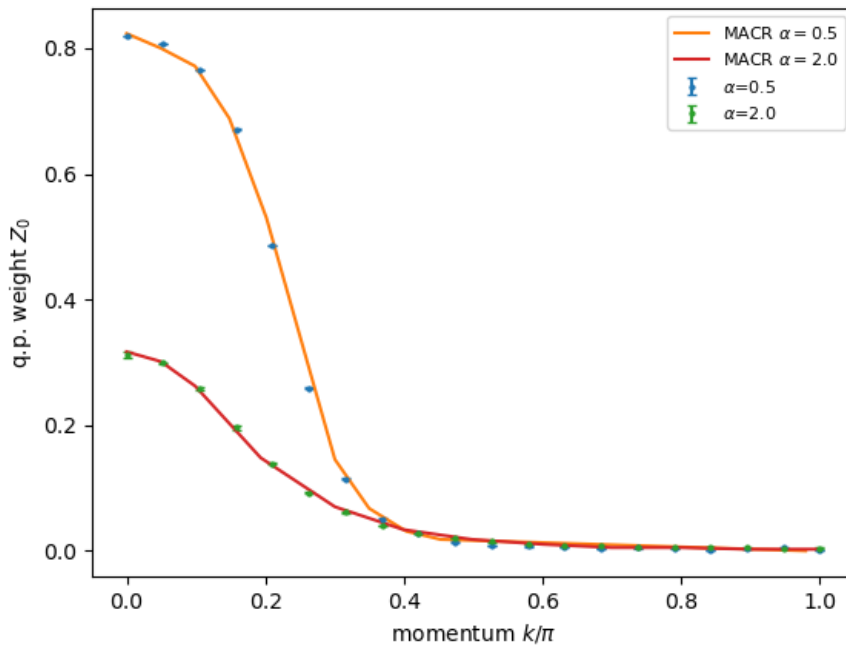
Figure 4.17: q.p. weight Z_0 vs. momentum, 1D lattice, $\gamma = 0.5$.
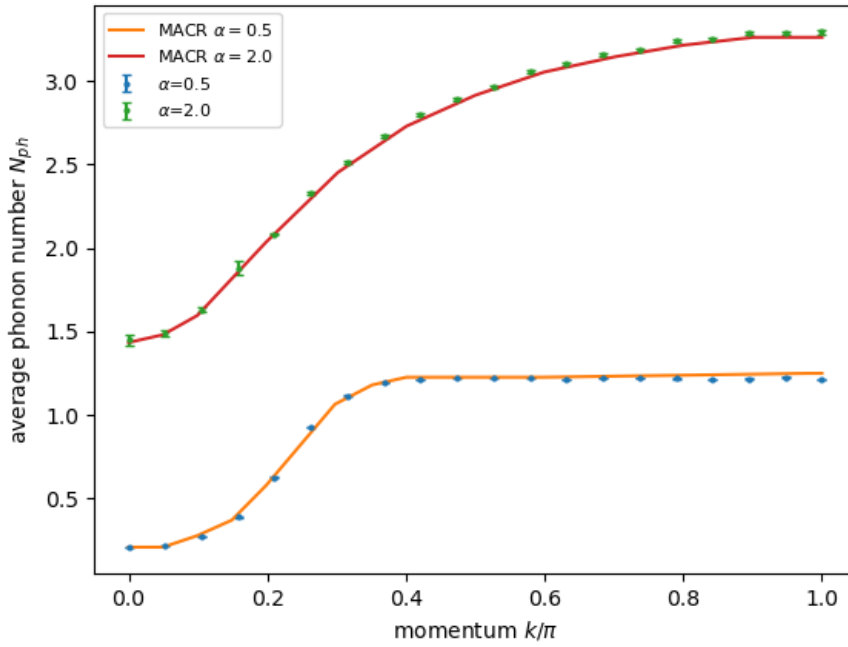
Figure 4.18: Average phonon number vs. momentum, 1D lattice, $\gamma = 0.5$.
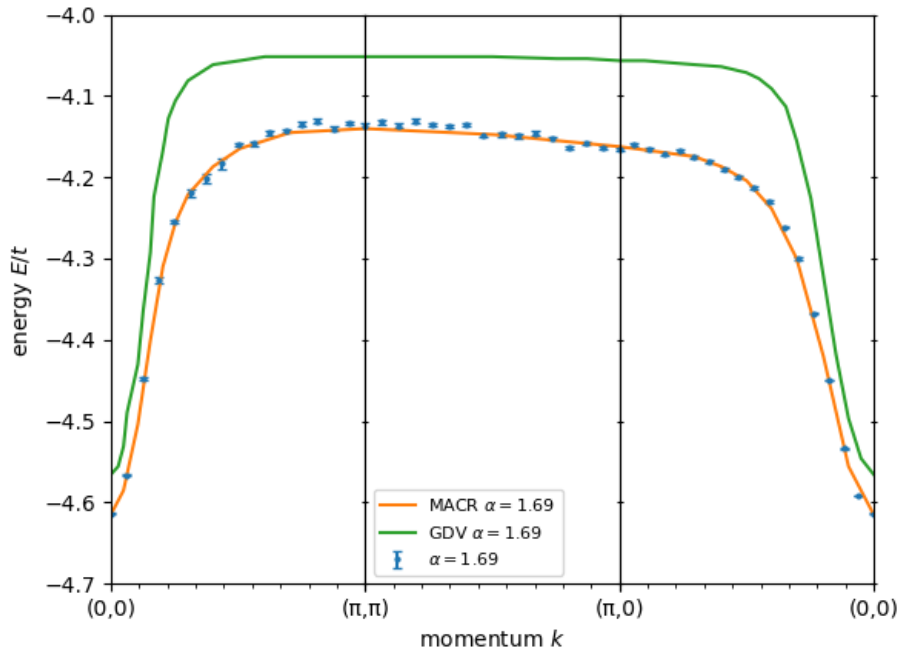
Figure 4.19: Energy vs. momentum, 2D lattice, $\gamma = 0.5$.
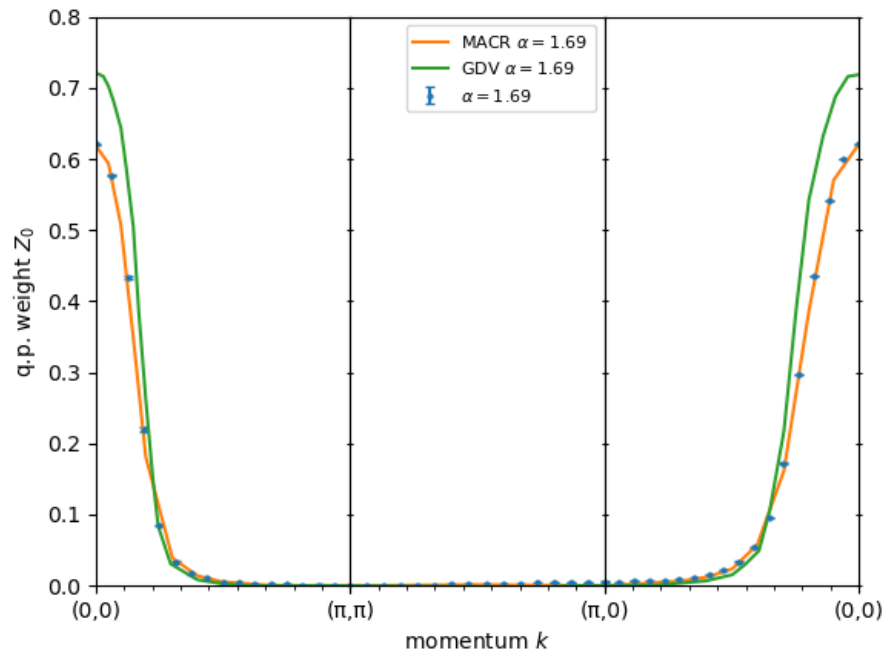
Figure 4.20: q.p. weight Z_0 vs. momentum, 2D lattice, $\gamma = 0.5$.
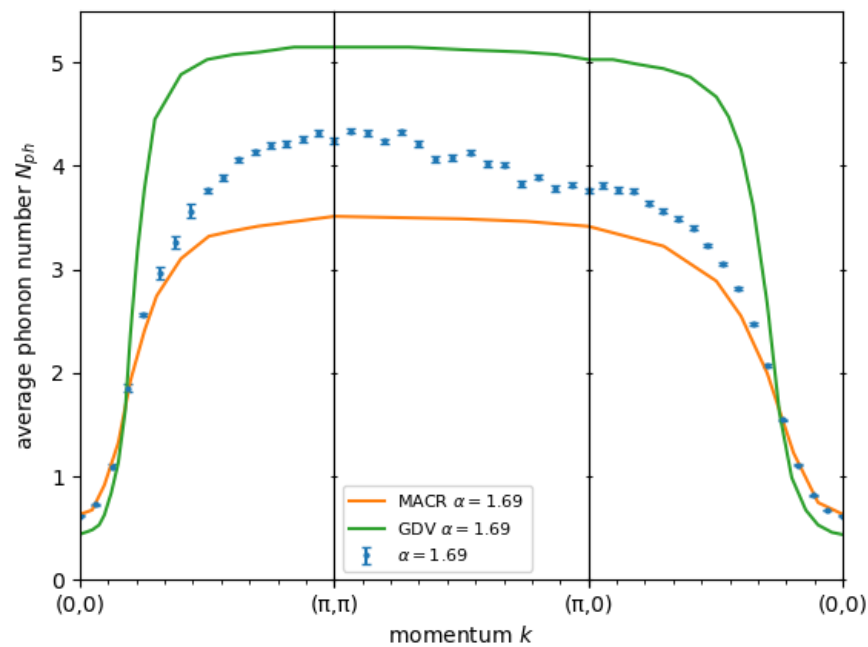
Figure 4.21: Average phonon number vs. momentum, 2D lattice, $\gamma = 0.5$.

Chapter 5

Conclusions and future work

The results showed good agreement with the reference data in general, which was somewhat expected as the method was developed with the polaron problem in mind, specifically the Fröhlich Hamiltonian, which differs just by the form of the electron-phonon interaction and electron dispersion. The quality of the present implementation has been validated with existing analytical perturbation theory results and previous DMC simulations. This work represents a systematic analysis of the main Holstein polaron properties in 1D, 2D and 3D, which was not fully carried out in literature.

The strong coupling behavior of the ground state energy and average phonon number was found to match very well the perturbation theory results (Figures 4.1 and 4.4), which means that the coupling range considered was enough to enter the strong coupling regime for these estimators. For the energy only, this was partly due to having included higher order term in the perturbative expansion. In contrast, the effective mass is still a bit far from the perturbation theory limit in the coupling range considered, especially for low values of the γ parameter (Figure 4.5): computing the effective mass in the coupling range where perturbation theory becomes a reasonable approximation is very expensive, at least in the present implementation.

Significant deviation from Macridin's and Goodvin's data was obtained for the momentum dependence of the average phonon number in 2D (Figure 4.21). This computation was expensive, and it can be seen that the data points still do not quite converge to a smooth line. Particularly suspicious is the deviation with respect to Macridin's result, since the same method is employed. This point will

be further explored in the future, as well as the computation of the 3D energy dispersion.

The biggest difficulties encountered during this work were related to the convergence of certain estimators for certain ranges of the parameter space. Simulations require more time in order to produce reliable results when the dimensionless coupling constant α and dimensionality are increased. Decreasing the adiabaticity ratio γ (while keeping fixed the hopping t) is also problematic, because convergence is attained at larger times due to the condition $\tau \gg (\omega_0)^{-1}$ [21] for the validity of the estimator expressions. Diagrams with a larger τ require more points to achieve the same "density" than with smaller τ.

As for the momentum dependence, when the 1D results were obtained the first time, the **k** region where the dispersion flattens was problematic: it was showing fast "oscillations" in the values of the energy and average phonon number observables, meaning that convergence was not achieved. This was attributed primarily to a too low total acceptance ratio, which was slowing down the development of the Markov chain. To improve the results, a series of improvements were introduced into the code: the total acceptance ratio was increased by both introducing a new type of update which is always accepted, the *shift-vertex* update, and by switching to better suited exponential distributions for the parameter τ_2 in the *add-internal* update and the parameters τ_1, τ_2 in the *add-external* update.

Since this implementation is single-threaded and results for different momentum and coupling are obtained by running independent simulation with the parameter of interest varied, the different runs can be launched in parallel. This was useful in particular when running the code on the Vienna Scientific Cluster, since the larger number of cores in the node of a cluster can be exploited. On the cluster, a batch of 16 simulations (one per core) was run each time on a single node.

This provided only limited benefit for the coupling dependence, since the overall execution time is largely dominated by the runs with the biggest couplings.

For the momentum dependence instead, this provides a significant speed-up since the time required to perform a certain number of iteration is spread out more evenly (it increases in the beginning as momentum is increased but reaches a plateau around the middle of the Brillouin zone).

Future improvements may consist in using a better memory representation for diagrams and faster implementations of the update procedures, following advice

contained in [24]. The algorithm could also be modified into the Self-Energy Diagrammatic Monte Carlo, in which the self-energy is sampled instead of the Green function. The self-energy diagram expansion has fewer terms and should therefore prove faster [23]. An even faster technique is Bold Diagrammatic Monte Carlo [29] where the bare propagator is replaced with a *dressed propagator* so that each diagram accounts for many diagrams of the self-energy expansion at once.

Chapter 6

Acknowledgments

Bibliography

[1] L. Ferrari, "Appunti per il corso di complementi di struttura della materia," 2018.

[2] S. B. D. Altland Alexander, *Condensed Matter Field Theory, Second Edition.* Cambridge University Press, 2 ed., 2010.

[3] G. D. Mahan, *Many-particle physics.* Physics of solids and liquids, Plenum Press, 2nd ed ed., 1990.

[4] H. Fröhlich, H. Pelzer, and S. Zienau, "Xx. properties of slow electrons in polar materials," *The London, Edinburgh, and Dublin Philosophical Magazine and Journal of Science*, vol. 41, no. 314, pp. 221–242, 1950.

[5] L. D. Landau and S. I. Pekar, "Effective mass of a polaron," *Zh. Eksp. Teor. Fiz. 18*, p. 419–423, 1948.

[6] F. Giustino, *Looking inside a polaron.* Workshop "Polarons in the 21st Century", 2019.

[7] M. Gell-Mann and F. Low, "Bound states in quantum field theory," *Phys. Rev.*, vol. 84, pp. 350–354, Oct 1951.

[8] R. D. Mattuck, *A guide to Feynman diagrams in the many-body problem.* Dover books on physics and chemistry, Dover Publications, 2nd ed ed., 1992.

[9] R. P. Feynman, "Space-time approach to quantum electrodynamics," *Phys. Rev.*, vol. 76, pp. 769–789, Sep 1949.

[10] N. Metropolis, A. W. Rosenbluth, M. N. Rosenbluth, A. H. Teller, and E. Teller, "Equation of state calculations by fast computing machines," *The Journal of Chemical Physics*, vol. 21, no. 6, pp. 1087–1092, 1953.

[11] J. Gubernatis, N. Kawashima, and P. Werner, "Quantum monte carlo methods: Algorithms for lattice models," Cambridge University Press, 2016.

[12] T. Holstein, "Studies of polaron motion: Part i. the molecular-crystal model," *Annals of Physics*, vol. 8, no. 3, pp. 325 – 342, 1959.

[13] T. Holstein, "Studies of polaron motion: Part ii. the "small" polaron," *Annals of Physics*, vol. 8, no. 3, pp. 343 – 389, 1959.

[14] A. Romero, D. Brown, and K. Lindenberg, "Solving the holstein molecular crystal model," 10 1997.

[15] A. Macridin and G. A. Sawatzky, *Phonons, charge and spin in correlated systems.* PhD thesis, Rijksuniversiteit Groningen, 2003.

[16] I. G. Lang and Y. A. Firsov, "Kinetic theory of semiconductors with low mobility," vol. 16, no. 5, 1963.

[17] B. Lau, "Two aspects of electron-phonon interactions." report for the course PHYS503, University of British Columbia.

[18] D. J. Griffiths, *Introduction to quantum mechanics.* Benjamin Cummings, 2 ed., 2004.

[19] F. Marsiglio, "Pairing in the holstein model in the dilute limit," *Physica C: Superconductivity*, vol. 244, no. 1, pp. 21 – 34, 1995.

[20] N. Prokof'ev and B. Svistunov, "Polaron problem by diagrammatic quantum monte carlo," *Phys. Rev. Lett.*, vol. 81, 1998.

[21] A. Mishchenko, N. Prokof'ev, A. Sakamoto, and B. Svistunov, "Diagrammatic quantum monte carlo study of the fröhlich polaron," *Phys. Rev. B*, vol. 62, 09 2000.

[22] T. Hahn, "Diagrammatic Quantum Monte Carlo for the Fröhlich polaron," Master's thesis, University of Vienna, 2017.

[23] D. Marchand, *Polaron physics beyond the Holstein model.* PhD thesis, University of British Columbia, 2011.

[24] N. Prokof'ev, *Diagrammatic Monte Carlo*, vol. 15 of *Many-Body Methods for Real Materials*. Verlag des Forschungszentrum Jülich, 2019.

[25] R. Bellman, R. Corporation, and K. M. R. Collection, *Dynamic Programming*. Rand Corporation research study, Princeton University Press, 1957.

[26] G. L. Goodvin, M. Berciu, and G. A. Sawatzky, "Green's function of the holstein polaron," *Phys. Rev. B*, vol. 74, p. 245104, Dec 2006.

[27] P. E. Kornilovitch, "Continuous-time quantum monte carlo algorithm for the lattice polaron," *Phys. Rev. Lett.*, vol. 81, pp. 5382–5385, Dec 1998.

[28] P. E. Kornilovitch, "Ground-state dispersion and density of states from path-integral monte carlo: Application to the lattice polaron," *Phys. Rev. B*, vol. 60, pp. 3237–3243, Aug 1999.

[29] N. V. Prokof'ev and B. V. Svistunov, "Bold diagrammatic monte carlo: A generic sign-problem tolerant technique for polaron models and possibly interacting many-body problems," *Phys. Rev. B*, vol. 77, p. 125101, Mar 2008.

[30] P. Virtanen, R. Gommers, T. E. Oliphant, M. Haberland, T. Reddy, D. Cournapeau, E. Burovski, P. Peterson, W. Weckesser, J. Bright, S. J. van der Walt, M. Brett, J. Wilson, K. J. Millman, N. Mayorov, A. R. J. Nelson, E. Jones, R. Kern, E. Larson, C. J. Carey, İ. Polat, Y. Feng, E. W. Moore, J. VanderPlas, D. Laxalde, J. Perktold, R. Cimrman, I. Henriksen, E. A. Quintero, C. R. Harris, A. M. Archibald, A. H. Ribeiro, F. Pedregosa, P. van Mulbregt, and SciPy 1.0 Contributors, "SciPy 1.0: Fundamental Algorithms for Scientific Computing in Python," *Nature Methods*, vol. 17, pp. 261–272, 2020.

[31] C. R. Harris, K. J. Millman, S. J. van der Walt, R. Gommers, P. Virtanen, D. Cournapeau, E. Wieser, J. Taylor, S. Berg, N. J. Smith, R. Kern, M. Picus, S. Hoyer, M. H. van Kerkwijk, M. Brett, A. Haldane, J. Fernández del Río, M. Wiebe, P. Peterson, P. Gérard-Marchant, K. Sheppard, T. Reddy, W. Weckesser, H. Abbasi, C. Gohlke, and T. E. Oliphant, "Array programming with NumPy," *Nature*, vol. 585, p. 357–362, 2020.

[32] Wes McKinney, "Data Structures for Statistical Computing in Python," in *Proceedings of the 9th Python in Science Conference* (Stéfan van der Walt and Jarrod Millman, eds.), pp. 56 – 61, 2010.

[33] J. D. Hunter, "Matplotlib: A 2d graphics environment," *Computing in Science Engineering*, vol. 9, no. 3, pp. 90–95, 2007.

[34] J. P. Ellis, "Tikz-feynman: Feynman diagrams with tikz," *Computer Physics Communications*, vol. 210, p. 103–123, Jan 2017.